NUREG/CR-5710

Stress-Corrosion-Cracking Studies on Candidate Container Alloys for the Tuff Repository

Prepared by
J. A. Beavers, C. L. Durr

Cortest Columbus Technologies, Inc.

Prepared for
U.S. Nuclear Regulatory Commission

AVAILABILITY NOTICE

Availability of Reference Materials Cited in NRC Publications

Most documents cited in NRC publications will be available from one of the following sources:

1. The NRC Public Document Room, 2120 L Street, NW., Lower Level, Washington, DC 20555

2. The Superintendent of Documents, U.S. Government Printing Office, P.O. Box 37082, Washington, DC 20013-7082

3. The National Technical Information Service, Springfield, VA 22161

Although the listing that follows represents the majority of documents cited in NRC publications, it is not intended to be exhaustive.

Referenced documents available for inspection and copying for a fee from the NRC Public Document Room include NRC correspondence and internal NRC memoranda; NRC bulletins, circulars, information notices, inspection and investigation notices; licensee event reports; vendor reports and correspondence; Commission papers; and applicant and licensee documents and correspondence.

The following documents in the NUREG series are available for purchase from the GPO Sales Program: formal NRC staff and contractor reports, NRC-sponsored conference proceedings, international agreement reports, grant publications, and NRC booklets and brochures. Also available are regulatory guides, NRC regulations in the *Code of Federal Regulations*, and *Nuclear Regulatory Commission Issuances*.

Documents available from the National Technical Information Service include NUREG-series reports and technical reports prepared by other Federal agencies and reports prepared by the Atomic Energy Commission, forerunner agency to the Nuclear Regulatory Commission.

Documents available from public and special technical libraries include all open literature items, such as books, journal articles, and transactions. *Federal Register* notices, Federal and State legislation, and congressional reports can usually be obtained from these libraries.

Documents such as theses, dissertations, foreign reports and translations, and non-NRC conference proceedings are available for purchase from the organization sponsoring the publication cited.

Single copies of NRC draft reports are available free, to the extent of supply, upon written request to the Office of Administration, Distribution and Mail Services Section, U.S. Nuclear Regulatory Commission, Washington, DC 20555.

Copies of industry codes and standards used in a substantive manner in the NRC regulatory process are maintained at the NRC Library, 7920 Norfolk Avenue, Bethesda, Maryland, for use by the public. Codes and standards are usually copyrighted and may be purchased from the originating organization or, if they are American National Standards, from the American National Standards Institute, 1430 Broadway, New York, NY 10018.

NUREG/CR-5710

Stress-Corrosion-Cracking Studies on Candidate Container Alloys for the Tuff Repository

Prepared by
J. A. Beavers, C. L. Durr

Cortest Columbus Technologies, Inc.

Prepared for
U.S. Nuclear Regulatory Commission

AVAILABILITY NOTICE

Availability of Reference Materials Cited in NRC Publications

Most documents cited in NRC publications will be available from one of the following sources:

1. The NRC Public Document Room, 2120 L Street, NW., Lower Level, Washington, DC 20555

2. The Superintendent of Documents, U.S. Government Printing Office, P.O. Box 37082, Washington, DC 20013-7082

3. The National Technical Information Service, Springfield, VA 22161

Although the listing that follows represents the majority of documents cited in NRC publications, it is not intended to be exhaustive.

Referenced documents available for inspection and copying for a fee from the NRC Public Document Room include NRC correspondence and internal NRC memoranda; NRC bulletins, circulars, information notices, inspection and investigation notices; licensee event reports; vendor reports and correspondence; Commission papers; and applicant and licensee documents and correspondence.

The following documents in the NUREG series are available for purchase from the GPO Sales Program: formal NRC staff and contractor reports, NRC-sponsored conference proceedings, international agreement reports, grant publications, and NRC booklets and brochures. Also available are regulatory guides, NRC regulations in the *Code of Federal Regulations*, and *Nuclear Regulatory Commission Issuances*.

Documents available from the National Technical Information Service include NUREG-series reports and technical reports prepared by other Federal agencies and reports prepared by the Atomic Energy Commission, forerunner agency to the Nuclear Regulatory Commission.

Documents available from public and special technical libraries include all open literature items, such as books, journal articles, and transactions. *Federal Register* notices, Federal and State legislation, and congressional reports can usually be obtained from these libraries.

Documents such as theses, dissertations, foreign reports and translations, and non-NRC conference proceedings are available for purchase from the organization sponsoring the publication cited.

Single copies of NRC draft reports are available free, to the extent of supply, upon written request to the Office of Administration, Distribution and Mail Services Section, U.S. Nuclear Regulatory Commission, Washington, DC 20555.

Copies of industry codes and standards used in a substantive manner in the NRC regulatory process are maintained at the NRC Library, 7920 Norfolk Avenue, Bethesda, Maryland, for use by the public. Codes and standards are usually copyrighted and may be purchased from the originating organization or, if they are American National Standards, from the American National Standards Institute, 1430 Broadway, New York, NY 10018.

DISCLAIMER NOTICE

NUREG/CR-5710

Stress-Corrosion-Cracking Studies on Candidate Container Alloys for the Tuff Repository

Manuscript Completed: April 1992
Date Published: May 1992

Prepared by
J. A. Beavers, C. L. Durr

Cortest Columbus Technologies, Inc.
2704 Sawbury Boulevard
Columbus, OH 43235

Prepared for
Division of Regulatory Applications
Office of Nuclear Regulatory Research
U.S. Nuclear Regulatory Commission
Washington, DC 20555
NRC FIN D1692

RELATED DOCUMENTS

The following is a listing of Topical Reports summarizing the research performed in the various tasks of the program issued to Cortest Columbus Technologies, Inc. (CC Technologies):

"Environmental Effects On Corrosion In The Tuff Repository." NUREG/CR-5435 published February, 1990.

"Potentiodynamic Polarization Studies On Candidate Container Alloys For The Tuff Repository." NUREG/CR-5708 published January, 1992.

"Immersion Studies On Candidate Container Alloys For The Tuff Repository." NUREG/CR-5598 published May, 1991.

Pitting, Galvanic, and Long-Term Corrosion Studies on Candidate Container Alloys for the Tuff Repository". NUREG/CR-5709 published January, 1992.

ABSTRACT

Cortest Columbus Technologies, Inc. (CC Technologies) investigated the long-term performance of container materials used for high-level waste packages as part of the information needed by the Nuclear Regulatory Commission (NRC) to assess the Department of Energy's application to construct a geologic repository for high-level radioactive waste. At the direction of the NRC, the program focused on the Tuff Repository. This report summarizes the results of Stress-Corrosion-Cracking (SCC) studies performed in Tasks 3, 5 and 7 of the program. Two test techniques were used; U-bend exposures and Slow-Strain-Rate (SSR) tests. The testing was performed on two copper-base alloys (Alloy CDA 102 and Alloy CDA 715) and two Fe-Cr-Ni alloys (Alloy 304L and Alloy 825) in simulated J-13 groundwater and other simulated solutions for the Tuff Repository. These solutions were designed to simulate the effects of concentration and irradiation on the groundwater composition. All SCC testing on the Fe-Cr-Ni Alloys was performed on solution-annealed specimens and thus issues such as the effect of sensitization on SCC were not addressed.

Both Alloy 825 and Alloy 304L was resistant to SCC in the J-13 well water and in the J-13 well water that was concentrated by a factor of about 80 by evaporation. Alloy 825 was resistant to SCC in all other environments evaluated including chloride solutions containing up to 100 000 ppm Cl in the presence of H_2O_2, even though crevice corrosion occurred in some of these environments. Alloy 304L was resistant to SCC in J-13 well containing 1000 ppm added Cl. Alloy 304L underwent SCC in only one liquid phase exposure condition; J-13 well water with 100 000 ppm added Cl. Alloy 304L also underwent SCC in four vapor phase exposure conditions, all in the presence of H_2O_2. Of the four solutions in which Alloy 304L underwent cracking, three were prepared with simulated J-13 well water and added Cl (1000 ppm Cl and 10 000 ppm Cl as NaCl and 10 000 ppm Cl as $CaCl_2$) while one solution, Solution Number 20, was taken from the Task 2 experimental test matrix. Solution Number 20 contained 1000 ppm Cl as well as 200 ppm F and 200 ppm NO_2^-.

Both Alloy CDA 102 and Alloy CDA 715 were found to be resistant to SCC in Solution Number 7 from the Task 2 experimental test matrix, in simulated J-13 well water and in the simulated water concentrated approximately 80 times. Alloy CDA 715 was also resistant to SCC in all other environments evaluated including $NaNO_2$ at concentrations up to 1M. Alloy CDA 102 underwent SCC in $NaNO_2$ environments at concentrations as low as approximately 200 ppm. The presence of species from simulated J-13 well water appeared to inhibit SCC of Alloy CDA 102 in the dilute $NaNO_2$ solution. On the other hand, anodic polarization of Alloy CDA 102 specimens in $NaNO_2$ solutions, to simulate radiolysis products, increased susceptibility to SCC. In SSR tests performed on Alloy CDA 102 at 90°C in $NaNO_2$ solutions, cracking only occurred under anodic polarization, suggesting that the potential range, relative to the free-corrosion potential, shifted in the noble direction with increasing temperature.

TABLE OF CONTENTS

TABLE OF CONTENTS (continued)

LIST OF FIGURES

LIST OF FIGURES (Continued)

LIST OF FIGURES (Continued)

LIST OF TABLES

LIST OF TABLES (Continued)

EXECUTIVE SUMMARY

The Department of Energy (DOE) is conducting a program for the disposal of high-level radioactive waste in a deep-mined geologic repository. The Nuclear Regulatory Commission (NRC), which is responsible for regulating high-level radioactive waste disposal, will review DOE's application for the construction and operation of the repository. To assist in evaluating DOE's application, the NRC's Office of Nuclear Regulatory Research is developing an understanding of the long-term performance of the geologic repository. As part of this effort, Cortest Columbus Technologies, Inc. (CC Technologies) was awarded a contract to investigate the long-term performance of container materials used for high-level waste packages. At the direction of the NRC, the program focused on the Tuff Repository. The scope of work consisted of employing relatively short-term electrochemical techniques to examine a wide range of possible failure modes. Long-term tests (1-2 years) were used to verify the short-term studies.

This report summarizes the results of Stress-Corrosion-Cracking (SCC) studies performed in Tasks 3, 5 and 7 of the program. The testing was performed on two copper-base alloys (Alloy CDA 102 and Alloy CDA 715) and two Fe-Cr-Ni alloys (Alloy 304L and Alloy 825) in simulated J-13 groundwater and other simulated solutions for the Tuff Repository. All SCC testing on the Fe-Cr-Ni Alloys was performed on solution-annealed specimens and thus issues such as the effect of sensitization on SCC were not addressed.

The objective of Task 3 was to evaluate the corrosion performance of the candidate alloys in simulated Tuff repository environments under various exposure conditions (immersed, vapor phase, and alternate immersion). These immersion tests included U-bend SCC specimens and were performed in a simulated J-13 well water and two other environments selected from the experimental test matrix from Task 2 of the program.

The objective of Task 7 was to evaluate the corrosion performance of the candidate alloys in simulated Tuff repository environments under long-term exposures. The long-term exposures included U-bend specimens and were also performed in the simulated J-13 well water. However, in these tests, the solutions were allowed to concentrate by means of evaporation and periodic addition of fresh solution. Thus, these studies were designed to evaluate the effects of alternate wetting and drying of the canister and the concentration of ionic species over time. In Task 7, immersion testing of U-bend specimens of both the Fe-Cr-Ni alloys also was conducted in solutions containing added chloride. The purpose of these tests was to provide data for comparison with Slow-Strain-Rate (SSR) tests performed under similar exposure conditions.

In Task 5 of the program, the SSR technique was used to evaluate the SCC of the candidate alloys in simulated repository environments. The primary objective of Task 5 was to identify environmental conditions under which the candidate alloys will undergo SCC. A secondary objective of Task 5 was to assess the SSR technique for evaluating long-term SCC performance. The alloy-environment combinations that were investigated were selected on the basis of the results of cyclic-potentiodynamic-polarization studies performed in Task 2 (NUREG/CR-5708) and the results of a literature search performed in Task 1 (NUREG/CR-5435). These included simulated J-13 well water, simulated J-13 water containing specific ionic species, sodium nitrite solutions (copper-base alloys), chloride solutions (Fe-Cr-Ni alloys) and two other solutions (Solution Number 20 (Fe-Cr-Ni alloys) and Solution Number 7 (copper-base alloys)) that were

designed to simulate the chemical effects resulting from concentration and irradiation of the groundwater.

Alloy 825 was resistant to SCC in all environments evaluated including simulated J-13 well water, simulated J-13 well water concentrated by a factor of about 80, and chloride solutions containing up to 100 000 ppm Cl in the presence of H_2O_2, even though crevice corrosion occurred in some of these environments. The concentrated simulated J-13 well water solution contained 675 ppm Cl based on a post-test chemical analysis.

Alloy 304L was resistant to SCC in the J-13 well water and in the J-13 well water that was concentrated by a factor of about 80 by evaporation. The U-bend test results also indicated that Alloy 304L was resistant to SCC in J-13 well containing 1000 ppm added Cl. Alloy 304L U-bend specimens underwent SCC in only one liquid phase exposure condition; J-13 well water with 100 000 ppm added Cl.

Alloy 304L U-bends also underwent SCC in four vapor phase exposure conditions, all in the presence of H_2O_2. Of the four solutions in which Alloy 304L underwent cracking, three were prepared with simulated J-13 well water and added Cl (1000 ppm Cl and 10 000 ppm Cl as NaCl and 10 000 ppm Cl as $CaCl_2$) while one solution, Solution Number 20, was taken from the Task 2 experimental test matrix. Solution Number 20 contained 1000 ppm Cl as well as 200 ppm F and 200 ppm NO_2^-. The occurrence of SCC only in the vapor phase in the latter environments suggests that SCC may be more likely in the vapor phase in the repository. This behavior may relate to the availability of the oxidant, H_2O_2, to the metal in the vapor phase.

Discrepancies were observed, in two environments, between the SSR and the U-bend test techniques, where SCC occurred with U-bend specimens of Alloy 304L but not with SSR specimens of that alloy. However, insufficient data were obtained to conclude that the SSR technique provides erroneous results in assessing the SCC behavior of Alloy 304L in chloride containing environments. Nevertheless, the discrepancies observed are disconcerting and indicate that further research is needed.

Both Alloy CDA 102 and Alloy CDA 715 were found to be resistant to SCC in Solution Number 7 from the Task 2 experimental test matrix, in simulated J-13 well water and in the simulated water concentrated approximately 80 times. Alloy CDA 715 was also resistant to SCC in all other environments evaluated including $NaNO_2$ at concentrations up to 1M. Possible incipient cracks were observed in the necked region of one specimen tested in the latter environment but the possible cracking could not be reproduced in two subsequent SSR tests.

In SSR tests performed on Alloy CDA 102, SCC was observed in $NaNO_2$ environments at concentrations as low as approximately 200 ppm. The presence of species from simulated J-13 well water appeared to inhibit SCC of Alloy CDA 102 in the dilute $NaNO_2$ solution. On the other hand, anodic polarization of Alloy CDA 102 specimens in $NaNO_2$ solutions, to simulate radiolysis products, increased susceptibility to SCC. In SSR tests performed on Alloy CDA 102 at 90°C, cracking only occurred under anodic polarization in $NaNO_2$ solutions, suggesting that the potential range, relative to the free-corrosion potential, shifted in the noble direction with increasing temperature.

An analysis of mechanical property and secondary cracking from the SSR tests on Alloy CDA 102 was performed to determine the most reliable indicator of SCC. Ultimate tensile strength did not correlate well with SCC crack velocity. On the other hand, time to failure, percent reduction in area, and percent elongation correlated well with SCC crack velocity. However, crack depth and crack velocity were found to be the most reliable indicators of susceptibility to SCC for Alloy CDA 102.

1. INTRODUCTION

The Department of Energy (DOE) is conducting a program for the disposal of high-level radioactive waste in a deep-mined geologic repository. The Nuclear Regulatory Commission (NRC), which is responsible for regulating high-level radioactive waste disposal, will review DOE's application for the construction and operation of the repository. To assist in evaluating DOE's application, the NRC's Office of Nuclear Regulatory Research is developing an understanding of the long-term performance of the geologic repository. As part of this effort, CC Technologies was awarded a contract to investigate the long-term performance of container materials used for high-level waste packages. At the direction of the NRC, the program focused on the Tuff Repository. The scope of work consisted of employing relatively short-term electrochemical techniques to examine a wide range of possible failure modes. Long-term tests (1-2 years) were used to verify the short-term studies.

This report summarizes the results of Stress-Corrosion-Cracking (SCC) studies performed in Tasks 3, 5 and 7 of the program. The testing was performed on two copper-base alloys (Alloy CDA 102 and Alloy CDA 715) and two Fe-Cr-Ni alloys (Alloy 304L and Alloy 825) in simulated J-13 groundwater and other simulated solutions for the Tuff Repository. The SCC testing in Tasks 3 and 7 consisted of exposures of U-bend specimens of the four alloys to the simulated repository environments while the testing in Task 5 consisted of Slow-Strain-Rate (SSR) tests of those alloys in similar environments.

2. BACKGROUND - THE TUFF REPOSITORY ENVIRONMENT

2.1 Nominal Environment

The Tuff Repository will be located in the Topopah Spring Member of the Paintbrush Tuff under Yucca Mountain, 100 miles northwest of Las Vegas, Nevada in the Nevada Test Site (NTS). The site is located in an extremely arid zone with about 15 cm/year annual precipitation. The evaporation-transpiration rates also are very high so the net water percolating down from the surface is of the order of a few millimeters per year (Montazer - 1984).

Tuff is an igneous rock of volcanic origin and is composed of volcanic rock fragments (shards) and ash. The structure of the tuff deposits depends on the cooling rate and degree of compaction after the volcanic eruption. The rock shards weld together and the compacted material may remain glassy or may devitrify. A layered structure develops; a densely welded core surrounded above and below by zones of material decreasing in density and strength. In the post-depositional period, alteration of the tuff layers occurs. Crystallization transforms the glassy material to feldspar plus quartz or cristobalite. Zeolitization produces hydrous silicates by reaction of the glassy material with groundwater. A typical stratigraphy of the tuff at the NTS is shown in Figure 2.1. A more detailed description of these tuff layers is found in Johnstone-1981.

The potential repository horizon is in the lower, densely welded and devitrified portion of the Topopah Spring Member located 700 to 1400 feet above the static water table. The bulk rock at the horizon is composed of rhyolite with a small range in composition as shown in Table 2.1. This small variation in geochemistry demonstrates that the host rock may be considered uniform, according to Glassley-1986.

A reference water used in many repository studies has been taken from Well J-13. That well is located near the repository site and produces water which has flowed through the Topopah Spring Member, where it lies at a lower elevation and is in the saturated zone. The J-13 well water is the best available source of water from the Topopah Spring Member, but may not be a good approximation of the actual water that will be present in the repository.

The location of the repository above the static water table has a maior impact on the anticipated environment. First of all, the environment will be aerated; the J-13 well water contains 5.7 ppm dissolved oxygen which presumably represents a lower limit for oxygen. This condition is unique in that the plans for all other repositories, either in the United States or elsewhere, have called for locations below the static water table where conditions are deaerated (anoxic).

A second feature of the location of the repository above the water table is the elimination of the hydrostatic head on the waste container. At the repository elevation, the boiling point for water is about 95°C, and thus the environment at the waste package surface will be steam and air during the early life of the repository.

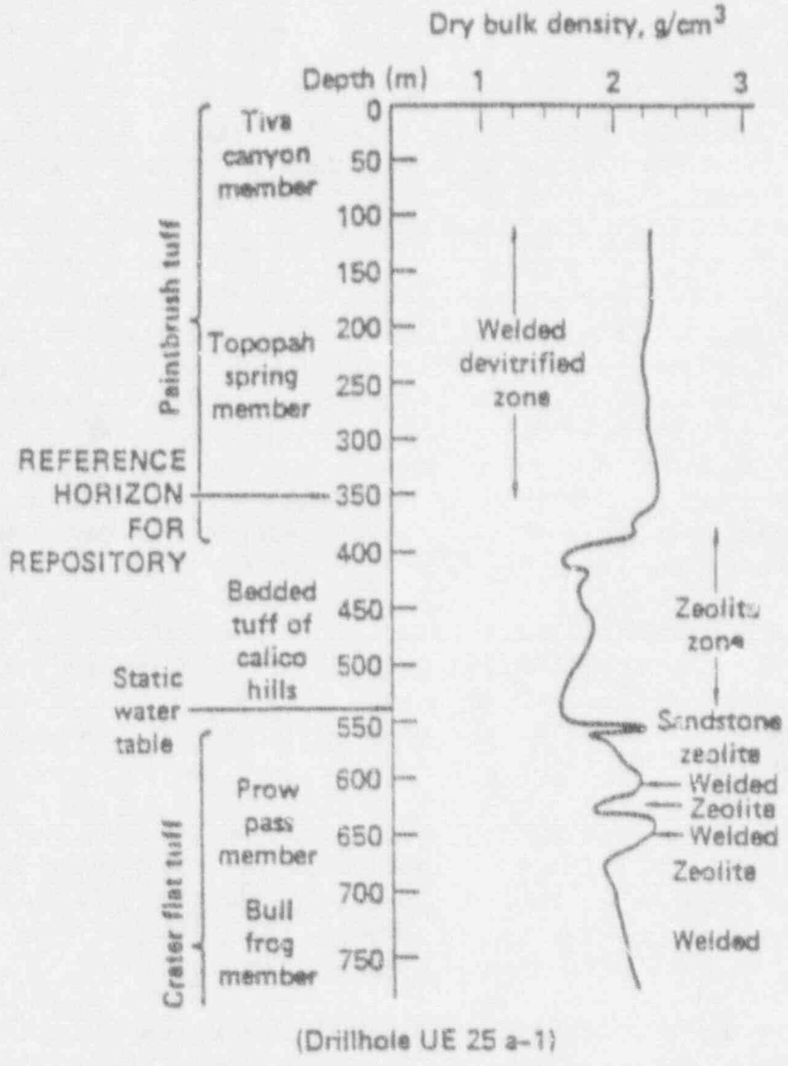

Figure 2.1 Representative Stratigraphic Section In Nevada Tuff (Drillhole UE25 a-1) (McCright-1984).

Table 2.1 Percentages Of Major Constituents In Topopah Springs Tuff, Drill Core USW GU-3, Samples 60, 61 And 62. Fe_2O_3 Represents Total Iron (Schuraytz-1985).

Constituent	60	61	62	Average	Std Dev
SiO_2	78.4	78.9	78.9	78.73	0.24
Al_2O_3	12.0	12.3	12.2	12.17	0.12
Fe_2O_3	1.016	0.973	1.000	0.996	0.018
CaO	0.492	0.451	0.480	0.474	0.017
MgO	0.1271	0.1281	0.1126	0.123	0.007
TiO_2	0.1108	0.0927	0.0984	0.101	0.008
Na_2O	4.07	3.92	4.25	4.08	0.13
K_2O	3.71	3.18	2.94	3.28	0.32
P_2O_2	0.01	0.01	0.03	0.02	0.01
MnO	0.0624	0.0455	0.0488	0.052	0.007

2.1.1 Thermal Effects

The repository is being designed for two types of waste packages; spent fuel and processed defense high level waste in the form of borosilicate glass. The spent fuel will have the highest thermal output of between 1.3 and 3.3 Kw per container, while the glass will have an output of 0.25 to 0.47 Kw per container. The temperature histories of the waste packages are sensitive functions of the thermal properties of the near-field rock, the specific configuration of boreholes and emplacement drifts, heat transfer mode as well as container output power; none of these factors has been precisely defined. Comparative canister surface temperatures as a function of time are shown in Figure 2.2 for one set of conditions. Note that the canister surface for spent fuel remains above the boiling temperature over at least a 300 year period following emplacement.

These elevated temperatures should exclude liquid water from the near field of the repository for several hundred years, although liquid water may be present in the pores in the rock up to 140°C. It is also possible that vadose water may come in contact with some of the waste packages during periods of liquid water movement through the repository.

A consequence of the elevated temperature in the repository will be the interaction of groundwater with the host rock in the vicinity of the waste package. A number of interaction studies has been performed over temperatures ranging from 90-250°C with core wafers, crushed core wafers in gold-bags and PTFE-lined (polytetrafluoroethylene) autoclaves. Rapid shifts in chemistry occurred with crushed rock as opposed to wafers because of the higher surface area with the former. Changes in solution concentration at 90°C were minor; whereas, more pronounced shifts occurred at 150°C. Results obtained by Knauss-1985a for crushed core material at 150°C are given in Figures 2.3 and 2.4. These data show that the silicon (Si) concentrations increased from about 30 ppm to around 150 ppm within 60 days, while the sodium (Na) concentration only increased slightly over the test period. The concentrations of aluminum[1] (Al), magnesium (Mg) and calcium (Ca) decreased with time while that of potassium[1] (K) was not greatly affected by thermal interaction; the pH decreased very slightly.

Another consequence of the elevated temperatures in the repository will be the boiling of groundwater in the vicinity of the waste package. This will lead to the concentration of the species, both beneficial and deleterious, in the groundwater. Abraham (1986) has performed some solution analyses on boiling J-13 groundwaters at Brookhaven National Laboratory. The solutions were boiled in the presence of tuff rock and specimens of several stainless steels. The results are summarized in Table 2.2. These data show that the composition of J-13 well water changed quite dramatically as a result of boiling. The stable concentrations of most species after one year were more than an order of magnitude higher than those in the J-13 well water. Some species, such as SO_4^{2-}, NO_3^-, Ca^{2+} and K^+ exhibited a maximum in concentration after only a few months which suggests the precipitation of compounds such as $CaSO_4$, etc.

The concentration of the species in the 10X J-13 well water also increased with exposure time in these tests. Although the magnitudes of the increases were smaller than those observed for

---

[1]Both aluminum and potassium exhibited initial transient increases in concentrations.

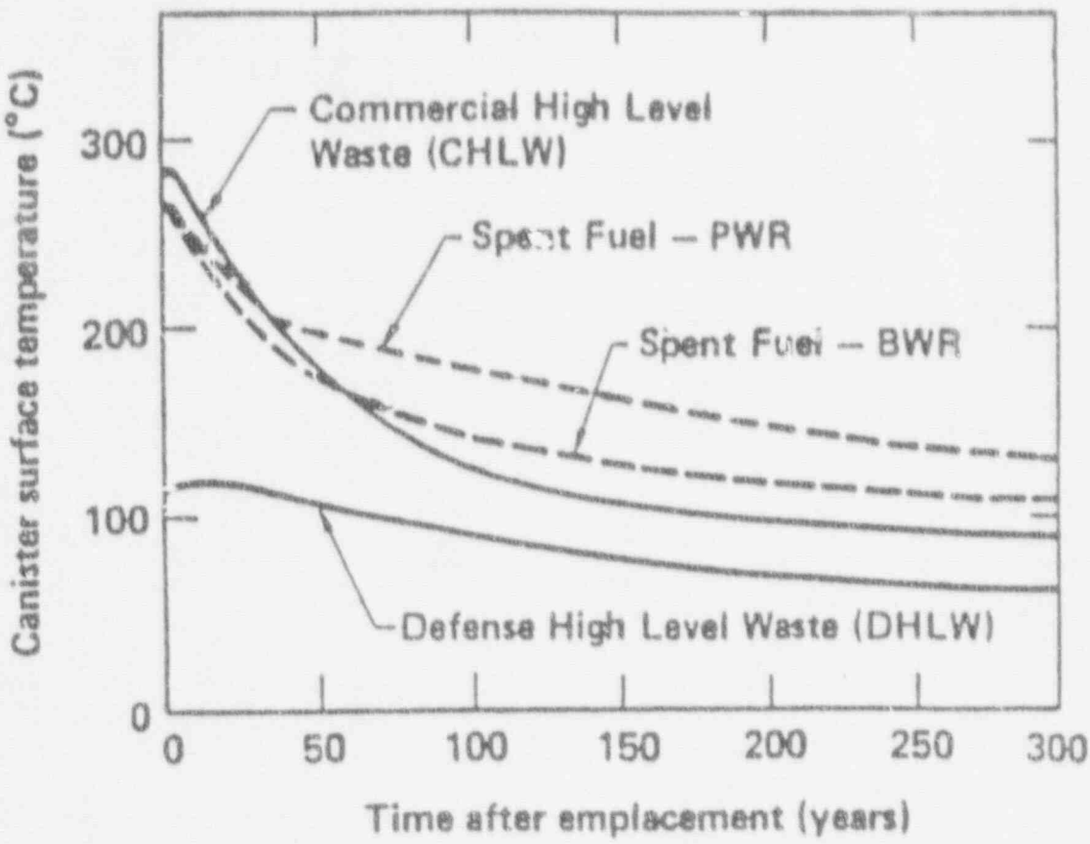

Figure 2.2 Comparative Canister Surface Temperature-Time Profiles For Different Waste Packages In A Tuff Repository (Vertical Emplacement, 50 kW/acre Areal Loading) (McCright-1984).

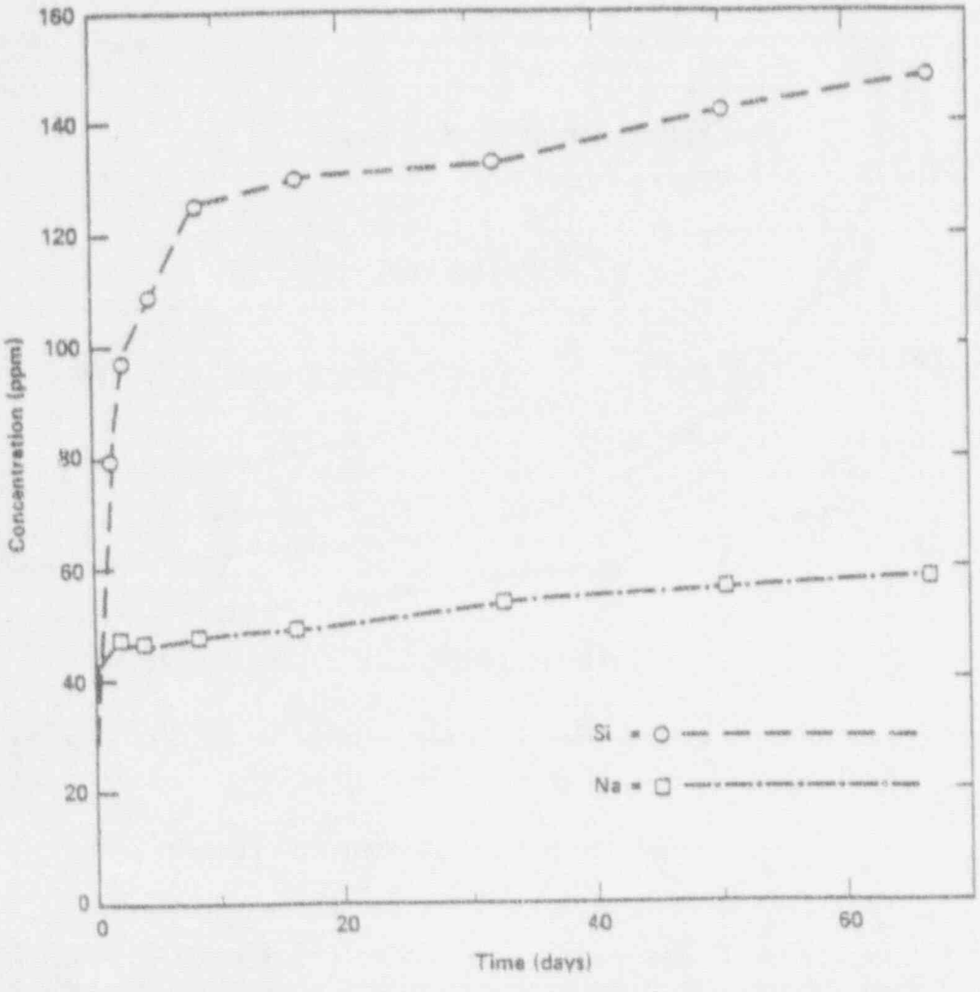

Figure 2.3 Silicon And Sodium Concentrations In J-13 Well Water Reacted With Crushed G-1 Material At 150°C As A Function Of Time In Days (Knauss-1985a).

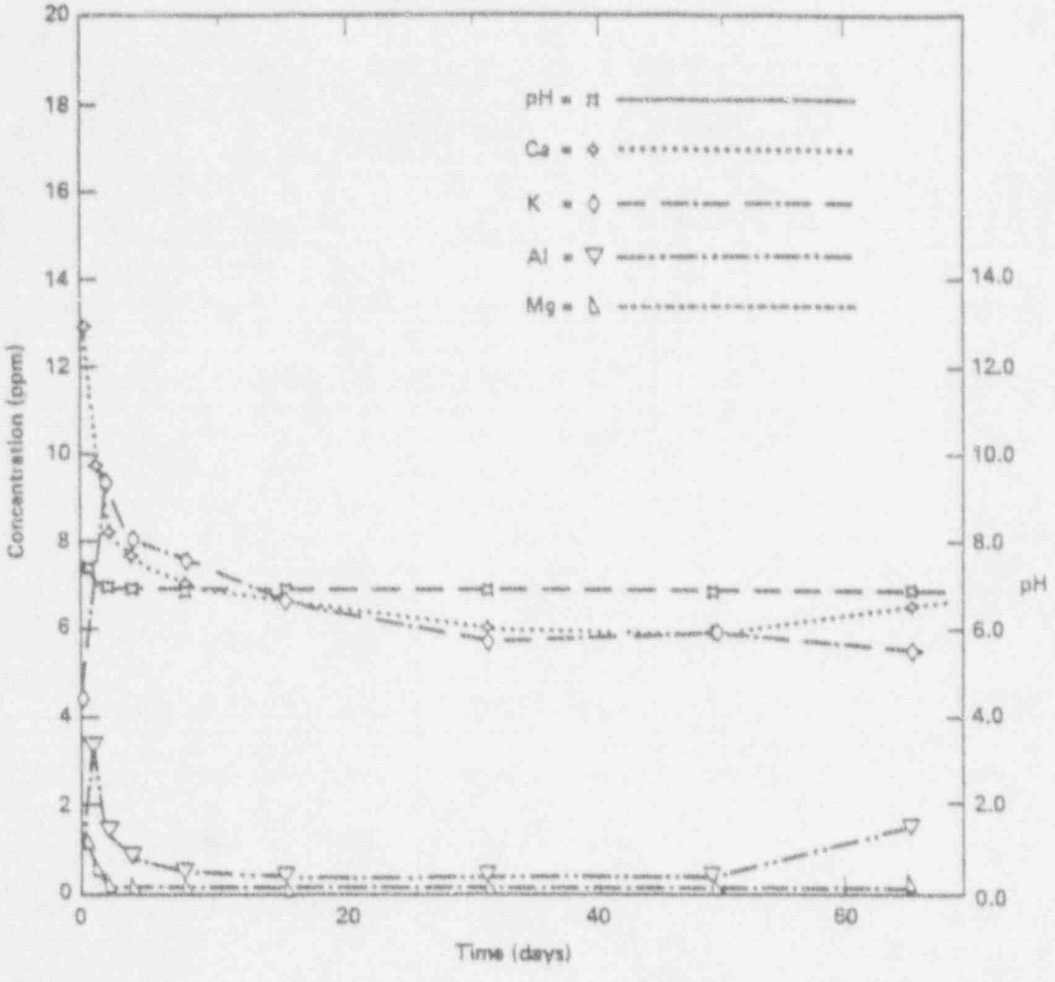

Figure 2.4 Aluminum, Potassium, Calcium, Magnesium, And pH Analyses From J-13 Well Water Reacted With Crushed G-1 Material At 150°C As A Function Of Time In Days (Knauss-1985a).

Table 2.2 Chemical Composition Of Test Solutions At The End Of Corrosion Tests (µg/ml) (Undiluted And Filtered Solution) (Abraham-1986).

	Reference	Synthetic J-13 Water			10-Times Conc. J-13 Water		
	J-13 Groundwater	3-Mo. Test	6-Mo. Test	1-Yr. Test	3-Mo. Test	6-Mo. Test	1-Yr. Test
Na^+	45	N.D.*	464	510	867	738	908
K^+	4.9	238	244	106	244	214	139
Ca^{2+}	14	308	161	104	301	164	129
Sn^{2+}	N.D.	3.4	0.4	1.0	4.4	0.5	1.2
F^-	2.2	12.1	4	6.31	14	5	21.1
Cl^-	7.5	130	236	161	330	211	260
NO_3^-	5.6	460	750	482	—	522	672
SO_4^{2-}	22	820	552	588	1300	1260	976
SiO_2	61	414	451	458	408	488	406
pH at room temperature	8.5	8.4	9.0	9.3	8.4	8.9	9.3

*N.D. = Not determined

the J-13 well water, the actual final concentrations of the species in the tests with the 10X J-13 well water were higher than those in the standard J-13 well water. As in the J-13 well water, maximum concentrations were observed for some species in the boiling 10X J-13 well water after a few months.

2.1.2 Radiation Effects

Relatively little research has been performed on the influence of the radiation field on the environment in the Tuff repository. On the other hand, a number of articles discuss, in general terms, the anticipated role of radiation in altering the repository environment while research on the effects of radiation on water and dilute aqueous solutions is much more extensive. As described by McCright-1984, the highest levels of radiation will occur on emplacement and the levels will begin to decay. The radiation of interest with regard to container corrosion will be gamma radiation. Interaction of the gamma radiation with either the container or the host rock is also expected to be minimal. Thus, the primary problem is the interaction of the gamma radiation field with the liquid and gas phases in the repository. Although most of the fission products responsible for gamma radiation decay rapidly, the repository environment will consist of air and water vapor during the time period when radiation levels will be high.

Radiolysis products expected in the moist-air system are not well established. Some experimental research regarding the temperature effects on radiolysis products has been performed by Van Konynenburg (1986) and others. Their research indicates that, above 135°C, the dominant species are NO, N_2O, and O_3. Between 120° and 135°C, NO_2, N_2O_4, H_2O, and O_3 are the dominant products, while below 120°C, the most abundant products are HNO_3 and H_2O with small amounts of O_3.

In liquid water at high radiation levels, small amounts of nitrates and nitrites will also be produced. However, the simultaneous presence of liquid water and high radiation fields are possible only intermittently during periods of liquid water movement through the repository.

Glass (1985 and 1986) reviewed the literature and performed electrochemical studies in irradiated J-13 well water. These studies concluded that the primary effect of radiation of J-13 well water is to produce the dominant oxidizing species O_2 and H_2O_2 with smaller concentrations of O^-_2 and still smaller concentrations of HO_2. Irradiation of water containing CO_2 or HCO_3 with O_2 was found to produce carboxylic acids (formic and oxalic).

Studies focused on the effects of radiation on water and dilute aqueous solutions concluded that a host of transient radicals, ions, and stable molecular species is created by gamma radiation. Some of these species are as follows: H, OH, e^-_{aq}, H_3O^+, OH^-, H_2, H_2O_2, O_2, O_2^- and HO_2. While these species only consider the breakdown of the water molecule, many other species are generated by reactions with other species in the groundwater.

2.2 Simulated Environments

2.2.1 Simulated J-13 Well Water

In Task 2 of this program, Cyclic-Potentiodynamic-Polarization (CPP) tests were performed in simulated and actual J-13 well water (Tuff groundwater). The purpose of these tests was to reproduce and verify the polarization behavior observed by McCright at Lawrence Livermore National Laboratory and to establish that the simulated J-13 well water produced similar corrosion behavior to the actual Tuff groundwater. To reproduce the behavior observed by McCright (Figure 2.5), the following test conditions were used: Actual J-13 well water, a scan rate of 3.6 V/hr, temperature of 80°C, aerated conditions, and an initial exposure of 1-2 hours prior to performing the CPP test. The potentiodynamic-polarization technique is discussed in more detailed in Appendix A. The J-13 well water used in this subtask of the NRC program initially was obtained from Oak Ridge National Laboratories. Due to the difficulty in obtaining actual J-13 well water required over the duration of the program, a simulated J-13 well water was used in most other tasks. This simulated J-13 well water was previously developed by Battelle Memorial Institute. The composition of the simulated J-13 well water is given in Table 2.3.

The results of experiments performed with Alloy CDA 102, under the above conditions in simulated J-13 well water and actual in J-13 well water, are shown in Table 2.4 and Figures 2.6 and 2.7, respectively. The curves are similar, with slight differences in the polarization parameters of E_b (breakdown potential), E_{rp} (repassivation potential), and i_{cor} (corrosion current). Repetition of these experiments verified the similarities. Although the passive current density is lower for the curves produced in this study, as compared to McCright's data, the polarization behavior reasonably reproduces the behavior shown by McCright in Figure 2.5. The above results produce two important findings that are critical to the remaining work performed in this project:

(1) Prepared solutions can reasonably simulate actual well waters extracted from the Tuff site, and

(2) The experimental procedures used for the NRC project are capable of reproducing the polarization behavior observed at Lawrence Livermore National Laboratory under similar test conditions.

2.2.2 Selected Simulated Environments

In Task 2 of the program, a statistically based experimental test matrix was formulated in an effort to evaluate the influence on corrosion of the possible range of environmental variables that may occur over the life of the canister. The major difficulty encountered in designing these synthetic test solutions is in defining the geochemistry and the actual environments to which the canister will be exposed. The J-13 well water is probably the most dilute environment that can be expected within the Tuff Repository since boiling of the groundwater and its interaction with the

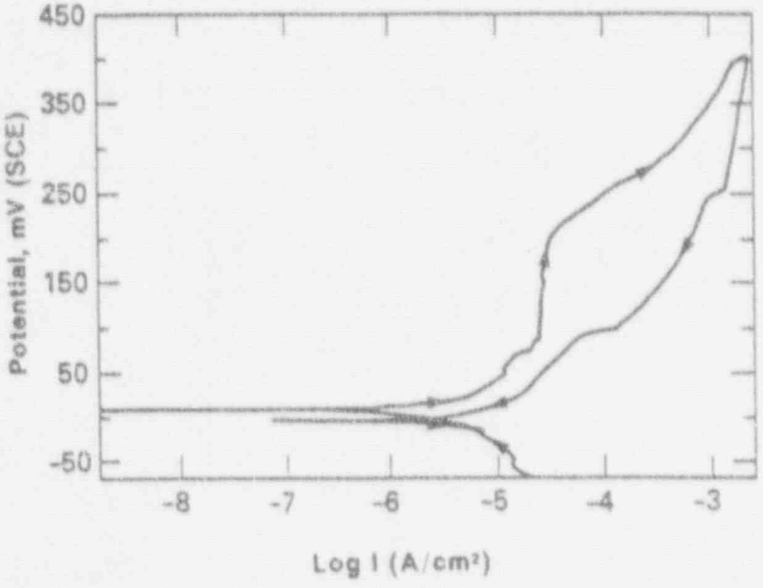

Figure 2.5 CPP Curve For Alloy CDA 102 In Actual J-13 Well Water At 80°C (Scan Rate: 1 mV/s) (McCright-1985).

Table 2.3 Chemical Composition Of Simulated Tuff Groundwater And J-13 Well Water From Yucca Mountain, Nevada (For Comparison).

Environmental Variable	Actual Chemical Used	J-13* ppm	Simulated J-13‡ ppm
Na^+	$NaHCO_3$	44.0	46.0
K^+	KCl, KF	5.1	5.5
Mg^{2+}	$MgCl_2 \cdot 6H_2O$	1.9	1.7
Ca^{2+}	$Ca(NO_3)_2 \cdot 4H_2O$, $CaSO_4 \cdot \frac{1}{2}H_2O$	12.5	12.0
SiO_2	H_2SiO_3	58.	64.2
F^-	KF	2.2	1.7
Cl^-	KCl, $MgCl_2 \cdot 6H_2O$	6.9	6.4
HCO_3^-	$NaHCO_3$	125.	121.
NO_3^-	$Ca(NO_3)_2 \cdot 4H_2O$	9.6	12.4
SO_4^{2-}	$CaSO_4 \cdot \frac{1}{2}H_2O$	18.7	19.2
pH		7.6	7.0 ± 0.2
TDS		291.5	290.3

*Knauss, 1985

‡Beavers, 1987

The pH adjustment was accomplished by bubbling carbon dioxide through the solution.

Table 2.4 CPP Parameters For The Candidate Alloys In Actual And Simulated J-13 Well Water.

Alloy	J-13 Well Water	Temperature °C	Initial Exposure Hours	Scan Rate V/hr	E_{corr} V, SCE	I_{corr} µA/cm²	E_{pit}/E_b V, SCE	E_{prot}/E_{rp} V, SCE
CDA 102	Actual *	80	1 - 2	3.6	-0.011	5.78	+0.201	+0.092
CDA 102	Simulated	80	1	3.6	-0.015	0.13	+0.161	-0.140
CDA 102	Actual	80	1	3.6	+0.004	0.31	+0.212	-0.179

* McCright - 1985.

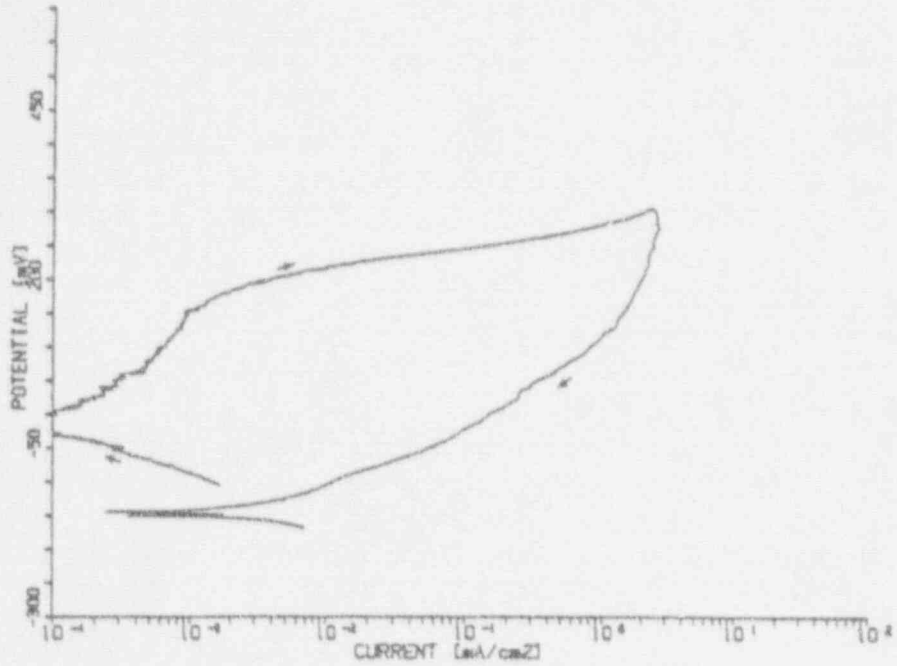

Figure 2.6 CPP Curve For Alloy CDA 102 In Simulated J-13 Well Water At 80°C Following A One Hour Initial Exposure (Beavers-1991b).

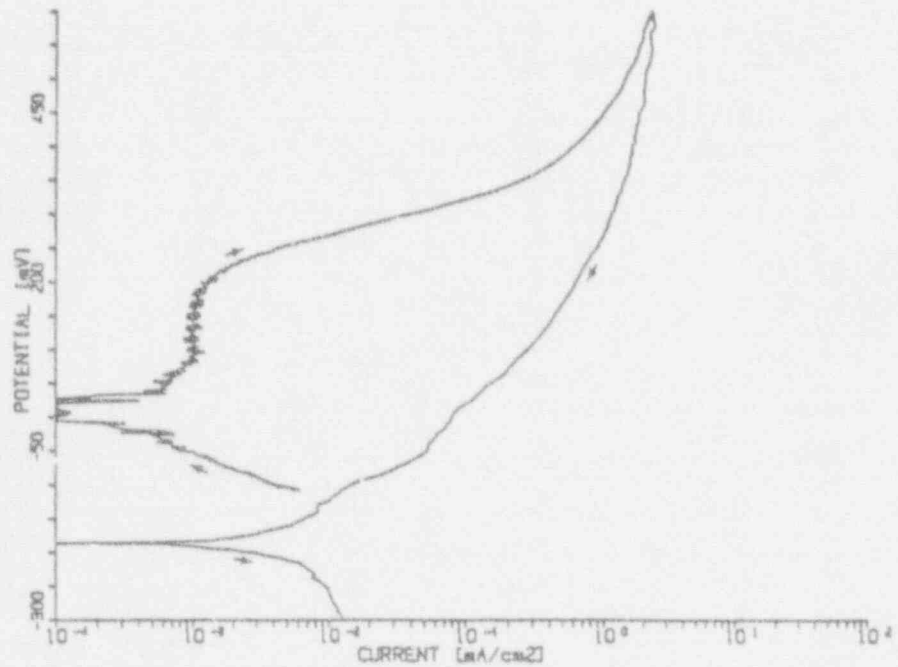

Figure 2.7 CPP Curve For Alloy CDA 102 In Actual J-13 Well Water At 80°C Following A One Hour Initial Exposure (Beavers-1991b).

host rock at elevated temperatures will tend to concentrate most species. The presence of the radiation field will generate new species, such as nitrates, carboxylic acids and hydrogen peroxide. Those species that are not volatile also may concentrate at the surface of the canister as a result of the combination of boiling and radiation.

The test matrix of simulated environments was designed as a screening matrix to identify important species, or regions of the environmental factor space, with respect to corrosion of the container materials, where additional research is needed. Each individual test solution represented individual points within the factor space. While it is not known whether these specific environments will be encountered, the maximum concentrations of the majority of the species within the solutions are thought to be reasonable, based on a thorough review of the literature (Beavers-1990). Further details of the Task 2 studies are given in the Topical Report referenced as Beavers-1991b.

Table 2.5 gives the compositions of the synthetic test solutions used in the Task 3, 5, and 7 SCC studies summarized in this report. Solution Numbers 7 and 20 were selected from the Task 2 experimental matrix and were used for testing the copper-base and Fe-Cr-Ni alloys, respectively. The selection of a specific composition was based primarily on the CPP behavior observed in Task 2 as opposed to the likelihood that a specific composition would exist in the repository. Solution Number 20 was found to be a pitting environment for the Fe-Cr-Ni alloys at 90°C as evidenced by the large hysteresis loop on the polarization curves shown in Figures 2.8 and 2.9. Solution Number 7 was found to be an active-corrosion environment for the copper-base alloys at 90°C. The polarization curves for these alloys are given in Figures 2.10 and 2.11. A summary of the CPP parameters for the selected alloys in simulated J-13 well water, Solution Number 20, and Solution Number 7 is given in Table 2.6.

The remaining solutions were prepared with additions of specific cracking agents, identified in a literature survey performed in Task 1 of the program. These agents included chlorides and hydrogen peroxide for the Fe-Cr-Ni alloys and nitrites for the copper-base alloys. CPP tests were performed with each of the chloride-containing solutions used with the Fe-Cr-Ni alloys to obtain the pitting and protection potentials (E_{pit}, E_{prot}). Appendix B gives the CPP curves for these alloy-environment systems and the CPP parameters determined from these curves.

Table 2.5 Composition Of J-13 Well Water And Selected Solutions From The Task 2 Experimental Matrix Used In The SCC Studies.

Environmental Species	J-13 Well Water mg/l	Simulated J-13 Well Water mg/l	Solution No. 20 mg/l	Solution No. 7 mg/l
pH	7.6	7.0 ± 0.2	10.0	5.0
SiO_2	58	64.2	2.2	215
HCO_3^-	125	121	0.4	0.4
F^-	2.2	1.7	200	0.04
Cl^-	6.9	6.4	1000	1000
NO_3^-	9.3	12.4	0.2	0.2
SO_4^{2-}	18.7	19.2	*	*
NO_2^-	—	—	200	0
H_2O_2	—	—	0.0	0
Al^{3+}	0.012	—	0.8	0.0004
Fe^{2+}	0.006	—	0.0	0.0
Ca^{2+}	12.5	12.0	0.8	0.8
Mg^{2+}	1.9	1.7	0.8	0.8
K^+	5.1	5.5	408	0.08
Na^+	44	46	*	*
PO_4^{3-}	0.12	—	2.0	2.0
Oxalic Acid	—	—	0.0	172

*Na^+ and SO_4^{2-} were used to balance the composition.

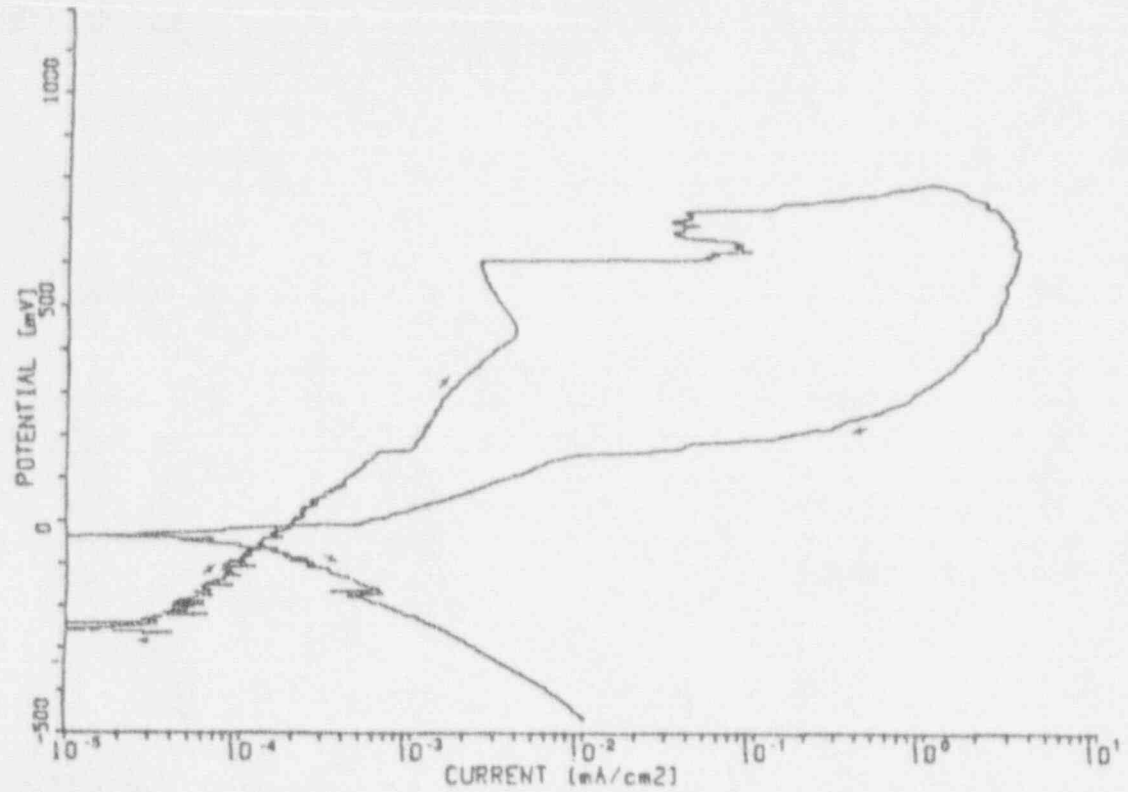

Figure 2.8 CPP Curve For Alloy 825 In Test Solution Number 20 At 90°C (Beavers-1991b).

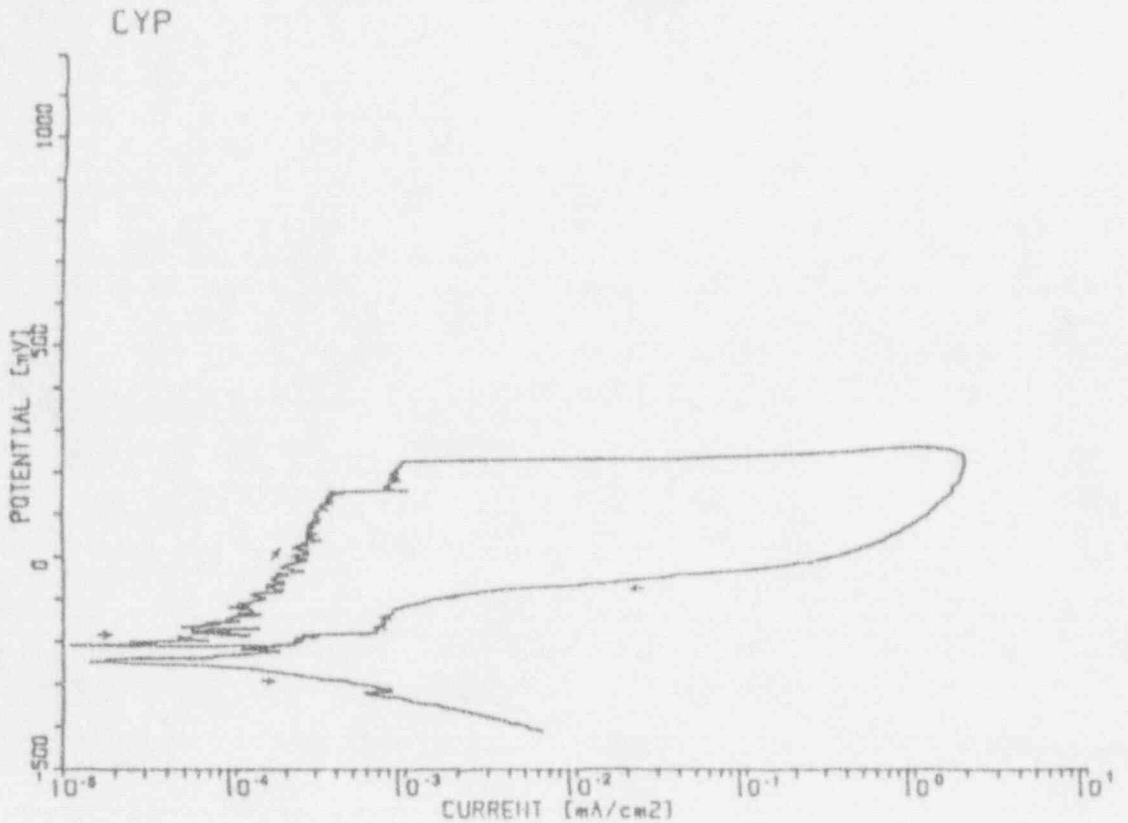

Figure 2.9 CPP Curve For Alloy 304L In Test Solution Number 20 At 90°C (Beavers-1991b).

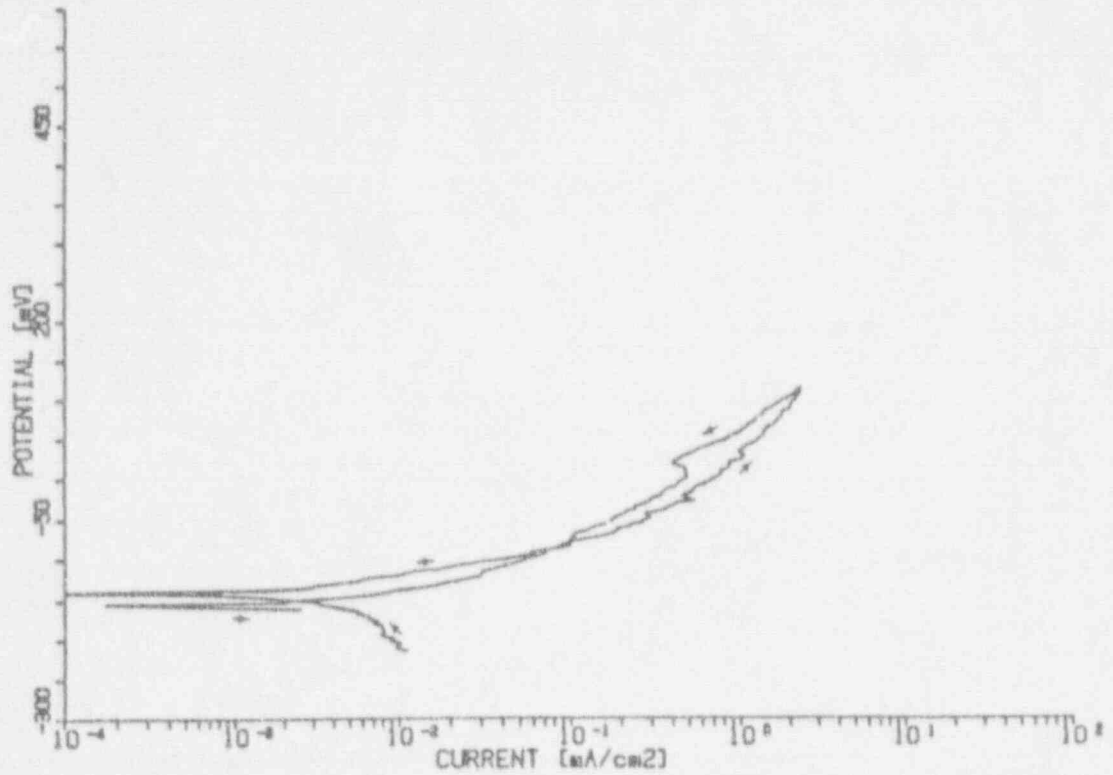

Figure 2.10 CPP Curve For Alloy CDA 102 In Test Solution Number 7 At 90°C (Beavers-1991b).

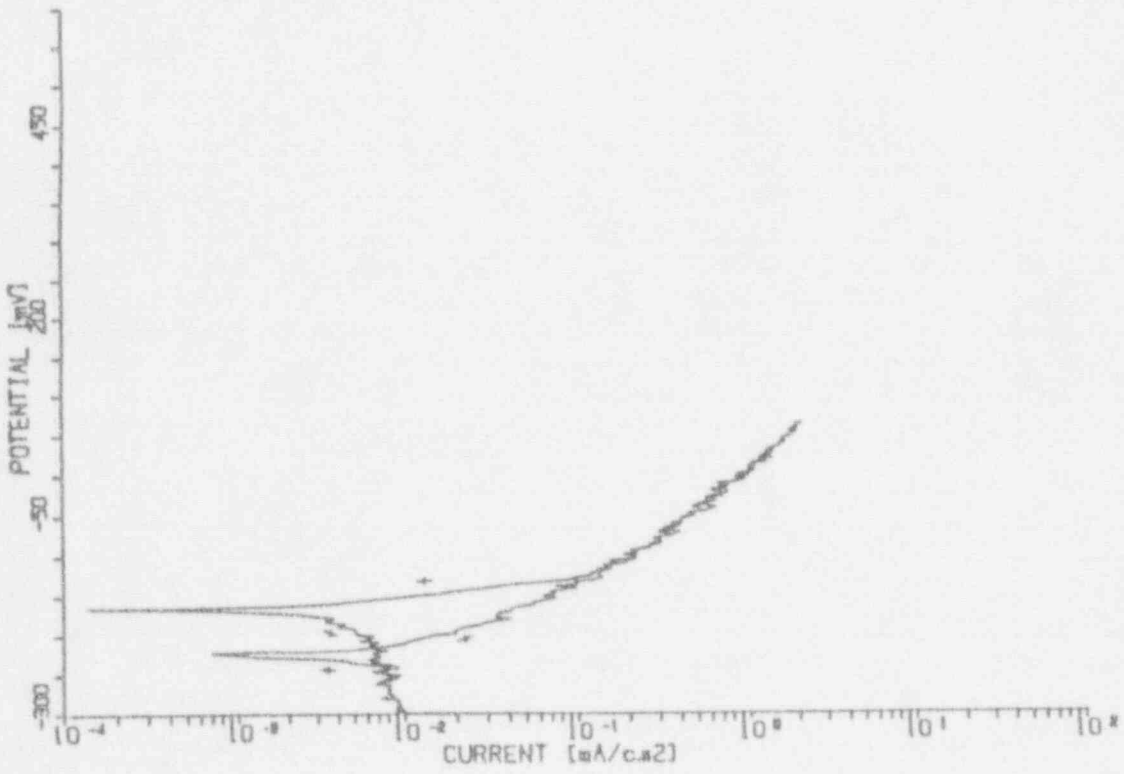

Figure 2.11 CPP Curve For Alloy CDA 715 In Test Solution Number 7 At 90°C (Beavers-1991b).

Table 2.6 Summary Of The Polarization Parameters For Selected Alloys In Simulated J-13 Well Water, Solution Number 20 And Solution Number 7 At 90°C.

Test Solution	Alloy	Solution Temp °C	E_{cor} V,SCE	I_{cor} A/cm^2 x 10^{-6}	E_{pit}/E_b V,SCE	E_{prot}/E_{rp} V,SCE	Comments
J13*	304L	90	-0.125	0.12	+0.800	+0.800	No pitting.
J13*	I825	90	-0.650	0.08	+0.700	+0.700	No pitting.
J13*	CDA 102	90	-0.030	2.00	+0.140	-0.035	Local changes in oxide.
J13*	CDA 715	90	-0.265	0.41	+0.180	+0.080	Local changes in oxide, local active attack with a few shallow pits.
20	304L	90	-0.205	0.13	+0.210	-0.110	Pitting.
20	I825	90	-0.250	0.05	+0.610	+0.150	Pitting.
7	CDA 102	90	-0.140	6.6	-0.140	-0.140	No pitting, local oxide growth.
7	CDA 715	90	-0.150	23	-0.150	-0.200	No pitting; active areas.

*Simulated J-13 Well Water

3. EXPERIMENTAL APPROACH

3.1 Candidate Alloys Evaluated

Two classes of alloys were evaluated in this study; Fe-Cr-Ni alloys and copper-base alloys. The candidate Fe-Cr-Ni alloys evaluated were Type 304L Stainless Steel (Alloy 304L) and Incoloy Alloy 825 (Alloy 825). The candidate copper-base alloys evaluated were CDA 102 Copper (Alloy CDA 102) and Copper-30 Nickel (Alloy CDA 715). The compositions of the candidate alloys are given in Appendix C.

3.2 Constant-Strain (U-Bend) Testing

Immersion testing of U-bend specimens was performed in Task 3 and Task 7 of the overall program. The objective of Task 3 was to evaluate the corrosion performance of the candidate alloys under various exposure conditions (immersed, vapor phase, and alternate immersion). The objective of Task 7 was to evaluate the corrosion performance of the candidate alloys in long-term exposures. The Task 3 test matrix consisted of four alloys, three environments (Simulated J-13 well water, Solution Number 7, and Solution Number 20), and four test conditions (liquid phase, vapor phase, vapor-liquid interface, and alternate immersion). All Task 3 tests were performed at 90°C. Table 3.1 shows the specimen types, exposure conditions and exposure times for each of the vessels. As shown in the table, constant strain (U-bend) specimens were included in the sample matrix to evaluate the susceptibility to stress-corrosion cracking after selected hours of exposure. The exposure tests were performed in four-liter glass resin kettles. These vessels, as shown in Figure 3.1, have a removable lid, four ground glass access ports in the lid, electrical resistance heating mantles, and glass Leibig condensers. With the exception of the vapor-liquid interface specimens and electrochemical monitors, all specimens were exposed in triplicate and designed so that individual "racks" of specimens could be removed and evaluated at three different exposure times to assess the time dependence of the corrosion process for periods up to 2000 hours.

Test specimens were mounted on Alloy C276 threaded rods and electrically isolated from the rods with tetrafluoroethylene (TFE) washers. Serrated TFE washers were clamped to the creviced coupons to create a TFE-metal crevice. U-bend specimens did not contain crevice washers. Following the exposure periods, the specimens were examined optically at 30X magnification. Metallography was performed on specimens that appeared to exhibit SCC at 30X magnification. Further information on the experimental approach used for the coupons is given in the Topical Report for Task 3 of the program which was published as NUREG/CR-5596.

Long-term, boil-down tests were performed with coupons and U-bend specimens in Task 7 of the program. These tests were performed with each of the four candidate container alloys in simulated J-13 water at 90°C for a period of 80 weeks. Unlike in the 3-month immersion studies conducted in Task 3, and described above, the long-term studies were designed to evaluate the

Table 3.1 Summary Of Specimens Used In The Task 3 Immersion Studies.

Vessel	Conditions	Specimen Type	Number Of Specimens	Exposure	Time	Hours	Total Number Of Specimens
1	Vapor	Creviced	3	500	1000	2000	9
1	Vapor	Uncreviced	3	500	1000	2000	9
1	Liquid	Creviced	3	500	1000	2000	9
1	Liquid	Uncreviced	3	500	1000	2000	9
1	V/L Interface	Machined Rod	1			2000	1
1	Vapor	Electrochemical Monitor	1			2000	1
2	Vapor	U-Bend	3	500	1000	2000	9
2	Liquid	U-Bend	3	500	1000	2000	9
2	Alt Immersion	Creviced	3			2000	3
2	Alt Immersion	Uncreviced	3			2000	3
2	Alt Immersion	U-Bend	3			2000	3

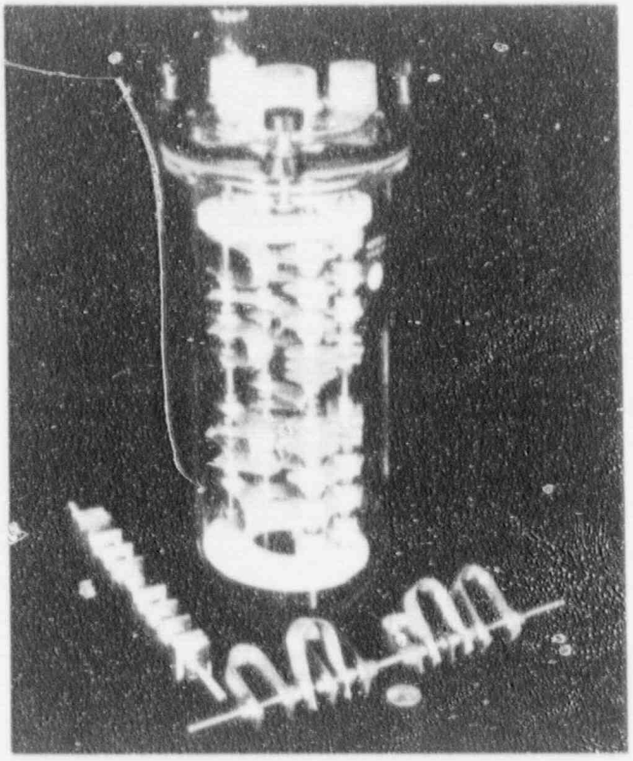

Figure 3.1 Glass Resin Kettles Used In The Task 3 Immersion Studies.

effects of wetting and drying of the candidate alloys and the effects from the concentration of salts over time.

The exposure tests were performed in the four-liter glass resin kettles described above in accordance with ASTM G31. As before, coupons and U-bend specimens were exposed in triplicate and their placement was designed so that individual racks of specimens could be removed and evaluated after three different exposure periods. Table 3.2 is a summary of the specimens used in the boil-down studies. Standard-sized U-bend specimens, prepared in accordance to ASTM G30, were included to evaluate the susceptibility to SCC at the end of the exposure period. The U-bend specimens did not have serrated crevices.

Every week, for 80 weeks, 1800 ml of freshly-prepared simulated J-13 water was added to each test vessel to completely cover the test specimens. Dry air was passed through the vessels. The rate of air flow and the cooling water flow rate in the condensers were adjusted to obtain nearly complete evaporation in one week. Following the exposure periods, the specimens were examined optically at 20X magnification.

Immersion testing of U-bend specimens of both the Fe-Cr-Ni alloys also was conducted in solutions containing added chloride. The purpose of these tests was to provide data for comparison with SSR tests performed under similar exposure conditions. Three tests were performed at 90°C in simulated J-13 water containing 1000, 10 000, and 100 000 ppm Cl as NaCl and 10 000 ppm Cl as $CaCl_2$. Hydrogen peroxide (H_2O_2) additions were made in two of the tests to simulate the effects of radiolysis. Hydrogen peroxide is expected to be generated as a result of radiolysis of the groundwater in the Tuff Repository.

These SCC studies were also performed in four-liter glass resin kettles described above. Triplicate U-bend specimens, prepared in accordance to ASTM G-30, were exposed to each of the four salt environments for a period of 20 minutes. The specimens were then inverted so as to be exposed to the vapor above the condensed phase for the duration of the exposure. Triplicate specimens were also exposed to the liquid phase for the entire exposure period. Humidified air was passed over the specimens in the vapor phase. Visual inspections were performed weekly for evidence of cracking. Daily additions of 200 ppm H_2O_2 were made in several of the experiments and the corrosion potentials were monitored over the exposure period. Each of the three experiments was continued for at least 100 days (2416 hours).

3.3 Slow-Strain-Rate (SSR) Testing

In Task 5 of the program, the Slow-Strain-Rate (SSR) technique was used to evaluate the SCC of the candidate alloys in simulated repository environments. The primary objective of Task 5 was to identify environmental conditions under which the candidate alloys will undergo SCC. A secondary objective of Task 5 was to assess the SSR technique for evaluating long-term SCC performance.

The SSR tests were performed with cylindrical tensile specimens whose dimensions are shown in Figure 3.2. A smaller specimen configuration was used in some tests and is illustrated in Figure 3.3. Prior to testing, the specimen dimensions were accurately measured with calibrated

Table 3.2 Summary Of Specimens Used In Task 7 Long-Term Boil-Down Studies.

Vessel	Alloy	Specimen Type	Number Of Specimens	Exposure Time Hours			Total Number Of Specimens
1	I825	Creviced U-Bend	3 3	4000 —	8000 —	13 400 13 400	9 3
2	304L	Creviced U-Bend	3 3	4000 —	8000 —	13 400 13 400	9 3
3	CDA 715	Creviced U-Bend	3 3	4000 —	8000 —	13 400 13 400	9 3
4	CDA 102	Creviced U-Bend	3 3	4000 —	8000 —	13 400 13 400	9 3

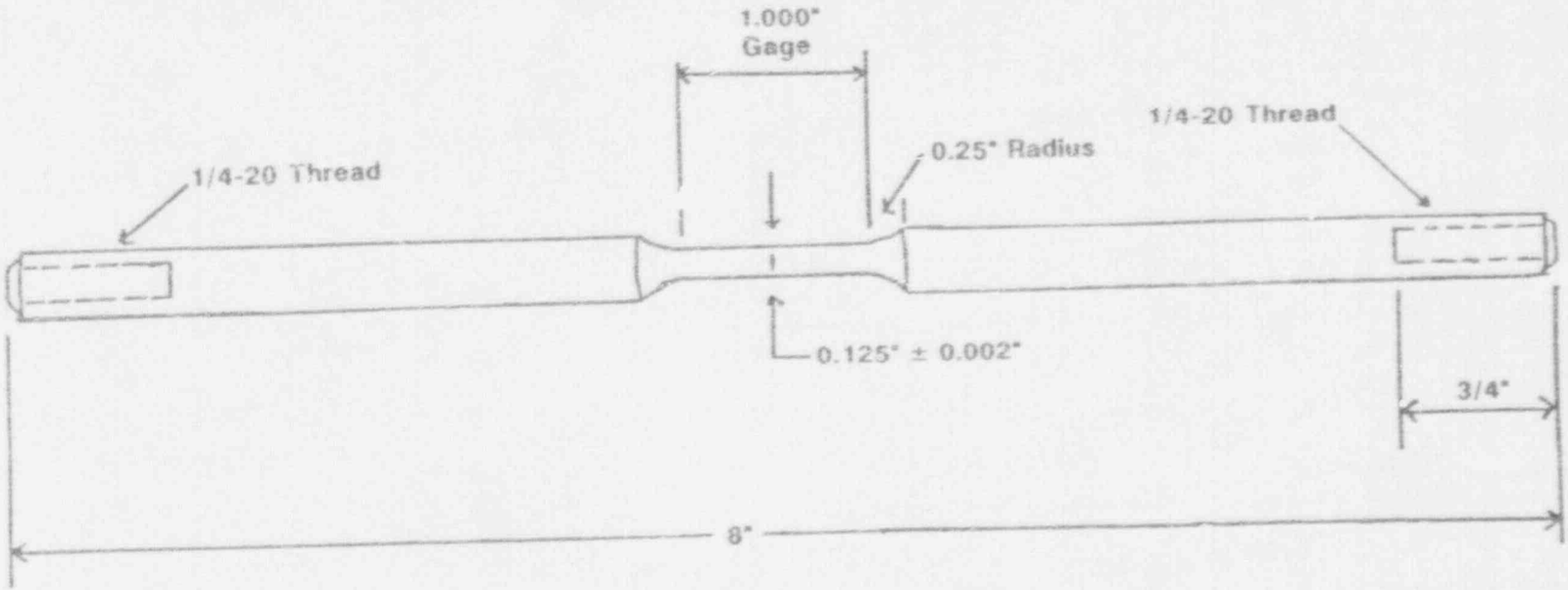

Figure 3.2 Schematic Of The Slow-Strain-Rate Specimen Used In Task 5.

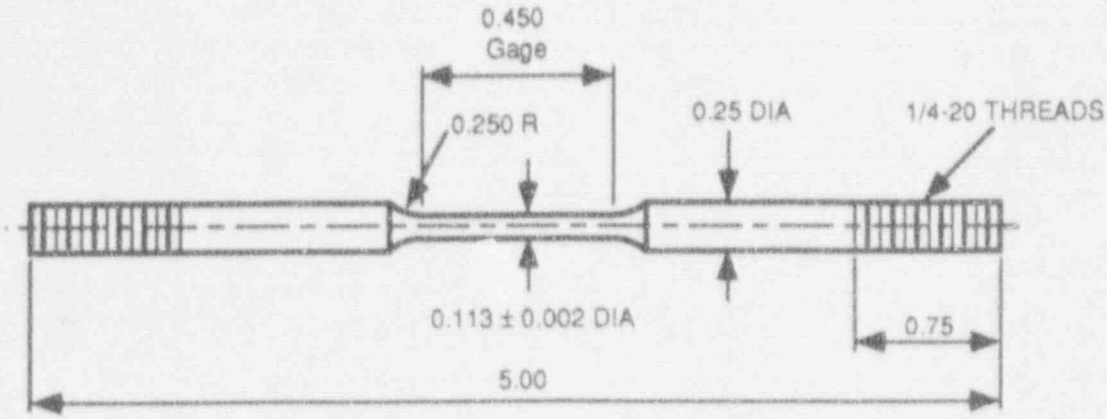

Figure 3.3 Schematic Of The Alternate Slow-Strain-Rate Specimen Used In Task 5.

calipers. In addition, gage marks were placed on either side of the reduced gage section and the distance between these marks was measured. The specimen was mounted in a tetrafluorothylene (TFE) test vessel in the SSR load unit. The test vessel was then filled with the appropriate electrolyte and the ancillary equipment (thermocouple, heat tape, condenser, Luggin probe, etc) was attached. The cell was then heated to the desired temperature and the gas flow was started. The free-corrosion potential was monitored and, once it stabilized, the specimen was polarized to the desired potential (where appropriate). The cross-head of the load frame was started and the specimen was strained to failure.

Following failure, the test cell was cooled to room temperature, the electrolyte was drained, and the specimen was removed. The dimensions of the specimen were then remeasured with calibrated calipers. The reduction in area, in percent, was calculated by the simple formula:

$$\text{Reduction in Area} = \frac{A_i - A_f}{A_i} \times 100 \qquad (3.1)$$

where A_i = initial cross sectional area of the gage section
A_f = final cross sectional area of necked region of gage section.

Similarly, the percent elongation is calculated by the formula:

$$\text{Percent Elongation} = \frac{L_f - L_i}{L_i} \times 100 \qquad (3.2)$$

where L_i = initial length of the gage section of the specimen
L_f = final length of the gage section of the specimen.

The ultimate tensile strength was calculated by dividing the maximum load in the test by the original cross sectional area. All of these calculations are standard strength-of-materials calculations. Metallography was performed on specimens which exhibited SCC at 30X magnification.

A variety of environments was used for the SSR testing. Alloy 304L was tested in the vapor above Solution Number 20 and in the liquid and vapor phase of simulated J-13 well water with and without specific ionic species. The ionic species included carbon dioxide (CO_2), bicarbonate (HCO_3), $CO_2 + H_2O_2$, $HCO_3 + H_2O_2$, and chloride (Cl). The following types and concentrations of chloride were evaluated: 1000 ppm, 10 000 ppm, and 100 000 ppm Cl as NaCl and 10 000 ppm Cl as $CaCl_2$. Alloy 825 was also evaluated in simulated J-13 water containing these same types and concentrations of salt.

The copper-base alloys were SSR tested in sodium nitrite ($NaNO_2$) solutions. Nitrite is a possible radiolysis product that is reported to cause SCC in copper-base alloys. Alloy CDA 102 was tested in both $NaNO_2$ and in simulated J-13 water containing $NaNO_2$. Alloy CDA 715 was tested only in $NaNO_2$.

4. RESULTS

Stress-corrosion-cracking (SCC) studies were performed in Tasks 3, 5, and 7 of the overall program. The objective of Task 3 was to evaluate the corrosion performance of the candidate alloys in simulated Tuff repository environments under various exposure conditions (immersed, vapor phase, and alternate immersion). These immersion tests included U-bend SCC specimens and were performed in simulated J-13 well water and two other environments selected from the experimental test matrix from Task 2 of the program.

The objective of Task 7 was to evaluate the corrosion performance of the candidate alloys in simulated Tuff repository environments under long-term exposures. The long-term exposures included U-bend specimens and were also performed in the simulated J-13 well water. However, in these tests, the solutions were allowed to concentrate by means of evaporation and periodic addition of fresh solution. Thus, these studies were designed to evaluate the effects of alternate wetting and drying of the canister and the concentration of ionic species over time. In Task 7, immersion testing of U-bend specimens of both the Fe-Cr-Ni alloys also was conducted in solutions containing added chloride. The purpose of these tests was to provide data for comparison with Slow-Strain-Rate (SSR) tests performed under similar exposure conditions.

In Task 5 of the program, the SSR technique was used to evaluate the SCC of the candidate alloys in simulated repository environments. The primary objective of Task 5 was to identify environmental conditions under which the candidate alloys will undergo SCC. A secondary objective of Task 5 was to assess the SSR technique for evaluating long-term SCC performance. The alloy-environment combinations that were investigated were selected on the basis of the results of cyclic-potentiodynamic-polarization studies performed in Task 2 (NUREG/CR-5708) and the results of a literature search performed in Task 1 (NUREG/CR-5435).

4.1 Fe-Cr-Ni Alloys

4.1.1 U-Bend Tests

4.1.1.1 Task 3

Constant-strain (U-bend) specimens of Alloy 304L and Alloy 825 were tested in simulated J-13 well water and in Solution Number 20 in immersion tests performed in Task 3 of the overall program. Further information on these experiments may be found in Section 3 of this report and in NUREG/CR-5598. U-bend specimens of both Alloy 304L and Alloy 825 were evaluated for SCC following exposure to the liquid and to the vapor above simulated J-13 well water at 90°C. No SCC was observed after 510, 1011, or 2039 hours of exposures to either the liquid or vapor phases.

Solution Number 20 was selected for study from the Task 2 experimental matrix because it was found to be an active pitting environment for the Fe-Cr-Ni alloys, based on the results of

potentiodynamic-polarization tests. The composition of Solution Number 20 is given in Table 2.5 where it can be seen that the solution is high in the aggressive species chloride and fluoride, and nitrite, which is an inhibitor for Fe-Cr-Ni alloys. Table 2.5 also shows that Solution Number 20 does not contain hydrogen peroxide (H_2O_2).

The immersion tests with both Alloy 304L and Alloy 825 in Solution Number 20 were extended beyond the 2000 hours exposure time originally planned due to the low corrosion rates observed with the coupons and the absence of significant localized corrosion or SCC. In an attempt to promote pitting and SCC of the specimens, by moving the corrosion potential into the pitting range, 200 ppm of hydrogen peroxide (H_2O_2) was added daily to each of the test kettles after approximately 2200 hours of exposure for a period of seven working days and the change in potential was monitored. Hydrogen peroxide is expected to be generated as a result of radiolysis of the groundwater in the Tuff Repository. Following each H_2O_2 addition, a noble potential spike occurred, followed by a potential decline. In an attempt to slow the potential decay, larger doses of H_2O_2 were added over the next seven-day period. Figures 4.1 and 4.2 illustrate the changes in the corrosion potentials as a function of test time for each of the two alloys.

Alloy 825 appeared to catalyze the H_2O_2 degradation as shown by the sharp decline in potential, even at very high H_2O_2 concentrations. Alloy 304L showed a much narrower range of potential change and the H_2O_2 appeared to degrade much slower. Effervescence from the H_2O_2 was also observed in the kettle containing Alloy 304L considerably longer than in the kettle containing Alloy 825. The hydrogen peroxide was allowed to degrade over the weekend following the 4800 ppm addition before terminating the test.

The corrosion potentials were compared with E_{pit} and E_{prot} for each of the alloys. Potentials for Alloy 825 remained below E_{prot} prior to the H_2O_2 additions. The H_2O_2 raised the potential above E_{prot} (+90 mV (SCE)), but it fell far short of E_{pit} (+690 mV (SCE)). Evaluation of Alloy 825 specimens showed only a few shallow pits on one coupon in the liquid phase and very slight etching on the remaining liquid-phase coupons. U-bend specimens were also evaluated for SCC at the end of the exposure. No SCC was observed in any of the U-bend specimens of Alloy 825.

The corrosion potentials for Alloy 304L fell between E_{pit} (+400 mV (SCE)) and E_{prot} (-150 mV (SCE)) during the entire 2855 hours of exposure. Although the H_2O_2 increased the potential slightly, it was insufficient to raise the potential above E_{pit}. Corrosion potentials that fall between E_{pit} and E_{prot} suggest that pitting could possibly occur over an extended period of time. Specimen examination indicated very deep pits under the crevices on coupons in the liquid phase for Alloy 304L. U-bend specimens exposed to the vapor phase and one of the alternate immersion specimens exhibited SCC. No cracks were visible at 30X magnification in liquid-phase specimens. Pitting and etching also were severe on specimens that exhibited cracking.

Metallographic analysis showed the SCC to be transgranular in nature. Most of the cracks were found to originate from deep pits that had initiated in stressed portions of the U-bends. A photomicrograph of a U-bend specimen exhibiting SCC is shown in Figure D.1 in Appendix D. One possible explanation for pitting and cracking of only vapor-phase specimens may be related to the availability of the oxidant (H_2O_2) to the specimen surface through a condensed layer in the vapor phase.

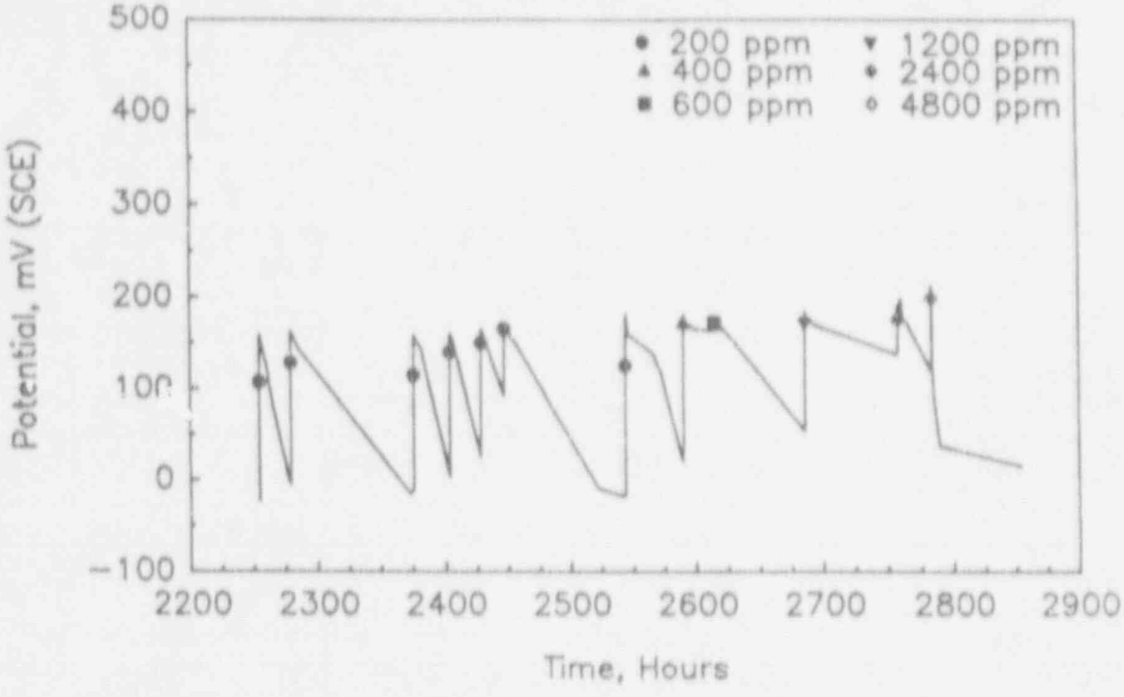

Figure 4.1 Corrosion Potential As A Function Of Test Time For Alloy 304L In Solution Number 20 At 90°C, Showing The Effects Of H_2O_2 Additions.

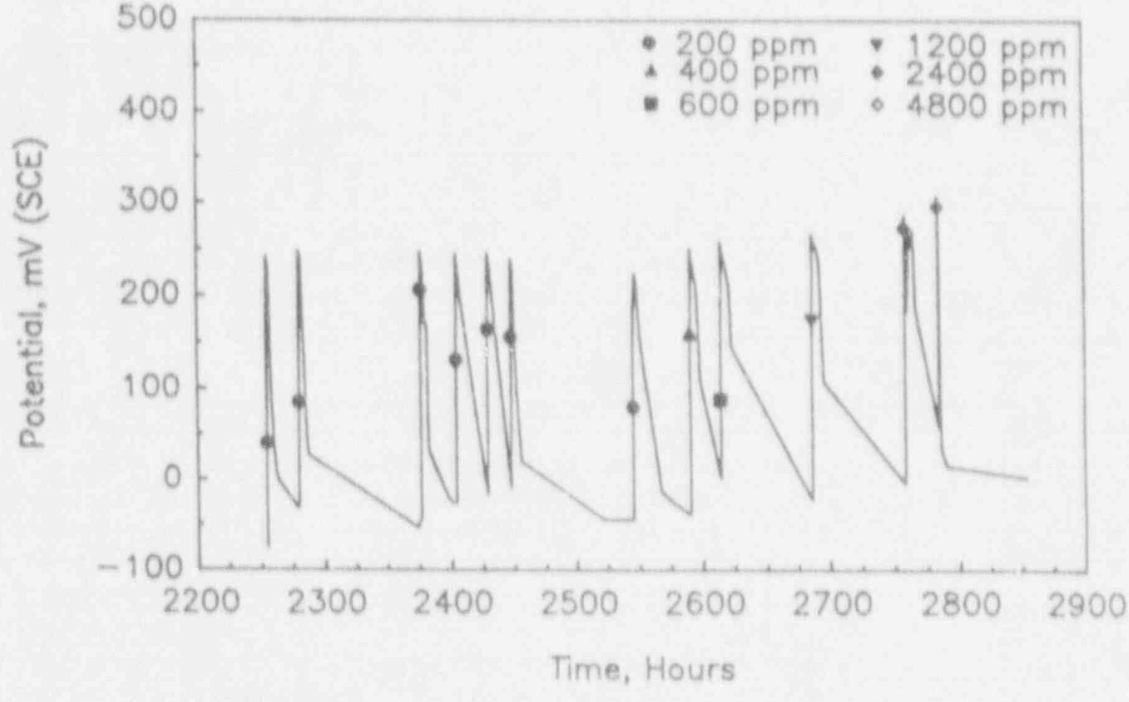

Figure 4.2 Corrosion Potential As A Function Of Test Time For Alloy 825 In Solution Number 20 At 90°C, Showing The Effects Of H_2O_2 Additions.

4.1.1.2 Task 7

In Task 7 of the program, constant-strain (U-bend) specimens of Alloy 304L and Alloy 825 were evaluated in long-term (80 week), boil-down tests with simulated J-13 well water and in 100-day immersion tests in simulated J-13 well water containing added chloride salts. Further information on these experiments may be found in Section 3 of this report and in NUREG/CR-5709.

The long-term, boil-down tests were performed at 90°C and the simulated J-13 well water was allowed to concentrate by evaporation and weekly solution additions over the 80 week exposure period. Weight-loss coupons and U-bend specimens were evaluated in these experiments. The U-bend specimens were examined at 30X magnification after 80 weeks of exposure. Optical examination revealed no attack or SCC of specimens of either Alloy 304L or Alloy 825.

Following the termination of the long-term, boil-down tests, duplicate samples of solution were obtained from each of the resin kettles and analyzed. Duplicate samples of simulated J-13 well water were also analyzed as a control and to act as a check on our quality assurance procedure for solution preparation. Table 4.1 summarizes the results of the solution analyses and compares these results with the predicted concentration assuming linearity of the weekly concentration over the 80 week exposure. These data show that the composition of the simulated J-13 well water was very similar to the calculated composition. These data also show that the composition of the solutions from the boil-down tests approximated the predicted composition assuming linear concentration, with a few exceptions. These exceptions included calcium, magnesium, silicon, and bicarbonate, which precipitated from solution, based on deposit analyses: see Table 4.2. Further details of these analyses are given in NUREG/CR-5709.

Three- to six-month exposure tests were performed with U-bend specimens of the Fe-Cr-Ni alloys in simulated J-13 well water containing various types and concentrations of added chloride salts. The primary purpose of these tests was to develop SCC data on the alloys for comparison with the results of the SSR tests. Testing was performed at 90°C in simulated J-13 water containing 1000, 10 000, and 100 000 ppm Cl as sodium chloride (NaCl) and 10 000 ppm Cl as calcium chloride ($CaCl_2$). The first and second series of tests were performed with Alloy 304L while the third series was performed with Alloy 825. In Test Series 1, no hydrogen peroxide was added to the test solutions while 200 ppm H_2O_2 was added daily to the test solutions in the second and third series of tests to simulate the effect of radiolysis. Vapor- and liquid-phase exposures were evaluated.

A summary of the results of the first two series of tests, in which Alloy 304L was evaluated, is given in Table 4.3. The first series of tests was originally planned for three months (~2000 hours) but in-situ examination of the specimens indicated no evidence of SCC and thus the experiment was extended to over 4000 hours. At the termination of the test, no SCC was evident based on in-situ examination. However, a detailed optical examination at 30X magnification revealed cracking in two liquid-phase specimens exposed to simulated J-13 well water containing 100 000 ppm chloride as NaCl. Large cracks were observed near the TFE washers under corrosion products. Metallography was completed on one of these specimens; a photomicrograph is shown in Figure D.2 in Appendix D. This figure shows that SCC of the specimen was associated with extensive pitting. This pitting had initiated beneath deposits near the TFE washers.

Table 4.1 Comparison Of The Compositions Of Simulated J-13 Well Water With The Compositions Of Solutions Following 80 Weeks Of Boil Down And Concentration.

Environmental Species	Calculated J-13 mg/l	Actual J-13 mg/l	Predicted J-13 After 80 weeks mg/l	I825 In J-13 mg/l*	304L In J-13 mg/l*	CDA 715 In J-13 mg/l*	CDA 102 In J-13 mg/l*
Nitrate, as N	2.8	2.8	224	264	224	154	179
Total Phosphorous, P	0.0	<0.1	0	1.1	0.7	0.5	0.6
Sulfate, SO_4	19.2	23.5	1536	1975	2050	1725	2125
Chloride, Cl	6.4	5 5	512	750	675	420	495
Fluoride, F	1.7	1.8	136	144	125	81.5	85
Calcium, Ca	12.0	10.0	960	2	3	2	2
Magnesium, Mg	1.7	1.5	136	<1	<1	<1	<1
Sodium, Na	46.0	42.0	3680	4450	3500	2450	2950
Potassium, K	5.5	6.3	440	380	230	240	200
Aluminum, Al	0.0	<0.2	0	<0.2	<0.2	<0.2	<0.2
Soluble Silicon, Si	30.0	27.5	2400	1170	1105	605	990
Alkalinity, HCO_3	121.0	102.0	—	0	0	0	0
Alkalinity, Phenolphthalein	0.0	0.0	—	4925	3820	2630	2990
Alkalinity, Total	121.0	102.0	—	7150	5700	3750	4330
pH	7.0 ± 0.2	7.0 ± 0.2	>7.0	10.68	10.44	10.41	10.41

* Average concentration from duplicate samples. NOTE: In all cases, J-13 well water was simulated.

Table 4.2 Compositions Of Precipitated Salts Following 80 Weeks Of Boil-Down Testing With Simulated J-13 Water At 90°C; Average Of Duplicate Tests.

Composition	ALLOY CDA 715		ALLOY CDA 102		ALLOY 304L		ALLOY 825	
	ICP	EDS[a]	ICP	EDS	ICP	EDS	ICP	EDS
Al	0.34%	—	0.39%	—	0.31%	—	0.40%	—
Si	24.41%	64.5%	25.46%	62.9%	25.47%	63.4%	25.61%	[illegible]%
Na	3.61%	—	3.74%	—	4.24%	—	4.09%	—
Mg	0.90%	—	1.01%	—	1.09%	—	0.93%	—
K	0.73%	3.3%	1.05%	4.7%	1.03%	3.8%	0.93%	3.0%
Ca	8.47%	32.2%	8.78%	32.4%	10.42%	32.8%	8.50%	29.4%
$CaCO_3$ (eq)	39.60%	—	36.20%	—	38.40%	—	35.60%	—
Sr	425 ppm	—	390 ppm	—	425 ppm	—	395 ppm	—
Ni	70 ppm	—	55 ppm	—	160 ppm	—	215 ppm	—
Cu	350 ppm	—	1610 ppm	—	65 ppm	—	<50 ppm	—
Fe	—	—	—	—	750 ppm	—	1870 ppm	—
Cr	—	—	—	—	<20 ppm	—	75 ppm	—
Mo	—	—	—	—	<2 ppm	—	<2 ppm	—
Cl	—	—	—	—	—	—	—	2.4%

a – EDS data normalized to 100%.
ICP – Inductively Coupled Plasma.
EDS – Energy Dispersive Spectroscopy.

Table 4.3 Summary Of Results Of Exposure Tests Performed On U-Bend Specimens Of Alloy 304L In Simulated J-13 Well Water Containing Added Chloride Salts.

Test N°	H_2O_2 Addition	Chloride Concentration (ppm)	Salt	Phase	Test Duration (hours)	Pitting/Crevice Corrosion	Time To SCC (hours)
1	No	1 000	NaCl	Vapor	4 344	Crevice	NC
1	No	1 000	NaCl	Liquid	4 344	—	NC
1	No	10 000	NaCl	Vapor	4 344	Crevice	NC
1	No	10 000	NaCl	Liquid	4 344	Crevice	NC
1	No	100 000	NaCl	Vapor	4 344	Crevice	NC
1	No	100 000	NaCl	Liquid	4 344	Crevice	4 344
1	No	10 000	$CaCl_2$	Vapor	4 344	Crevice, pitting **	NC
1	No	10 000	$CaCl_2$	Liquid	4 344	Crevice, pitting **	NC
2	Yes	1 000	NaCl	Vapor	2 416	—	184
2	Yes	1 000	NaCl	Liquid	2 416	Crevice	NC
2	Yes	10 000	NaCl	Vapor	2 416	Crevice	1 833
2	Yes	10 000	NaCl	Liquid	2 416	Crevice	NC
2	Yes	100 000	NaCl	Vapor	2 416	Crevice	NC
2	Yes	100 000	NaCl	Liquid	2 416	Crevice	NC
2	Yes	10 000	$CaCl_2$	Vapor	2 416	Crevice, pitting *	668
2	Yes	10 000	$CaCl_2$	Liquid	2 416	Crevice, pitting **	NC

NC = No cracking.
* = Pitting along edges of specimens.
** = Pitting near bend portion of one specimen.

In the second series of experiments, each of the four exposure tests, with U-bend specimens of Alloy 304L, was repeated with daily additions of H_2O_2 to simulate the effects of radiolysis. The corrosion potentials were monitored before and after each H_2O_2 addition and are exhibited graphically in Figure 4.3. These data clearly illustrate the noble shift in potential and the ensuing decline in potential as the H_2O_2 degraded. The values of E_{pit} and E_{prot} determined from the respective CPP curves (Appendix B) for each environment are also plotted on Figure 4.3. These data show that the maximum potentials achieved as a result of the H_2O_2 additions fell between E_{pit} and E_{prot} in the most dilute solution and exceeded E_{pit} in the other solutions.

Table 4.3 indicates the cumulative hours of exposure until SCC was observed in the second series of experiments with Alloy 304L. These data show that SCC was observed only in the vapor and in all of the test solutions except the most concentrated NaCl solution containing 100 000 ppm Cl. While pitting was present in many of the specimens, the cracking frequently was not associated with the pitting. Metallography was performed on one specimen that exhibited SCC from each environment. Photomicrographs of these specimens are shown in Figures D-3 through D-5.[5] These figures show extensive cracking in the stressed area of the U-bend specimens. These cracks were found to extend almost through the 0.16 cm (1/16 inch) thickness of each specimen.

In the third series of experiments, each of the four exposure tests was performed with U-bend specimens of Alloy 825 with the periodic additions of 200 ppm H_2O_2. The changes in potential from the H_2O_2 additions were monitored and are graphically illustrated in Figure 4.4. These data also clearly illustrates the noble shift in potential and the ensuing decline in potential as the H_2O_2 degraded. The values of E_{pit} and E_{prot} determined from the respective CPP curves (Appendix B) for each environment are also plotted on Figure 4.4. These data show that the corrosion potential consistently exceeded the pitting potential only in the most concentrated NaCl solution and in the $CaCl_2$ solution and was below the protection potential in the most dilute NaCl solution.

Low power optical examination of the specimens following 103 days of exposure indicated no evidence of SCC, as shown in Table 4.4. Heavy, localized attack at the TFE inserts in both the vapor- and liquid-phase specimens was evident. On the other hand, the uncreviced areas of the specimens were free of localized corrosion, with one exception. One vapor-phase specimen closest to the vapor-liquid interface of simulated J-13 water containing 10 000 ppm $CaCl_2$ exhibited a few pits. These pits were located in the stressed portion of the specimen but metallographic analysis indicated no evidence of SCC.

4.1.2 SSR Tests

The primary focus of the SSR testing of the Fe-Cr-Ni alloys was Alloy 304L. The SCC behavior was screened in a variety of possible cracking environments. Cursory tests were then performed with Alloy 825, an alloy that was expected to be more resistant to SCC.

Alloy 304L was tested in the liquid and vapor phases of simulated J-13 well water with and without specific ionic species. These ionic species included carbon dioxide (CO_2), bicarbonate (HCO_3), $CO_2 + H_2O_2$, $HCO_3 + H_2O_2$, and chloride (Cl). Tensile specimens of Alloy 304L were also

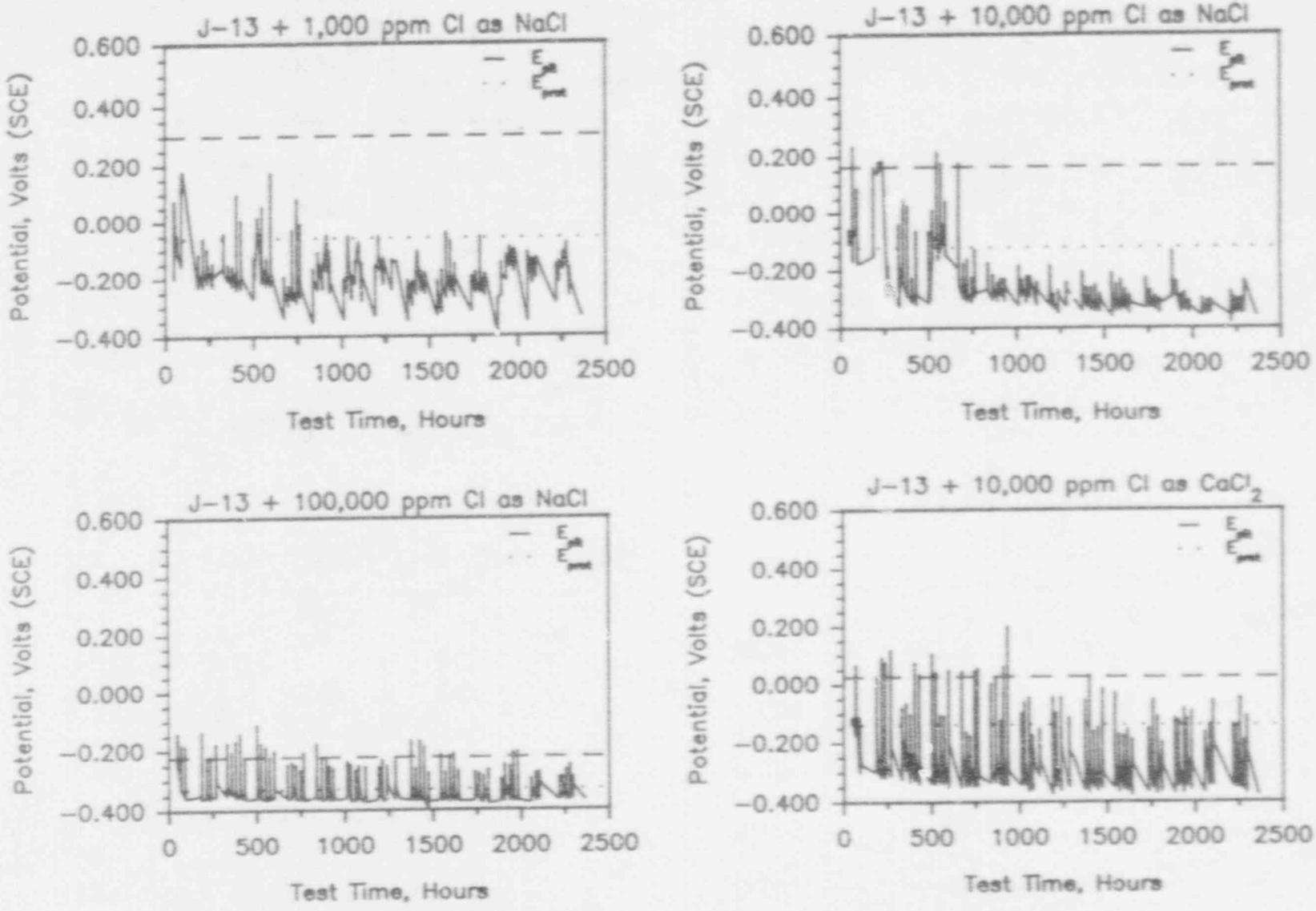

Figure 4.3 Corrosion Potential As A Function Of Test Time For U-Bend Specimens Of Alloy 304L Exposed To The Liquid Phase Of 90°C Aerated Simulated J-13 Well Water Containing Various Types And Concentrations Of Salt. Noble Spikes Indicate 200 ppm H_2O_2 Additions.

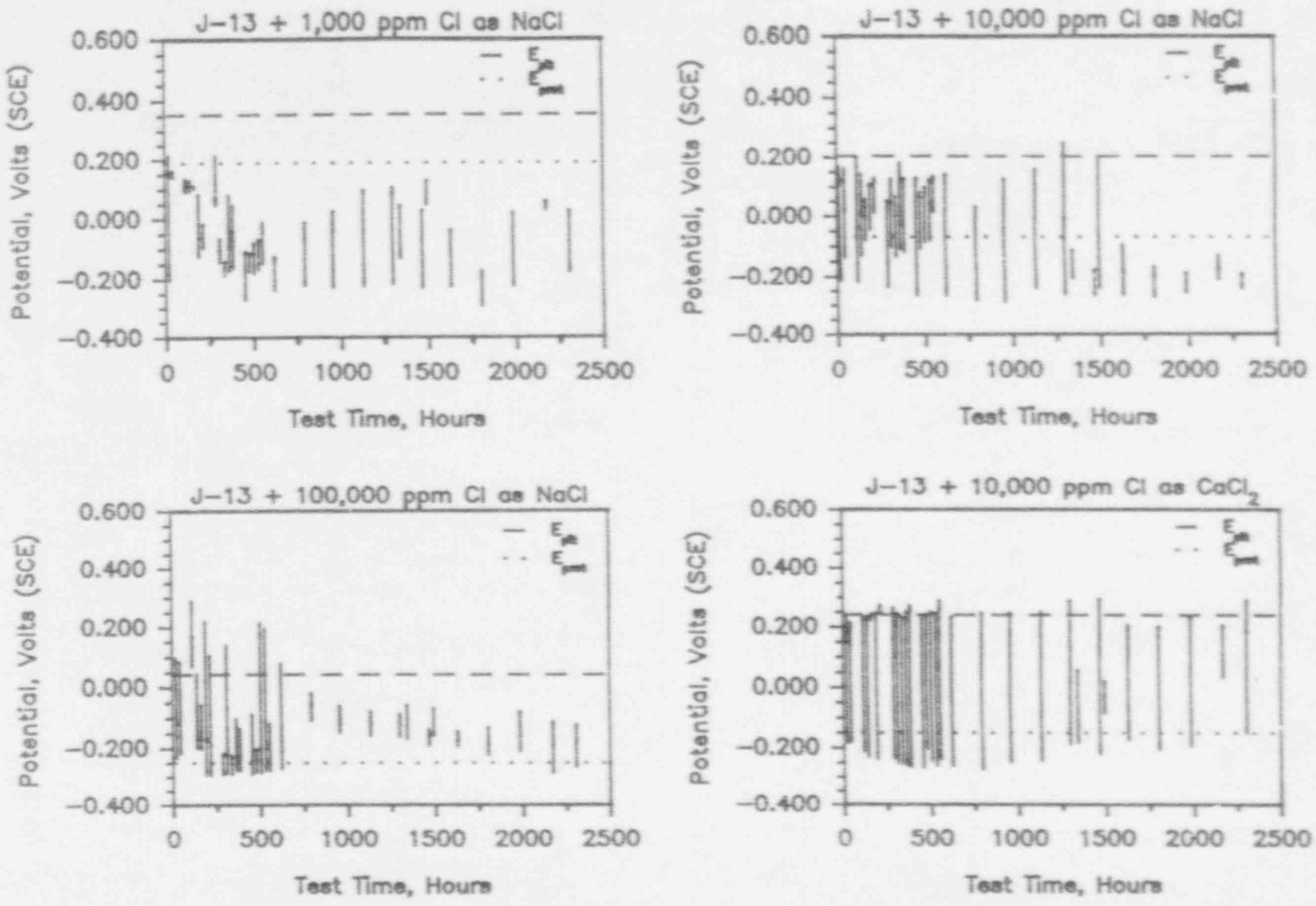

Figure 4.4 Corrosion Potential As A Function Of Test Time For U-Bend Specimens Of Alloy 825 Exposed To The Liquid Phase Of 90°C Aerated Simulated J-13 Well Water Containing Various Types And Concentrations Of Salt. Noble Spikes Indicate 200 ppm H_2O_2 Additions.

Table 4.4 Summary Of Results Of Exposure Tests Performed On U-Bend Specimens Of Alloy 825 In Simulated J-13 Well Water Containing Added Chloride Salts.

Test №	H_2O_2 Addition	Chloride Concentration (ppm)	Salt	Phase	Test Duration (hours)	Pitting/Crevice Corrosion	Time To SCC (hours)
3	Yes	1 000	NaCl	Vapor	2 472	Crevice	NC
3	Yes	1 000	NaCl	Liquid	2 472	Crevice	NC
3	Yes	10 000	NaCl	Vapor	2 472	Crevice	NC
3	Yes	10 000	NaCl	Liquid	2 472	Crevice	NC
3	Yes	100 000	NaCl	Vapor	2 472	Crevice, etching *	NC
3	Yes	100 000	NaCl	Liquid	2 472	Crevice	NC
3	Yes	10 000	$CaCl_2$	Vapor	2 472	Pitting **	NC
3	Yes	10 000	$CaCl_2$	Liquid	2 472	Crevice	NC

* = Localized etching in bend portion of one specimen.
** = Pitting in bend portion and along edges of specimens.

evaluated in the vapor above Solution Number 20 for comparison with results obtained with U-bend specimens tested in immersion studies in Task 3 of the program. Specimens of Alloy 825 were evaluated in simulated J-13 well water containing various types and concentrations of chloride for comparison with SSR results for Alloy 304L and results obtained with U-bend specimens of Alloy 825 tested in immersion studies in Task 7.

Initially, SSR tests were performed in simulated J-13 water to investigate the role of radiation on SCC of stainless steel. Pitman (1986) reported that a single specimen of solution-annealed Type 304L stainless steel had experienced SCC in the vapor above J-13 well water in the presence of 3×10^5 rads/hour gamma radiation at 90°C. Relatively little data are available on the radiation environment in the Tuff Repository but Yunker (1986) observed an apparent loss of HCO_3 in irradiated J-13 well water. This loss was associated with an increase in the concentration of CO_2 in the vapor above the liquid. Accordingly, both high and low levels of CO_2 and HCO_3 were evaluated. Experimentally, in the absence of a radiation field, it is not possible to have a high CO_2 partial pressure in the vapor and a low HCO_3 concentration in the liquid because of equilibrium considerations. H_2O_2 was included in the matrix since this is a common radiolysis product. An H_2O_2 concentration of about 10 mg/l was used based on analyses reported by Glass (1985).

Table 4.5 is a summary of the results of the initial SSR tests performed with Alloy 304L. No SCC was observed in any of these tests. The data in Table 4.5 indicate good ductility (as anticipated) for the solution-annealed Alloy 304L in the control tests, (in mineral oil), with about 20 percent elongation and over 70 percent reduction in area. In simulated J-13 well water and in simulated J-13 well water with CO_2, there was no evidence of SCC and the mechanical properties data were similar to those found in the control tests. These results are in agreement with results of the exposures of U-bend specimens of Alloy 304L to simulated J-13 water in the immersion studies performed in Task 3 of the program. SSR tests in simulated J-13 water without HCO_3 also showed similar mechanical properties to the control tests. The addition of H_2O_2 did not promote SCC in any of the environments tested at a strain rate of 1×10^{-6} sec^{-1}.

Some of the SSR tests (identified with a (c)) in Table 4.5 were performed with shorter specimens that had a shorter gage length (see Figure 3.3). These data, identified by a (c), show higher percent elongation, lower tensile strength, and longer failure times. These specimens came from a different heat of materials which probably accounts for the slightly different mechanical properties. It is also possible that the shorter gage length affected the elongation to failure and failure time. For the same strain rate, a shorter gage section specimen experiences a slower crosshead speed during straining, which reduces the strain rate during necking. Additional control tests were performed with the shorter specimens in mineral oil and those results are reported in Table 4.5 as Test Numbers M25 and M26.

A surprising result of the SSR data shown in Table 4.5 is the absence of SCC in specimens tested in the concentrated chloride solutions. Chloride is an established cracking agent and will likely concentrate in the repository. For the tests summarized in Table 4.5, no SCC was observed even at very high (10 000 ppm) Cl concentrations. Two of the tests at 1000 ppm Cl were potentiostated to +200 mV (SCE). This led to severe pitting but no SCC. To better control the extent of pitting of the specimens, a test was performed under galvanic control at a current density of 50 $\mu A/cm^2$. The extent of pitting was decreased, but again, no cracking occurred. Photomicrographs of one of the specimens are given in Figure D.6 in Appendix D.

Table 4.5 Summary Of Initial Results Of Slow-Strain-Rate Tests Performed On Solution-Annealed Specimens Of Alloy 304L Under Freely-Corroding Conditions At 90°C.

Electrolyte	Test No.	Strain Rate sec^{-1}	Potential mV (SCE)	Time To Failure Hours	Reduction In Area Percent	Elongation Percent	Ultimate Tensile Strength MPa	SCC	Crack Velocity x 10^{-6} mm/sec
Mineral Oil	M1	5×10^{-7}	—	107	73.0	20.0	701	None	—
Mineral Oil	M2	1×10^{-6}	—	61	74.6	20.3	688	None	—
Mineral Oil	M3	1×10^{-6}	—	63	71.3	20.5	667	None	—
Mineral Oil (c)	M25	1×10^{-6}	—	106	77.2	40.0	572		—
Mineral Oil (c)	M26	1×10^{-6}	—	106	77.0	38.9	606		—
J-13	M4	1×10^{-6}	-136	73	74.6	24.1	731	None	—
J-13	M5	1×10^{-6}	-113	71	72.2	23.7	652	None	—
J-13 *	M6	1×10^{-6}	—	73	73.8	24.3	619	None	—
J-13 *	M7	1×10^{-6}	—	82	76.2	28.2	652	None	—
J-13 + CO_2 (b)	M12	1×10^{-6}	—	73	74.6	24.2	657	None	—
J-13 + CO_2 (b)	M13	1×10^{-6}	-55	75	76.2	26.8	651	None	—
J-13 + CO_2 (a, b)	M10	1×10^{-6}	—	80	74.6	25.9	685	None	—
J-13 + CO_2 (a, b)	M11	1×10^{-6}	—	80	75.4	27.6	741	None	—
J-13 + CO_2 (b) + H_2O_2 (a, b, c)	M18	1×10^{-6}	—	122	78.5	41.4	588	None	—
J-13 + CO_2 (b) + H_2O_2 (a, b, c)	M19	1×10^{-6}	—	128	78.9	42.6	570	None	—
J-13 - HCO_3 (c)	M15	1×10^{-6}	+32	81	73.8	27.0	730	None	—
J-13 - HCO_3 (c)	M17	1×10^{-6}	-92	108	75.5	36.6	611	None	—
J-13 - HCO_3 + H_2O_2 (d)	M14	1×10^{-6}	+450	81	71.2	26.5	651	None	—
J-13 - HCO_3 + H_2O_2 (c, d)	M16	1×10^{-6}	+337	109	78.1	36.6	550	None	—
J-13 + 1000 ppm Cl (c)	M20	1×10^{-6}	[+200]	88	68.4	41.6	505	None (g)	—
J-13 + 1000 ppm Cl (c)	M21	1×10^{-6}	[+200]	82	66.9	28.2	524	None (g)	—
J-13 + 1000 ppm Cl (c)	M22R	1×10^{-6}	(e)	106	77.2	38.4	537	None (g)	—
J-13 + 1000 ppm Cl (c)	M23R	1×10^{-6}	(e)	112	74.6	38.8	544	None (g)	—
J-13 + 10 000 ppm Cl (c, f)	M27	1×10^{-6}	-181	102	84.0	36.2	585	None	—
J-13 + 10 000 ppm Cl (c, f)	M28	1×10^{-6}	—	102	76.1	32.2	533	None	—

J-13 = Simulated J-13 well water.
(a) = Vapor phase testing.
(b) = Pure CO_2 sparged through solution at a rate of about 10 ml/minute.
(c) = Smaller specimen configuration.
(d) = 15% H_2O_2 dripped into cell at rate of 0.02 ml/hour.
(e) = Galvanostated current, 50 $\mu A/cm^2$.
(f) = 100°C.
(g) = Pitting at 30X magnification.
[ ] = Polarized potential.

The original experimental approach in this task was to produce SCC in the Alloy 304L by increasing the chloride content of the J-13 well water and then to establish the relative chloride limits for cracking of Alloy 304L and Alloy 825. In light of the absence of cracking with Alloy 304L at relatively high chloride concentrations, the SSR tests were suspended and a survey of the literature was performed.

The search was performed, using the CORAB[2] computer program, on transgranular SCC of stainless steels in chloride environments. The purpose of the search was to identify the reason that we were unable to obtain chloride SCC of the Alloy 304L specimens even in high chloride (10 000 ppm Cl) environments. While several relevant articles were identified, the most useful study was performed by Mancia (1986) on SCC of Alloy 304 in 5M NaCl at 110°C. Results summarized in Figure 4.5 indicate that strain rates below about 5×10^{-7} sec^{-1} were required to obtain SCC in this system. On the NRC program, a strain rate of 1×10^{-6} sec^{-1} was used, which is above the cracking range according to Mancia (1986).

Based on the results of the literature survey, a second series of SSR tests was performed on Alloy 304L in solutions of varying chloride concentration and at varying potentials and strain rates. A summary of the results of these SSR tests is given in Table 4.6. Companion exposure tests were performed on U-bend specimens of Alloy 304L in similar environments in Tasks 3 and 7 of the program.

As shown in Table 4.6, duplicate SSR tests were performed with tensile specimens of Alloy 304L in the vapor phase above Solution Number 20 at 90°C at strain rates of 1×10^{-6} sec^{-1} and 1×10^{-7} sec^{-1}. Daily additions of 1000 ppm H_2O_2 were made to the test cells. The data in Table 4.6 show that SCC was only observed at the slower strain rate. Optical and metallographic examination of the specimens, tested at the higher strain rate of 1×10^{-6} sec^{-1} (Test Numbers 32 and 33), revealed pitting at the vapor-liquid interface but no SCC. Photomicrographs of the specimens tested at the slower strain rate (Tests Numbers 34 and 35) are given in Figures D.7 and D.8 in Appendix D. These figures show that transgranular SCC was associated with extensive pitting, which occurred at the vapor-liquid interface in the radius above the gage section.

As previously described, in Task 3 of the program, U-bend specimens of Alloy 304L were exposed at 90°C to the vapor above Solution Number 20 with periodic H_2O_2 additions. Metallographic analysis of the specimens indicated the presence of SCC which was transgranular and was found to originate from deep pits that had initiated in stressed portions of the U-bends. Therefore, the results of the U-bend tests were in agreement with the SSR tests when considering only the SSR tests at the slower strain rate.

Fourteen SSR tests were performed with Alloy 304L in the liquid and vapor phases of simulated J-13 well water with chloride additions. The following types and concentrations of chloride were evaluated: 1000, 10 000, and 100 000 ppm Cl as NaCl and 10 000 ppm Cl as $CaCl_2$. Of the 14 tests, 6 were performed in the vapor phase and 8 were performed in the liquid phase. In the vapor-phase testing, 200 ppm H_2O_2 was added to the test cell daily to simulate radiolysis, as in the immersion tests in Task 7. The liquid-phase tests were conducted in each of the four solutions both at the free-corrosion potential and polarized 50 mV above the pitting potential (E_{pit})

---

[2]National Association of Corrosion Engineers.

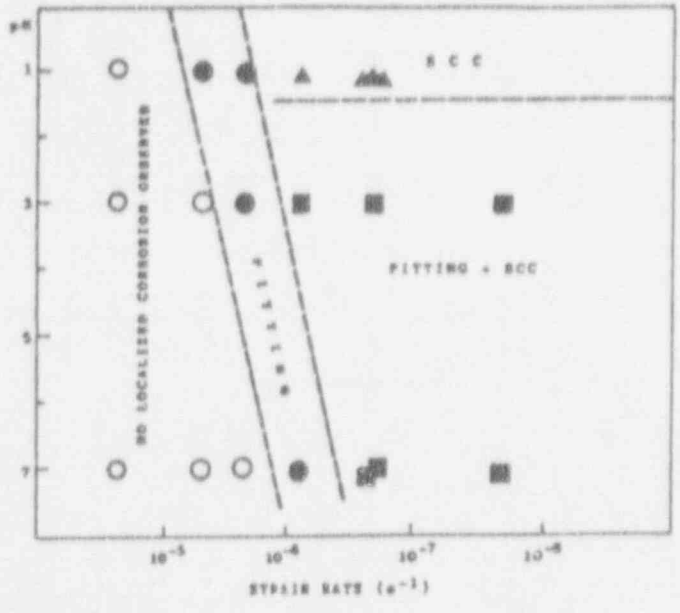

Figure 4.5 Effect Of Strain Rate And pH On The Localized Corrosion Morphology For Type 304 Stainless Steel In Aqueous 5M NaCl At 110°C (Mancia-1986).

Table 4.6 Summary Of Results Of Slow-Strain-Rate Tests Performed On Solution-Annealed Specimens Of Alloy 304L At 90°C For Comparison With Results From Immersion Testing Of Constant-Strain Specimens In Tasks 3 And 7.

Electrolyte	Test #	Strain Rate sec^{-1}	Potential mV (SCE)	Time To Failure Hours	Reduction In Area Percent	Elongation Percent	Ultimate Tensile Strength MPa	SCC	Crack Velocity x 10^{-6} mm/sec
Oil	M2	$1x10^{-6}$	—	61	74.6	20.3	688	None	—
Oil	M3	$1x10^{-6}$	—	63	71.3	20.5	667	None	—
Solution #20 [a]	32	$1x10^{-6}$	—	80.3	80.0	26.7	669	None[c]	—
Solution #20 [a]	33	$1x10^{-6}$	—	80.5	76.2	27.6	618	None[c]	—
Solution #20 [a]	34	$1x10^{-7}$	—	935.2	78.5	23.5	618	TG *	0.37
Solution #20 [a]	35	$1x10^{-7}$	—	550.7	75.4	17.7	646	TG *	0.66
J-13 + 1000 ppm Cl as NaCl	42	$1x10^{-6}$	-201	63.1	75.4	20.2	759	None	—
J-13 + 1000 ppm Cl as NaCl	45	$1x10^{-6}$	[+350]	15.4	—	—	450	‡	—
J-13 + 10 ppm Cl as NaCl	43	$1x10^{-6}$	-172	63.6	72.9	20.3	688	None	—
J-13 + 100 ppm Cl as NaCl	46	$1x10^{-6}$	[+213]	16.6	—	—	393	‡	—
J-13 + 100000 ppm Cl as NaCl	36	$1x10^{-6}$	-310	64.4	73.0	21.3	674	None	—
J-13 + 100000 ppm Cl as NaCl	37	$1x10^{-6}$	[-174]	69.3	68.6	23.7	618	TG	2.61
J-13 + 10000 ppm Cl as $CaCl_2$	44	$1x10^{-6}$	-140	59.2	75.4	21.4	688	None	—
J-13 + 10000 ppm Cl as $CaCl_2$	47	$1x10^{-6}$	[+76]	44.7	—	—	562	‡	—
J-13 + 1000 ppm Cl as NaCl [b]	38	$1x10^{-6}$	—	68.9	76.2	22.0	674	None	
J-13 + 1000 ppm Cl as NaCl [b]	55	$1x10^{-7}$	—	596.3	74.6	19.4	624	None[c]	—
J-13 + 10000 ppm Cl as NaCl [b]	39	$1x10^{-6}$	—	65.2	76.9	20.9	686	TG	3.41
J-13 + 100000 ppm Cl as NaCl [b]	40	$1x10^{-6}$	—	68.4	73.8	22.6	723	None	—
J-13 + 10000 ppm Cl as $CaCl_2$ [b]	41	$1x10^{-6}$	—	68.1	76.9	21.9	688	None	—
J-13 + 10000 ppm Cl as $CaCl_2$ [b]	54	$1x10^{-7}$	—	624.4	79.2	19.5	632	None	—

(a) Vapor phase; 1000 ppm H_2O_2 added daily.
(b) Vapor phase; 200 ppm H_2O_2 added daily.
(c) Pitting at 30X magnification.
* Probable transgranular, occurred in the radius above the gage section at the vapor-liquid interface.
‡ Severe pitting, unable to measure reduction in area and elongation.
[ ] Polarized potential; E_{pit} + 50 mV.

obtained from the respective cyclic-potentiodynamic-polarization curves. These CPP curves are given in Appendix B.

A summary of the results of these tests is also given in Table 4.6. These data show that all of the tests in the liquid phase were performed at the faster strain rate, 1×10^{-6} sec^{-1}; the program was terminated before the tests at the slower strain rate could be completed. The data in Table 4.6 show that, under freely-corroding conditions, no SCC was observed in any of the liquid-phase specimens of Alloy 304L, based on post-test optical examination of the specimens at 30X magnification. The mechanical property data also were very similar to data from the control tests performed in mineral oil.

In an effort to induce SCC, the SSR specimens were potentiostated to 50 mV above E_{pit} during the SSR testing in the four simulated J-13 well water/salt environments. These test results are shown in Table 4.6 as Test Numbers 45, 46, 37, and 47. The mechanical property data could not be obtained on several of these potentiostated specimens because they experienced significant metal loss due to pitting. The failure times for these specimens also were short as a result of the extensive pitting. Results of optical examinations of these specimens, at 30X magnification, indicated cracking in only one test environment, simulated J-13 water containing 100 000 ppm Cl as NaCl. Metallography was performed on this specimen and a photomicrograph is given in Figure D.9 in Appendix D. This photomicrograph illustrates extensive pitting and transgranular cracks radiating from these pits all along the gage section.

Six SSR tests were performed with tensile specimens of Alloy 304L in the vapor above simulated J-13 water containing each of the four salt concentrations. In these tests, the gage section was maintained in the vapor above the selected solution throughout the test. In each of the vapor-phase tests, 200 ppm H_2O_2 was added daily to simulate the effects of radiation. The results of these tests are shown in Table 4.6 as Test Numbers 38 through 41 and 54 and 55. Test Numbers 38 through 41 were conducted at a strain rate of 1×10^{-6} sec^{-1}. Test Numbers 54 and 55 were conducted at a strain rate of 1×10^{-7} sec^{-1}. For Alloy 304L specimens tested at a strain rate of 1×10^{-6} sec^{-1}, the mechanical property data for the vapor-phase specimens were similar to those for the liquid-phase and control specimens. Optical examination, at 30X magnification, indicated SCC of the specimen exposed to the vapor above simulated J-13 water containing 10 000 ppm Cl as NaCl. No SCC was visible in specimens tested above the other three solutions.

Following testing, each of the specimens tested in the vapor phase at a strain rate of 1×10^{-6} sec^{-1} was metallographically sectioned and examined. The purpose of the metallographic examinations was to determine whether any cracking originated from pits and corroded areas that formed at the vapor-liquid interface just above the gage section. These cracks would not necessarily be evident in a low power optical examination. Further examination of these specimens in cross-section revealed no evidence of SCC. The Alloy 304L specimen that experienced SCC, Specimen Number 39, was also metallographically examined. A photomicrograph of this specimen is given in Figure D.10 in Appendix D. This photomicrograph shows transgranular cracking and pits located in the radius above the gage section at the vapor-liquid interface.

SSR tests, Test Numbers 54 and 55, were performed on Alloy 304L at a strain rate of 1×10^{-7} sec^{-1} for comparison with tests numbered as 41 and 38, respectively. With the exception of the

strain rate, the companion tests were performed under the same conditions. Surprisingly, no SCC was observed in these tests at the slower strain rate. The specimen in Test Number 55 showed some pitting at the vapor-liquid interface outside of the gage section. Comparison of Test Numbers 55 and 38 show similar mechanical property data for both strain rates. Comparison of Test Numbers 54 and 41 also show similar mechanical property data.

Six cursory SSR tests were performed with tensile specimens of Alloy 825 in the vapor phase of simulated J-13 well water containing various types and concentrations of chloride. Duplicate control tests were also performed with Alloy 825 in mineral oil. These tests were performed in an effort to correlate SSR results with those obtained from long-term exposures of U-bend specimens in immersion tests in Task 7 of the program. As with the testing of Alloy 304L, 200 ppm H_2O_2 was added daily to simulate radiolysis. A summary of results for the SSR tests completed with Alloy 825 is given in Table 4.7. These data show similar mechanical properties for tests in the inert environment and tests in the simulated J-13 water/salt environments at the higher stress rate. Lower power optical examination of the SSR specimens of Alloy 825 showed no evidence of SCC.

The specimen exposed to the vapor above simulated J-13 water containing 100 000 ppm chloride as NaCl experienced pitting in the radius of the gage section at the vapor-liquid interface. Metallography was performed on this specimen and no evidence of SCC was found. Figure E.2 in Appendix E is a photomicrograph of that specimen.

An interesting observation from the mechanical property data in Table 4.7 is the lower values for percent elongation at the slower strain rate. This reduced elongation also is reflected in the time to failure data. The strain rate was reduced by a factor of 10 (from 10^{-6} sec^{-1} to 10^{-7} sec^{-1}) but the time to failure only increased by a factor of 5. The ultimate tensile strength also was higher at the slower strain rate. Since the reduction in area data were similar for the two strain rates, and no SCC was observed at either strain rate, the most reasonable interpretation of the data is that the effects are related to a strain-aging phenomena.

4.2 Copper-Base Alloys

4.2.1 U-Bend Tests

U-bend specimens of Alloy CDA 102 and Alloy CDA 715 were tested in simulated J-13 water and in Solution Number 7 in immersion tests performed in Task 3 of the overall program. Further information on those experiments may be found in NUREG/CR-5598. U-bend specimens of both Alloy CDA 102 and Alloy CDA 715 were evaluated for SCC after exposure to the liquid and to the vapor above simulated J-13 water at 90°C. No SCC was observed after 590, 1000, or 2024 hours of exposure although etching and pitting were observed in specimens of both alloys in the vapor and liquid phases.

Solution Number 7 was selected from the experimental test matrix where it was found to be an active-corrosion environment for the copper-base alloys based on potentiodynamic-polarization tests. The composition of Solution Number 7 is given in Table 2.5. The data in Table 2.5 show

Table 4.7 Summary Of Results Of Slow-Strain-Rate Tests Performed On Solution-Annealed Specimens Of Alloy 825 At 90°C For Comparison To Results From Immersion Testing Of Constant-Strain Specimens In Task 7.

Electrolyte	Test №	Strain Rate sec^{-1}	Potential mV (SCE)	Time To Failure Hours	Reduction In Area Percent	Elongation Percent	Ultimate Tensile Strength MPa	SCC	Crack Velocity x 10^{-4} mm/sec
Oil	52	$1x10^{-6}$	—	127.8	80.6	44.1	576	None	—
Oil	53	$1x10^{-6}$	—	121.8	77.8	41.4	548	None	—
J-13 + 1 000 ppm Cl as NaCl *	48	$1x10^{-6}$	—	126.3	80.0	43.1	570	None	—
J-13 + 1 000 ppm Cl as NaCl *	55	$1x10^{-7}$	—	596.3	74.6	19.4	624	None	—
J-13 + 10 000 ppm Cl as NaCl *	49	$1x10^{-6}$	—	122.8	76.9	42.3	551	None	—
J-13 + 100 000 ppm Cl as NaCl *	50	$1x10^{-6}$	—	123.7	80.6	42.8	590	None**	—
J-13 + 10 000 ppm Cl as $CaCl_2$ *	51	$1x10^{-6}$	—	127.5	79.2	42.2	582	None	—
J-13 + 10 000 ppm Cl as $CaCl_2$ *	54	$1x10^{-7}$	—	624.4	79.2	19.5	632	None	—

* Vapor phase; 200 ppm H_2O_2 added daily.

** Pitting in the radius above the gage section at the vapor-liquid interface.

that Solution Number 7 was high in chloride and oxalic acid and had a low pH. The U-bend specimens were evaluated at the end of the exposure. No SCC were observed for Alloy CDA 715 after 503, 1009, or 2014 hours of exposure although etching and pitting was observed in both the vapor and liquid phases. No SCC was observed for Alloy CDA 102 after the exposure periods although the liquid-phase specimens exhibited heavy etching.

U-bend specimens of Alloy CDA 102 and Alloy CDA 715 were also evaluated in long-term, boil-down tests with simulated J-13 water in Task 7 of the overall program. Further information on these experiments may be found in NUREG/CR-5709. Long-term, boil-down tests were performed with each of the copper-base alloys in simulated J-13 well water at 90°C for a period of 80 weeks. U-bends were evaluated in these experiments. The specimens were examined at 30X magnification after 80 weeks of exposure. Optical examination revealed no SCC of the specimens of either Alloy CDA 102 or Alloy CDA 715.

Following the termination of the long-term, boil-down tests, duplicate samples of solution were obtained from each of the resin kettles and analyzed. Results of the analysis are given in Table 4.1 and discussed in greater detail in Section 4.1.1.2. Briefly, these data show that the species in the solutions in the long-term, boil-down tests concentrated linearly with time, with the exception of four species that precipitated from the solutions; calcium, magnesium, silicon, and bicarbonate.

4.2.2 SSR Tests

The primary focus of the SSR testing of the copper-base alloys was with Alloy CDA 102. Cursory tests were performed with Alloy CDA 715. Initial control tests were performed with both Alloy CDA 102 and Alloy CDA 715 in mineral oil at 90°C. The remaining SSR testing focused on sodium nitrite environments, a compound that is a possible radiolysis product and has been reported to promote SCC of copper-base alloys.

A total of 22 SSR tests was performed with Alloy CDA 102 in various $NaNO_2$ solutions at 23°C and 90°C to evaluate the effects of nitrite concentration and temperature on SCC. Initial testing investigated low and high concentrations of $NaNO_2$ at both 23°C and 90°C. To simulate the repository environment, simulated J-13 well water containing $NaNO_2$ was also evaluated. Finally, some of the SSR test specimens were anodically polarized to simulate the effect of hydrogen peroxide (H_2O_2), a radiolysis product that will occur in the Tuff Repository.

To evaluate the effects of H_2O_2, the equivalent of 200 ppm H_2O_2 was added to the test cell prior to straining. The shift in potential was monitored and the anodic peak potential was recorded. To counteract the degradation of the H_2O_2, as evidenced by a rapid decline in potential, the test specimen was polarized to the anodic peak potential during the slow-strain-rate test.

A summary of the mechanical property data for the SSR tests completed on Alloy CDA 102 is given in Table 4.8 and in Figures 4.6 through 4.9. Metallography was performed on tensile specimens that exhibited SCC. Photomicrographs of the SCC are shown in Appendix F. The SSR data for Alloy CDA 102 in mineral oil exhibited very short times to failure, which suggests

Table 4.8 Summary Of Results Of Slow-Strain-Rate Tests Performed On Tensile Specimens Of Alloy CDA 102 In The Liquid Phase At A Strain Rate Of 1 X 10^{-6} Sec $^{-1}$.

Sodium Nitrite Concentration	Test Nº	Potential mV (SCE)	Time To Failure (hours)	Reduction In Area (percent)	Elongation (percent)	Ultimate Tensile Strength MPa	Temperature °C	SCC	Crack Velocity × 10^{-6}
Oil *	1	—	18.7	55.2	6.8	320	90	None	—
Oil *	2	—	20.1	45.8	7.2	343	90	None	—
1M	5	-13	23.4	53.8	7.9	393	23	Yes †	†
1M	7	+8	21.2	64.0	7.6	337	23	TG	1.97
0.005M	6	+12	26.0	79.2	9.5	348	23	Yes †	†
0.005M	8	+35	24.4	78.5	8.7	348	23	TG	1.02
0.005M	9	+17	20.5	53.8	7.1	320	90	None	—
0.005M	10	+13	22.3	57.0	7.8	298	90	None	—
1M	13	-2	20.0	49.3	7.3	309	90	None	—
1M	14	-17	21.2	43.4	5.9	292	90	None	—
0.005M in J-13	11	+8	22.0	57.0	7.1	309	90	None	—
0.005M in J-13	12	-7	20.4	52.7	7.5	309	90	None	—
1M in J-13	15	+6	21.0	58.0	7.4	303	90	None	—
1M in J-13	16	+15	21.1	49.3	6.4	309	90	None	—
0.005M in J-13	25	+40	25.0	76.9	9.6	340	23	None	—
0.005M in J-13	26	+29	26.0	79.2	9.4	351	23	None	—
0.005M	19	[+200]	21.4	63.0	8.9	337	23	TG	5.84
0.005M	20	[+174]	20.2	58.0	7.3	346	23	TG	5.09
1M	17	[+61]	18.0	53.8	6.1	337	23	TG	8.02
1M	18	[+68]	18.5	50.4	7.3	337	23	TG	5.26
0.005M	29	[+234]	21.3	58.0	7.5	309	90	TG	0.52
0.005M	31	[+246]	21.0	60.1	7.9	315	90	TG	1.19
1M	23	[+122]	11.6	10.8	4.0	315	90	TG	20.4
1M	24	[+121]	11.0	9.4	4.3	309	90	TG	12.6

* Control Test. † Not Sectioned.
TG Transgranular. [ ] Polarized Potential.

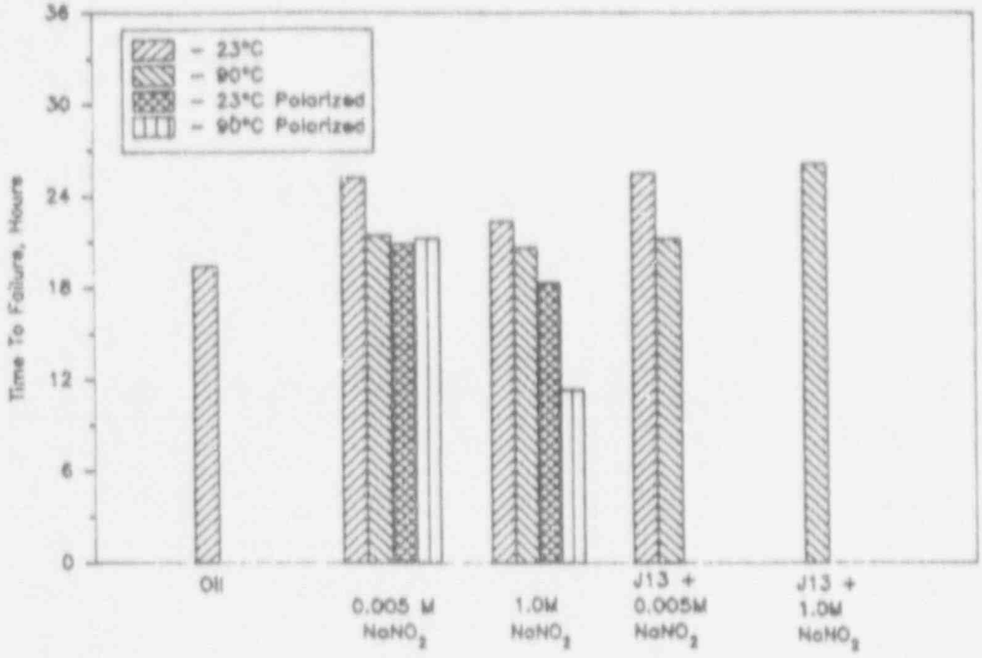

Figure 4.6 Time To Failure As A Function Of Environment, Temperature, And Polarization For Tensile Specimens Of Alloy CDA 102.

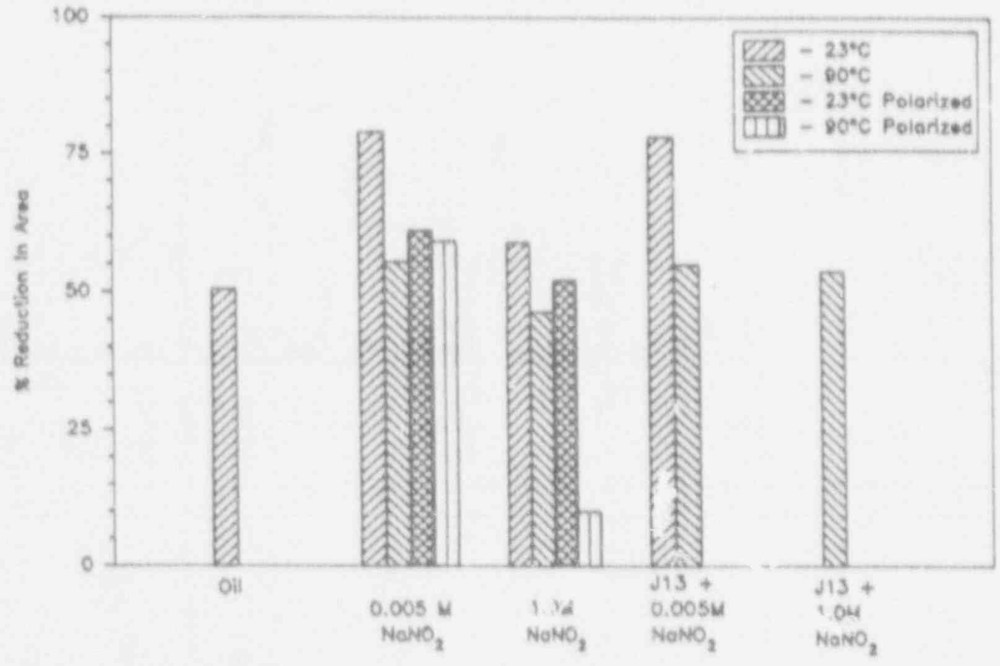

Figure 4.7 Percent Reduction In Area As A Function Of Environment, Temperature, And Polarization For Tensile Specimens Of Alloy CDA 102.

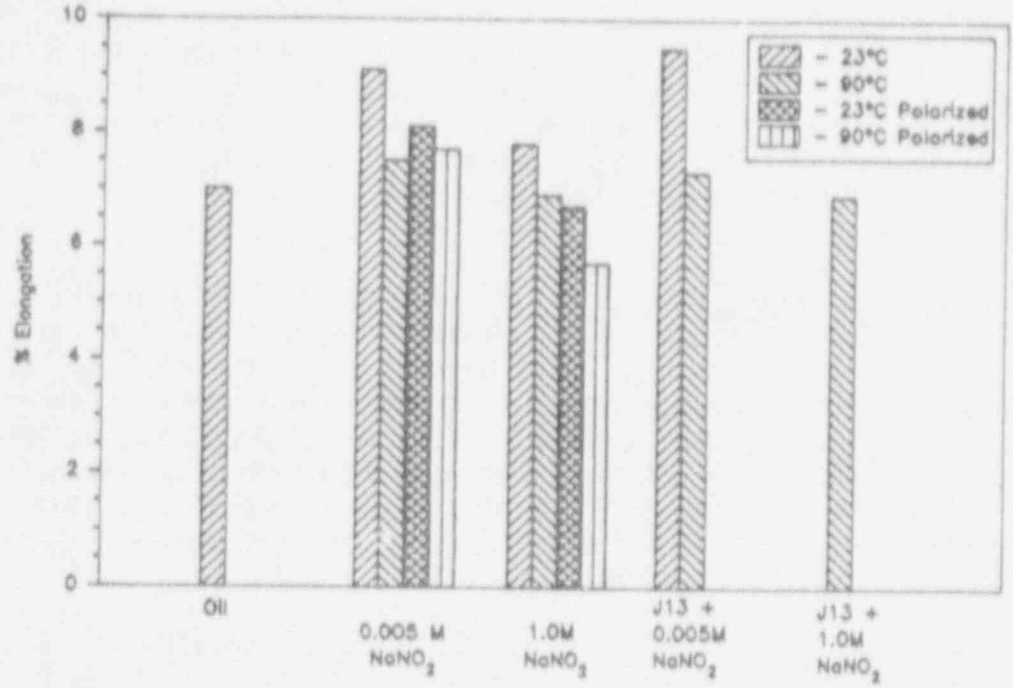

Figure 4.8 Percent Elongation As A Function Of Environment, Temperature, And Polarization For Tensile Specimens Of Alloy CDA 102.

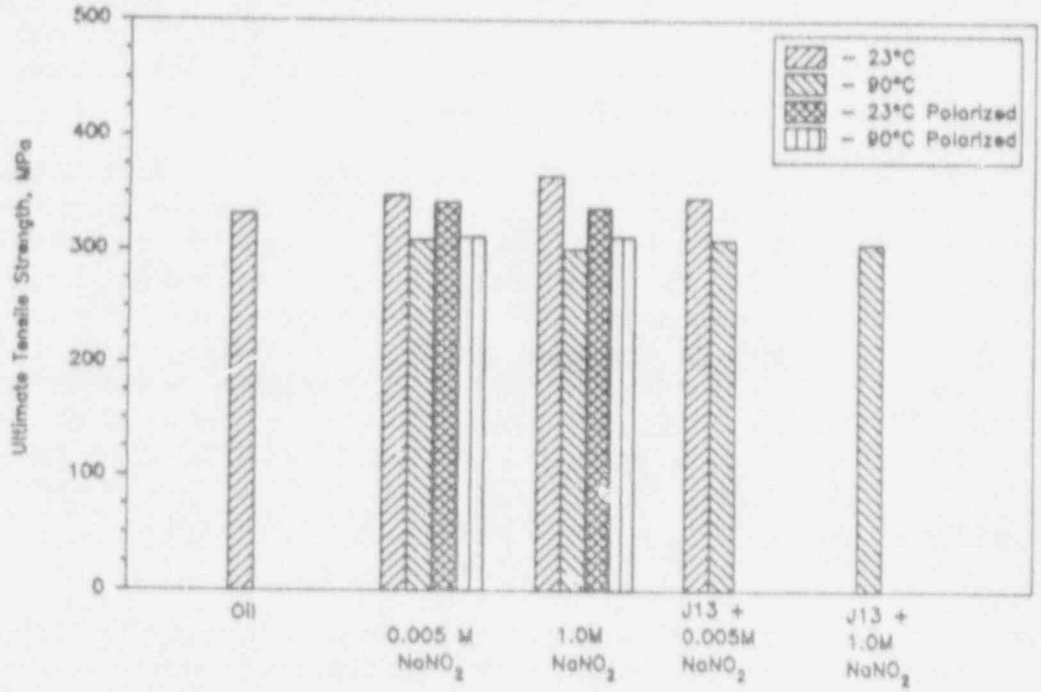

Figure 4.9 Ultimate Tensile Strength As A Function Of Environment, Temperature, And Polarization For Tensile Specimens Of Alloy CDA 102.

that the alloy was cold worked. A literature search was performed, using the CORAB computer program, to investigate the effect of cold working of copper-base alloys on susceptibility to SCC. The literature revealed that cold work had a minimal effect on SCC (Erzurum-1983). Accordingly, subsequent SSR tests were performed with this material. One advantage of the use of the cold-worked material is that the failure times are short for a given strain rate, making the testing more cost-effective.

Stress-corrosion cracking was observed in each of the four initial SSR tests in 0.005M and 1M $NaNO_2$ at 23°C (Test Numbers 5-8). Metallography was performed on one specimen from each test solution concentration. The analysis showed the SCC to be transgranular. Photomicrographs of the specimens at 100X magnification are shown in Figures F.1 and F.2 for 0.005M and 1M $NaNO_2$ solutions, respectively. As anticipated, cracking was more severe in the more concentrated nitrite solution as evidenced by the absence of significant necking, the deep cracks and the crack branching. The cracking that occurred in the specimen exposed to the low concentration of NO_2 appeared to be less severe with blunted crack tips. Crack branching was not observed in this specimen.

These four tests (Test Numbers 8, 10, 13, and 14) were repeated at 90°C to determine the effects of temperature on the cracking behavior in these environments. The results of these tests on Alloy CDA 102 showed that no SCC was observed in any of the tests performed under freely-corroding conditions at 90°C.

To more closely simulate the repository environment, SSR tests were performed in simulated J-13 well water containing 0.005M and 1M $NaNO_2$ at 90°C. As was observed in the straight nitrite solutions at 90°C, no SCC was observed in these tests. An additional SSR test was performed in simulated J-13 well water containing 0.005M $NaNO_2$ at 23°C. Surprisingly, no SCC was observed. This result contrasted with the results of a similar test performed in the straight nitrite solution where SCC was observed. One possible explanation for this behavior is that species present in the simulated J-13 well water inhibited SCC.

Finally, SSR tests were performed with specimens of Alloy CDA 102 which were anodically polarized to simulate oxidizing radiolysis products. These tests evaluated both high and low concentrations of $NaNO_2$ at both 23°C and 90°C. These data indicated shorter times to failure and less reduction in area as compared with previous, unpolarized tests. Cracking was also observed in each of the tests performed with specimens of Alloy CDA 102 which were anodically polarized. Another significant observation from the data in Table 4.8 is the fact that Alloy CDA 102 exhibited SCC in $NaNO_2$ at 90°C under anodic polarization, but not at the free-corrosion potential. These data indicate that the alloy is not immune to cracking at elevated temperature, as had been previously assumed, but that the cracking range had shifted away from the free-corrosion potential. The SCC observed with anodic polarization correlates well with the results of the literature search in which Gouda (1984) indicated that SCC was more severe when copper-base alloy specimens were anodically polarized.

Five cursory SSR tests were performed with tensile specimens of Alloy CDA 715. Duplicate control tests were performed in mineral oil, an inert environment. Triplicate tests were performed in 1M $NaNO_2$ at 23°C. In these latter tests, the specimens were anodically polarized to simulate the effects of H_2O_2. As in the test with Alloy CDA 102, 200 ppm H_2O_2 was added to the test cell prior to straining. The shift in potential was monitored and the anodic peak potential was

recorded. To counteract the degradation of the H_2O_2, as evidenced by a rapid decline in potential, the test specimen was polarized to the anodic peak potential during the slow-strain-rate test.

The mechanical property data for SSR tests with specimens of Alloy CDA 715 are summarized in Table 4.9. These data show that the nitrite solution did not significantly affect the mechanical property data. Optical examination of the specimens also was performed, at 30X magnification. Possible incipient cracking along slip planes was observed in the Alloy 715 specimen from the first test. On the other hand, the duplicate test showed no cracking. A third SSR test was performed in an effort to duplicate the observation. The third test showed only pitting at 30X magnification. Two of the specimens were sectioned and their photomicrographs are shown in Figures G.1 and G.2 in Appendix G. Figure G.1 shows pitting that measured from 0.02 to 0.036 mm in depth. Figure G.2 shows the possible incipient cracking.

Table 4.9 Summary Of Results Of Slow-Strain-Rate Tests Performed On Tensile Specimens Of Alloy CDA 715 In The Liquid Phase At A Strain Rate Of 1×10^{-6} Sec $^{-1}$.

Electrolyte	Test №	Potential mV (SCE)	Time To Failure (hours)	Reduction In Area (percent)	Elongation (percent)	Ultimate Tensile Strength MPa	Temperature °C	SCC	Crack Velocity $\times 10^{-4}$
Oil *	3	—	69.1	79.2	22.9	410	90	None	—
Oil *	4	—	67.9	80.6	23.7	393	90	None	—
1M $NaNO_2$	30	[+127]	74.6	85.3	26.7	433	23	None†	—
1M $NaNO_2$	27	[+64]	74.0	81.3	25.3	410	23	None	—
1M $NaNO_2$	28	[+33]	72.3	76.9	25.8	421	23	None‡	—

* = Control Test.
‡ = Pitting at 30X magnification.
† = Possibly incipient cracking at slip planes.
[ ] = Polarized Potential.

5. DISCUSSION

There were two goals of the SCC studies performed in the overall program; (1) to assess the SCC performance of the candidate alloys in simulated repository environments and (2) to evaluate SCC test techniques. Two test techniques were used; the U-bend test technique and the Slow-Strain-Rate (SSR) technique. Both techniques are performed with smooth, un-notched, specimens and thus, test the SCC initiation resistance of the alloys. Crack-propagation studies were not planned or performed on the program. Because SCC growth rates are generally high, a waste container would fail relatively rapidly, in comparison to the repository life, following initiation of SCC. This approach to the SCC testing is philosophically different from that used in the pitting studies where slowly propagating pits may be tolerable for some alloy systems. Stress-Corrosion-Cracking studies were performed on two alloy systems; Fe-Cr-Ni alloys and copper-base alloys.

5.1 Fe-Cr-Ni Alloys

Stress-corrosion testing was performed on two Fe-Cr-Ni alloys; Alloy 304L and Alloy 825. All SCC testing was performed on solution-annealed specimens and thus issues such as the effect of sensitization on SCC were not addressed. Alloy 825 was resistant to SCC in all environments evaluated including simulated J-13 well water, simulated J-13 well water concentrated by a factor of about 80, and chloride solutions containing up to 100 000 ppm Cl in the presence of H_2O_2, even though crevice corrosion occurred in some of these environments. The concentrated simulated J-13 well water solution contained 675 ppm Cl based on a post-test chemical analysis.

Table 5.1 summarizes the results of the SCC testing performed on the Alloy 304L specimens. These data show that Alloy 304L was resistant to SCC in the J-13 well water and in the J-13 well water that was concentrated by a factor of about 80 by evaporation. The U-bend test results, summarized in Table 5.1, also indicate that Alloy 304L was resistant to SCC in J-13 well containing 1000 ppm added Cl. Alloy 304L U-bend specimens underwent SCC in only one liquid-phase exposure condition; J-13 well water with 100 000 ppm added Cl.

Alloy 304L U-bends also underwent SCC in four vapor-phase exposure conditions, all in the presence of H_2O_2. Of the four solutions in which Alloy 304L underwent cracking, three solutions were prepared with simulated J-13 well water and added Cl (1000 ppm Cl and 10 000 ppm Cl as NaCl and 10 000 ppm Cl as $CaCl_2$) while one solution, Solution Number 20, was taken from the Task 2 experimental test matrix. Solution Number 20 contained 1000 ppm Cl as well as 200 ppm F and 200 ppm NO_2^-. The occurrence of SCC only in the vapor phase in the latter environments suggests that SCC may be more likely in the vapor phase in the repository. This behavior may relate to the availability of the oxidant, H_2O_2, to the metal in the vapor phase. Indeed, Pitman (1986) reported that solution-annealed Alloy 304L underwent transgranular SCC following 23 months of exposure above J-13 well water at 90°C in the presence of a gamma radiation field of 5×10^5 R/hour.

Table 5.1 Summary Of Results Of Stress-Corrosion-Cracking Tests Performed On Specimens Of Alloy 304L.

Environment	Phase	U-Bend Test	Slow-Strain-Rate Test	
			1×10^{-6} sec^{-1}	1×10^{-7} sec^{-1}
J-13 Well Water	Vapor Liquid	NC NC	NC NC	— —
Concentrated J-13 Well Water	Vapor Liquid	NC NC	NC NC	— —
Solution No. 20	Vapor Liquid	SCC NC	NC —	TG-SCC* —
J-13 + CO_2	Vapor Liquid	— —	NC NC	— —
J-13 + CO_2 + H_2O_2	Vapor Liquid	— —	NC —	— —
J-13 - HCO_3	Vapor Liquid	— —	— NC	— —
J-13 - HCO_3 + H_2O_2	Vapor Liquid	— —	— NC	— —
J-13 + 1000 ppm Cl as NaCl	Vapor Liquid	NC NC	— NC	— —
J-13 + 10000 ppm Cl as NaCl	Vapor Liquid	NC NC	— NC	— —
J-13 + 100000 ppm Cl as NaCl	Vapor Liquid	NC SCC	— TG-SCC*	— —
J-13 + 10000 ppm Cl as $CaCl_2$	Vapor Liquid	NC NC	— NC	— —
J-13 + 1000 ppm Cl as NaCl + H_2O_2	Vapor Liquid	SCC NC	NC —	NC —
J-13 + 10000 ppm Cl as NaCl + H_2O_2	Vapor Liquid	SCC NC	TG-SCC —	— —
J-13 + 100000 ppm Cl as NaCl + H_2O_2	Vapor Liquid	NC NC	NC —	— —
J-13 + 10000 ppm Cl as $CaCl_2$ + H_2O_2	Vapor Liquid	SCC NC	NC —	NC —

NC = No cracking SCC = Stress-Corrosion-Cracking TG-SCC = Transgranular SCC
P = Polarized specimen * = Containing H_2O_2

Table 5.1 compares the results of SCC tests performed on Alloy 304L using the SSR and U-bend test techniques. These data show that both techniques were used to evaluate 11 different environments. No SCC was observed for both techniques in 6 of the 11 environments. Of the remaining five environments, there were two discrepancies between the techniques, where SCC was observed in the U-bend tests but no cracking was observed in the SSR tests, even at the lower strain rate tested. These two environments were simulated J-13 well water containing H_2O_2 and 1000 ppm Cl (as NaCl) and 10 000 ppm Cl as $CaCl_2$. In one additional environment, Solution Number 20, SCC was observed in the U-bend test and in the SSR test at the slower strain rate but not at the higher strain rate. This behavior is consistent with that predicted by Mancia and Tamba (1986) for marginally aggressive SCC environments. In the remaining two environments, SCC was observed in the U-bend tests and in the SSR tests at the faster strain rate. It is the opinion of the authors that there is insufficient data obtained to conclude that the SSR technique provides erroneous results in assessing the SCC behavior of Alloy 304L in chloride containing environments. Nevertheless, the discrepancies observed are disconcerting and indicate that further research is needed.

5.2 Copper-Base Alloys

A review of the literature in Task 1 of the program indicated that SCC of copper-base alloys has been reported in numerous environments including sulfates, nitrates, nitrites, ammonia, humid air, and steam, see Table 5.2. While Cu-Zn alloys predominate, this may reflect, in part, the fact that brasses are used extensively and more stress-corrosion research has been performed on these alloys than on other alloys. It is generally established that pure copper and copper-nickel alloys are more resistant to SCC than are most other copper-base alloys. However, as shown in Table 5.2, these alloys are susceptible to SCC in several of the reported cracking environments.

Literature on the SCC of copper-base alloys in nitrates and nitrites was investigated further to aid in determining possible test solutions for the Task 5 research. No information was found pertaining to the effects from nitrates. Nitrites, however, were found to cause SCC in copper-base alloys in concentrations as low as 0.005M (as sodium nitrite, $NaNO_2$) at ambient temperature (Mattsson-1987). The literature also indicated that SCC was more severe when specimens of copper-base alloys were anodically polarized (Gouda-1984). A test matrix was drafted to evaluate the effects of nitrite concentration on SCC of the copper-base alloys. The test matrix was comprised of a low and high concentration of 0.005M $NaNO_2$ and 1M $NaNO_2$, respectively. The low concentration of 0.005M $NaNO_2$ was selected as this was approximately equivalent to the 200 ppm NO_2^- in the overall test solution matrix established in Task 2. Testing also was performed in the simulated J-13 well water.

Both Alloy CDA 102 and Alloy CDA 715 were found to be resistant to SCC in Solution Number 7 from the Task 2 experimental test matrix, in simulated J-13 well water and in the simulated water concentrated approximately 80 times. Both SSR and U-bend tests were performed in the simulated J-13 well water while only U-bend tests were performed in Solution Number 7 and in the concentrated well water solution. In SSR tests, Alloy CDA 715 was also resistant to SCC in all other environments evaluated including $NaNO_2$ at concentrations up to 1M. Possible incipient cracks were observed in the necked region of one specimens tested in the latter environment but the possible cracking could not be reproduced in two subsequent SSR tests.

Table 5.2 Summary Of Environments Known To Promote Stress-Corrosion Cracking Of Copper-Base Alloys (Beavers-1990).

Environment	Alloy	Reference
Ammonia	Pure Copper, Cu-Ni	Thompson-1944
Nitrites	Pure Copper	Benjamin-1983
Steam	Al Bronze	Klement-1959
Steam	Cu-Ni	Sato-1974a
Ammonia	Al Brass	Sato-1974a
Room Temperature Humid Air	Cu-Zn Alloys	Sato-1974b
SO_4^{2-}	Cu-Zn Alloys	Kawashima-1979
Nitrates	Cu-Zn	Graf-1969
ClO_3^-	Cu-Zn	Kawashima-1977

In SSR tests performed on Alloy CDA 102, SCC was observed in $NaNO_2$ environments at concentrations as low as approximately 200 ppm. The presence of species from simulated J-13 well water appeared to inhibit SCC of Alloy CDA 102 in the dilute $NaNO_2$ solution. On the other hand, anodic polarization of Alloy CDA 102 specimens, to simulate radiolysis products, increased susceptibility to SCC in $NaNO_2$ solutions. In SSR tests performed on Alloy CDA 102 at 90°C, cracking only occurred under anodic polarization, suggesting that the potential range, relative to the free-corrosion potential, shifted in the noble direction.

The literature survey performed on the SSR test technique did not indicate evidence of anomalous behavior with the technique for the copper-base alloys. On the other hand, a question arose in the testing concerning the best parameter for indicating susceptibility to SCC. Maximum crack depth in the specimen is generally agreed to be the best indicator of susceptibility but, to obtain this parameter, metallography or a Scanning Electron Microscope (SEM) examination of each SSR specimen is required. To aid in correlating the mechanical property data for Alloy CDA 102 with actual SCC, graphs of cracking velocity as a function of each of the mechanical properties were prepared and are shown in Figures 5.1 through 5.4. These graphs show that, in general, cracking velocity was inversely proportional to time to failure, percent reduction in area, and the percent elongation. For example, the higher the crack velocity, the shorter the time to failure with little reduction in the necked area, and consequently, less elongation. On the other hand, ultimate tensile strength did not correlate well with crack velocity.

However, actual crack depth, or velocities, calculated from these depths, are the most reliable indicators of SCC. As an example of the erroneous conclusions one could draw from the mechanical property data, note in Table 4.9 and Figures 4.6 and 4.7 that the tests in oil actually exhibited lower times to failure and reduction in areas than in some tests where cracking was observed.

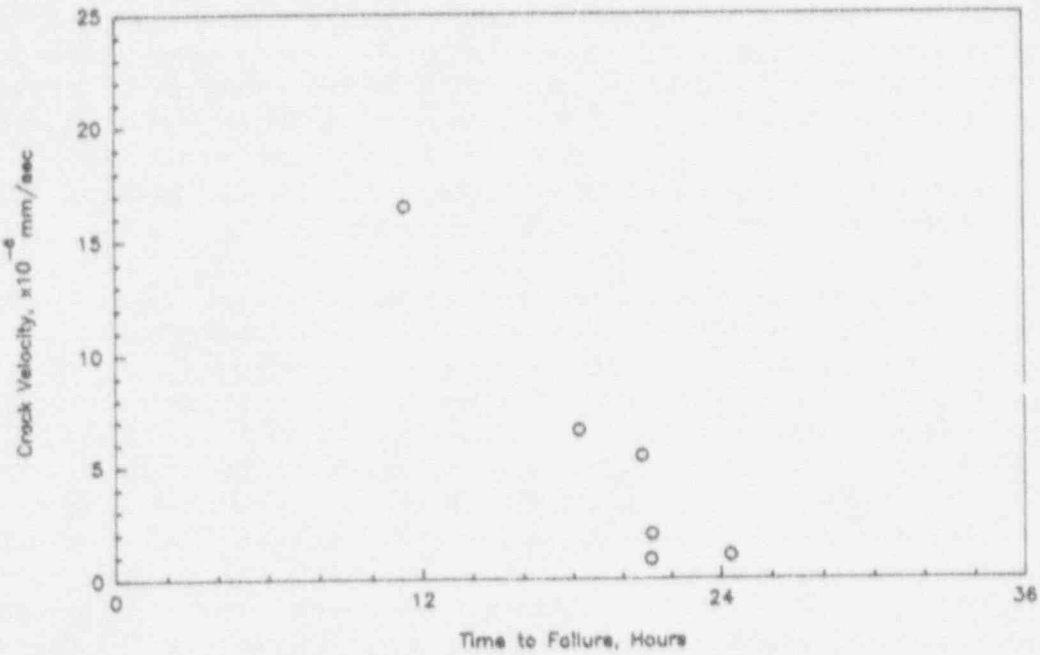

Figure 5.1 Crack Velocity As A Function Of Time To Failure For Tensile Specimens Of Alloy CDA 102 In $NaNO_2$ Environments.

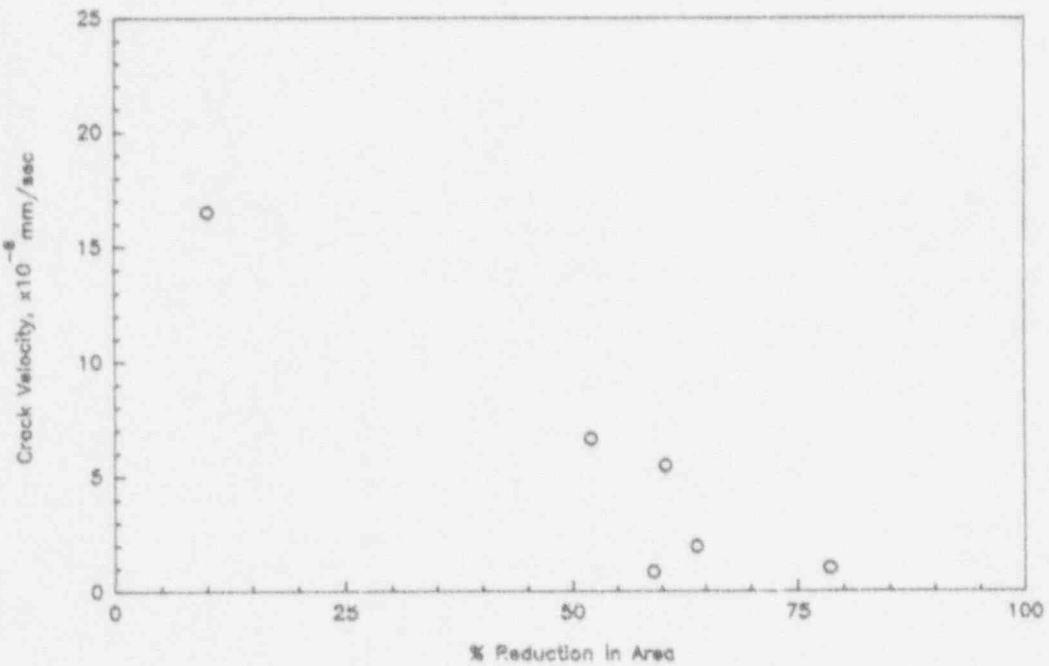

Figure 5.2 Crack Velocity As A Function Of Percent Reduction In Area For Tensile Specimens Of Alloy CDA 102 In $NaNO_2$ Environments.

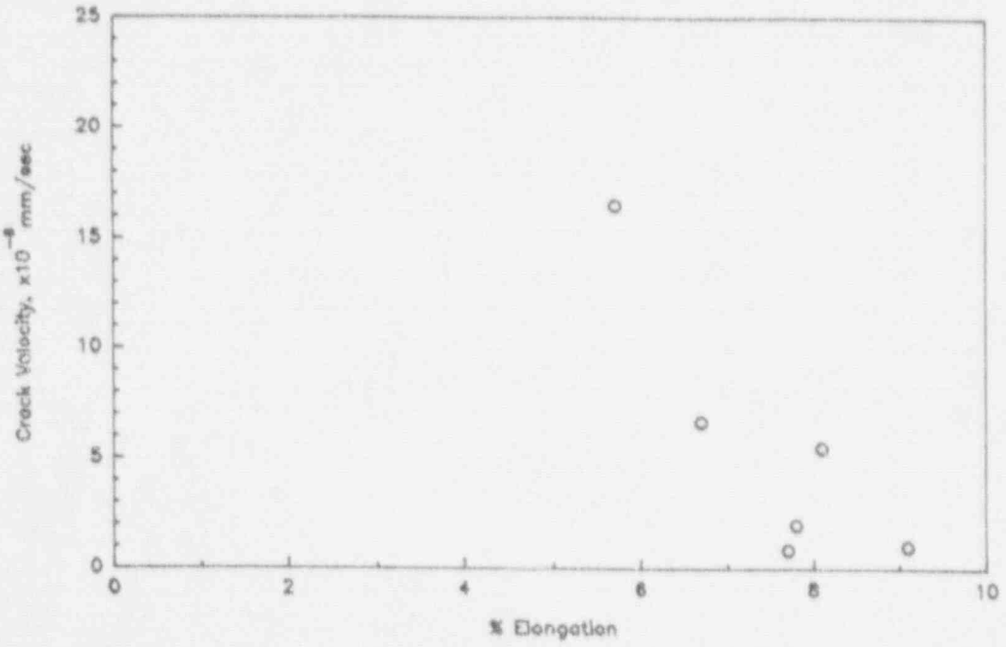

Figure 5.3 Crack Velocity As A Function Of Percent Elongation For Tensile Specimens Of Alloy CDA 102 In $NaNO_2$ Environments.

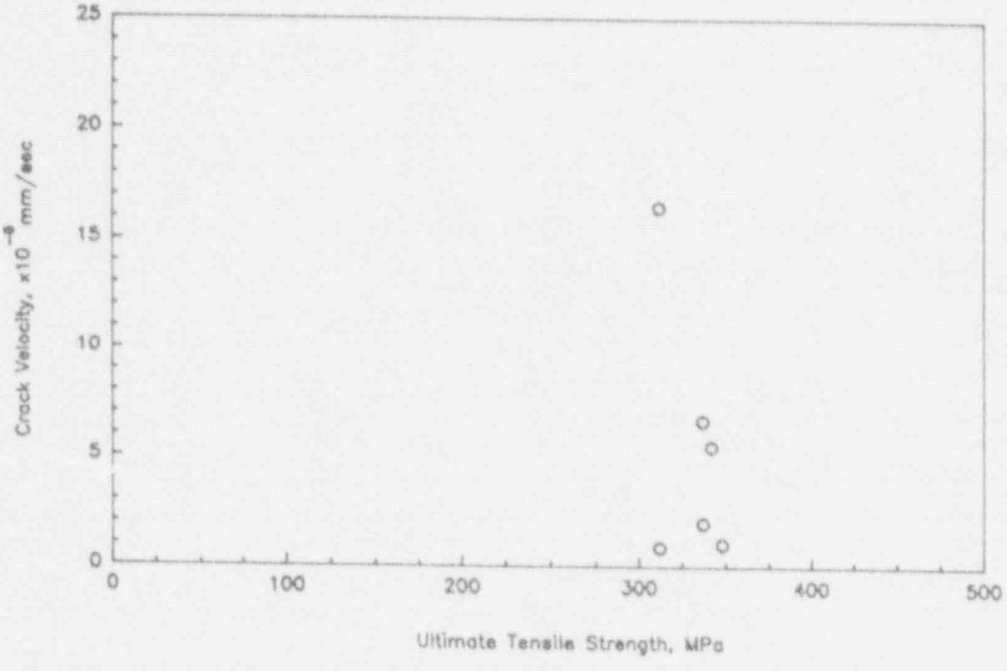

Figure 5.4 Crack Velocity As A Function Of Ultimate Tensile Strength For Tensile Specimens Of Alloy CDA 102 In $NaNO_2$ Environments.

6. CONCLUSIONS

6.1 Fe-Cr-Ni Alloys

1. Both Alloy 304L and Alloy 825 were found to be resistant to SCC in simulated J-13 well water and in the simulated water concentrated approximately eighty times.

2. Alloy 825 also was resistant to SCC in all other environments evaluated including chloride concentrations up to 100 000 ppm in the presence of H_2O_2, even though crevice corrosion occurred in some of these environments.

3. Alloy 304L underwent transgranular SCC in several of the chloride containing solutions examined.

4. Hydrogen peroxide additions to the chloride solutions appeared to decrease the minimum chloride concentration necessary to promote SCC of Alloy 304L.

5. Discrepancies were observed, in two environments, between the SSR and the U-bend test techniques, where SCC occurred with U-bend specimens of Alloy 304L but not with SSR specimens of that alloy.

6. Insufficient data were obtained to conclude that the SSR technique provides erroneous results in assessing the SCC behavior of Alloy 304L in chloride containing environments. Nevertheless, the discrepancies observed are disconcerting and indicate that further research is needed.

6.2 Copper-Base Alloys

1. Both Alloy CDA 102 and Alloy CDA 715 were found to be resistant to SCC in simulated J-13 well water and in the simulated water concentrated approximately eighty times.

2. Alloy CDA 715 was resistant to SCC in all environments evaluated including $NaNO_2$ at concentrations up to 1M; possible incipient cracks were observed in the necked region of one specimens tested in the latter environment but the possible cracking could not be reproduced in two subsequent SSR tests.

3. Alloy CDA 102 was susceptible to SCC in $NaNO_2$ environments at concentrations as low as approximately 200 ppm.

4. The presence of species from simulated J-13 well water inhibited SCC of Alloy CDA 102 in the dilute $NaNO_2$ solution.

5. Anodic polarization of Alloy CDA 102 specimens, to simulate radiolysis products, increased susceptibility to SCC.

6. In SCC tests performed at 90°C, cracking only occurred under anodic polarization, suggesting that the potential range, relative to the free-corrosion potential, shifted in the noble direction.

7. In SSR tests performed on Alloy CDA 102, ultimate tensile strength did not correlate well with SCC crack velocity.

8. Time to failure, percent reduction in area, and percent elongation correlated well with SCC crack velocity in SSR tests performed on Alloy CDA 102.

9. Crack depth or crack velocity are the most reliable indicators of susceptibility to SCC for Alloy CDA 102.

7. RECOMMENDATIONS FOR FURTHER RESEARCH

- SCC studies should be pursued in a broader range of possible repository environments.
- Possible discrepancies between SSR and other SCC test techniques should be investigated.
- Longer-term SCC initiation tests need to be performed, including the role of crevice corrosion and pitting on SCC initiation.
- Fracture mechanics-type tests should be considered as a means of accelerated testing.

8. REFERENCES

Abraham-1986 - Abraham, T., Jain, H., and Soo, P., "Stress-corrosion Cracking Tests On High-Level-Waste Container Materials In Simulated Tuff Repository Environments," Brookhaven National Laboratory, NUREG/CR-4619, BNL-NUREG-51996, June, 1986.

Beavers-1987 - Beavers, J. A. and Thompson, N. G., et al., "Long-Term Performance of Container Materials for High-Level Waste," NUREG/CR-4955, BMI-2155, September, 1987.

Beavers-1990 - Beavers, J. A. and Thompson, N. G., "Environmental Effects On Corrosion In The Tuff Repository," Cortest Columbus, Inc., Columbus, Ohio, NUREG/CR-5435.

Beavers-1991 - Beavers, J. A. and Durr, C. L., "Immersion Studies On Candidate Container Alloys For The Tuff Repository," Cortest Columbus Technologies, Inc., Columbus, Ohio, NUREG/CR-5598.

Beavers-1991a - Beavers, J. A. and Durr, C. L., "Pitting, Galvanic, And Long-Term Corrosion Studies On Candidate Container Alloys For The Tuff Repository," Cortest Columbus Technologies, Inc., Columbus, Ohio, NUREG/CR-5709.

Beavers-1991b - Beavers, J. A., Thompson, N. G., and Durr, C. L., "Potentiodynamic Polarization Studies On Candidate Container Alloys For The Tuff Repository," Cortest Columbus Technologies, Inc., Columbus, Ohio, NUREG/CR-5708.

Benjamin-1983 - Benjamin, L. A., Hardie, D. and Parkins, R. N., University of Newcastle-Upon-Tyne, England, Report No. 83-06/SKBF/KBS.

Erzurum-1983 - Erzurum, S. and Yeh, H. C., "The Effect Of Environment, Cold Work, And Crystallography On The Stress Corrosion Cracking Of C36000 Alloy," Corrosion, Vol. 39, No. 5, May, 1983.

Glass-1985 - Glass, R. S., Overturf, G. E., Van Konynenburg, R. A., and McCright, R. D., "Gamma Radiation Effects On Corrosion: I Electrochemical Mechanisms For The Aqueous Corrosion Processes Of Austenitic Stainless Steels," Lawrence Livermore National Laboratory, Livermore, CA, UCRL-92311, February, 1985.

Glass-1986 - Glass, R. S., Van Konynenburg, R. A., and Overturf, G. E., "Corrosion Processes Of Austenitic Stainless Steels And Copper-Based Materials In Gamma-Irradiated Aqueous Environments," Corrosion-86, Paper No. 258 and Lawrence Livermore National Laboratory, Livermore, CA, UCRL-92941, September, 1985.

Glassley-1986 - Glassley, W. E., "Reference Waste Package Environment Report," Lawrence Livermore National Laboratory, Livermore, CA, UCRL-53726, October 1, 1986.

Gouda-1984 - Gouda, V. K., Sayed, S. M., and El-Sayed, H. A., "Stress Corrosion Cracking Behavior Of Brass In Sodium Nitrite Solutions," Fourth International Congress On Metallic Corrosion, National Research Council of Canada, 1984.

Graf-1969 - Graf, L., "Stress-Corrosion Cracking In Homogeneous, Non-Supersaturated Alloys Containing Noble Or No Noble Metals," Fundamental Aspects Of Stress-Corrosion Cracking, Eds. Staehle, R.W., et al., NACE 1969, p. 197.

Johnstone-1981 - Johnstone, J. K. and Wolfsberg, K., editors, "Evaluation Of Tuff As A Medium For A Nuclear Waste Repository: Interim Status Report On The Properties Of Tuff," Sandia National Laboratories, SAND80-1464, July, 1981.

Kawashima-1977 - Kawashima, A., Agrawal, A. K. and Staehle, R. W., "Stress-Corrosion Cracking Of Admiralty Brass In Non-Ammoniacal Sulfate Solutions," J. Electrochem. Soc., Vol. 124, p. 1822.

Kawashima-1979 - Kawashima, A., Agrawal, A. K. and Staehle, R. W., "Stress-Corrosion Cracking - The Slow Strain Rate Technique," Ugiansky, G. M., Payer, J. H., ASTM STP 665, American Society For Testing and Materials.

Klement-1959 - Klement, J. F., Maersch, R. E. and Tully, P. A., Metal Progress, 75, (2), p. 83.

Knauss-1985a - Knauss, K. G., Beiriger, W. J. and Peifer, D. W., "Hydrothermal Interaction Of Crushed Topopah Spring Tuff and J-13 Water At 90, 150, and 250°C Using Dickson-Type, Gold-Bag Rocking Autoclaves," Lawrence Livermore National Laboratory, Livermore, CA, UCRL-53630, DE86-014752, May, 1985.

Knauss-1985b - Knauss, K. G., Beiriger, W. B., Peifer, D. W. and Piwinskii, A., "Reaction Of Solid Wafers Of Topopah Spring Tuff With J-13 Water At 90, 150, And 250°C In Dickson-Type, Gold-Bag Rocking Autoclaves: 1. Short-Term Experiments," Lawrence Livermore National Laboratory, Livermore, CA, UCRL-53645.

Mancia-1986 - Mancia, F. and Tamba A., Corrosion, Vol. 42, No. 6, p. 362, June, 1986.

Mattsson-1987 - Mattsson, E., "Focus On Copper In Modern Corrosion Research," Materials Performance, Vol. 26, No. 4, April, 1987.

McCright-1984 - McCright, R. D., Weiss, H., Juhas, M. C., and Logan, R. W., "Selection Of Candidate Canister Materials For High-Level Nuclear Waste Containment In A Tuff Repository," Lawrence Livermore National Laboratory, Livermore, CA, UCRL 89988 and Corrosion '84, Paper No. 198, April, 1984.

McCright-1985 - McCright, R. D., "FY 1985 Status Report On Feasibility Assessment Of Copper-Base Waste Package Container Materials In A Tuff Repository," Lawrence Livermore National Laboratory, Livermore, CA, UCID-20509, September, 1985.

Montazer-1984 - Montazer, P. and Wilson, W. E., "Conceptual Hydrologic Model Of Flow In The Unsaturated Zone, Yucca Mountain, Nevada," U. S. Geological Survey - Water Resources Investigation Report, USGS-WRI-84-4345, 1984.

Pitman-1986 - Pitman, S. G., Westerman, R. E., Haberman, J. H., "Corrosion And Slow Strain Rate Testing Of Type 304L Stainless Steel In Tuff Groundwater Environments," Pacific Northwest Laboratory, Richland, WA, PNL-SA-14396, DE87-006404, October, 1986.

Sato-1974a - Sato, S. and Nagata, K., "Stress-Corrosion Cracking Of Copper Alloys In Pure Steam And Water At High Temperatures," Boshoku Gijustu, Vol. 23, pp. 125-133.

Sato-1974b - Sato, S. and Nagata, K., "Case Studies On The Failures Of Copper And Copper Alloys By Stress-Corrosion Cracking," Sumitomo Light Metal Technical Reports, Vol. 15:3, pp. 174-185, July, 1974.

Schuraytz-1985 - Schuraytz, B., "Geochemical Gradients In The Topopah Spring Member Of The Paintbrush Tuff: Evidence For Eruption Across A Magmatic Interface," Lawrence Livermore National Laboratory, Livermore, CA, UCRL-53698.

Thompson-1944 - Thompson, D. H. and Tracy, A. W., Trans. AIME, 185, p. 100.

Van Konynenburg-1986 - Van Konynenburg, R. A., "Radiation Chemical Effects In Experiments To Study The Reaction Of Glass In A Gamma-Irradiated Air, Groundwater, And Tuff Environment," Lawrence Livermore National Laboratory, Livermore, CA, UCRL-53719.

Yunker-1986a - Yunker, W. H., "Corrosion Of Copper-Based Materials In Gamma Radiation," Westinghouse Hanford Company, HEDL-7612, DE87-005494, June, 1986.

Yunker-1986b - Yunker, W. H., Westinghouse Hanford Company, and Glass, R. S., Lawrence Livermore National Laboratory, "Long-Term Corrosion Behavior Of Copper-Base Materials In A Gamma-Irradiated Environment," UCRL-94500, DE87-007098, December, 1986.

APPENDIX A

THE POTENTIODYNAMIC POLARIZATION TECHNIQUE FOR CORROSION EVALUATION

APPENDIX A

The Potentiodynamic Polarization Technique For Corrosion Evaluation

The cyclic-potentiodynamic-polarization (CPP) technique was used in this project to provide an understanding of how the specific variables, environmental composition, temperature, and alloy composition affect the general and pitting corrosion behavior of the alloys in simulated repository environments.

In the CPP procedure, the polarity and magnitude of the current flow between a specimen of the material of interest and an inert counter electrode are measured as a function of electrochemical potential. For the anodic portions of the curve, the current measured is equal to the corrosion rate of the specimen if two conditions are met: (1) The electrochemical potential is far enough away from the open-circuit potential that the rate of the cathodic reaction is negligible; and (2) The rates of spurious oxidation reactions are negligible.

Schematics of anodic polarization curves showing several types of behavior are given in Figure A.1. For the active-corrosion case, the anodic curve is linear on an E-log i plot, and the forward and reverse scans are coincident. The presence of a peak in the anodic portion of the curve, followed by decreasing current, is generally indicative of the onset of passivation. The occurrence of hysteresis between the forward and reverse scans is indicative of pitting. Where the hysteresis loop is very large, the protection potential may be very close to the open-circuit potential, indicating a high probability of pitting in that particular environment.

The polarization behavior of the alloys was determined using conventional polarization techniques. The specific polarization equipment used for these experiments included a Princeton Applied Research Model 273 potentiostat coupled to a computer data-acquisition system or a Santron Electrochemical Measuring System. A two-compartment electrochemical cell was employed that utilized a saturated-calomel reference electrode (SCE) and a platinum counter electrode (Figure A.2). Originally, it was planned to use a three-compartment cell (working, counter, and reference compartments), but the relatively high resistance of several of the solutions prevented its use, and the two-compartment cell was used for all tests. The working electrode specimens were cylindrical rods that were drilled, tapped at one end, and sealed off using PTFE gaskets. The specimens were typically 1.3 cm in length with the diameter depending on the metal being tested. The electrodes were polished with successively finer grades of silicon carbide paper, finishing with a 600-grit grade.

A typical experiment consisted of the following procedure. Prior to testing, the working electrode was immersed in the test solution overnight while the solution was sparged with the desired gas mixture. The CPP test was then performed approximately 16 hours after immersion of the working electrode in the cell.

The working electrode lead was connected to the test specimen while the auxiliary (counter) electrode lead was connected to an inert electrode (platinum wire) placed in the test cell. The reference electrode lead was connected to the reference electrode which communicates with the test cell electrolyte through a small diameter tube filled with electrolyte, referred to as a Luggin

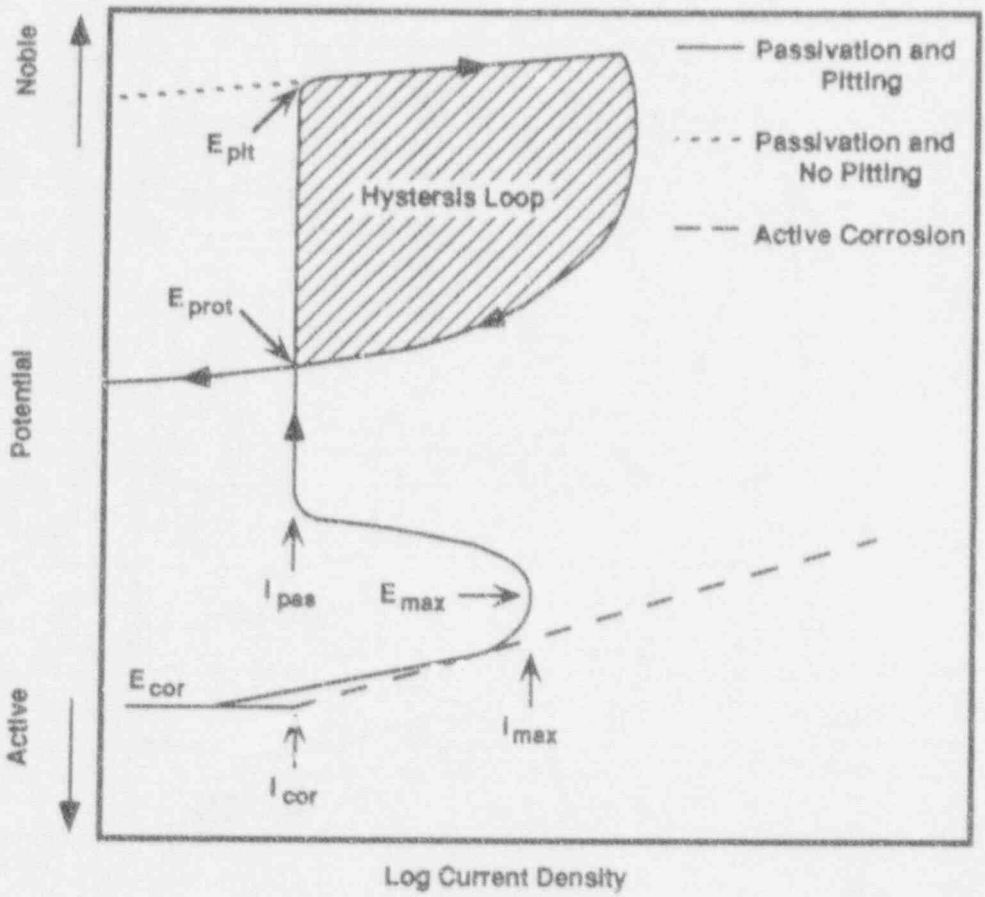

Figure A.1 Schematic Of Typical Anodic Potentiodynamic Polarization Curves.

E_{cor} = corrosion potential; E_{pit} = potential at which pits initiate on forward scan; E_{prot} = potential at which pits repassivate on reverse scan; i_{cor} = current density at the free-corrosion potential; i_{max} = current density at active peak; i_{pas} = current density in passive range.

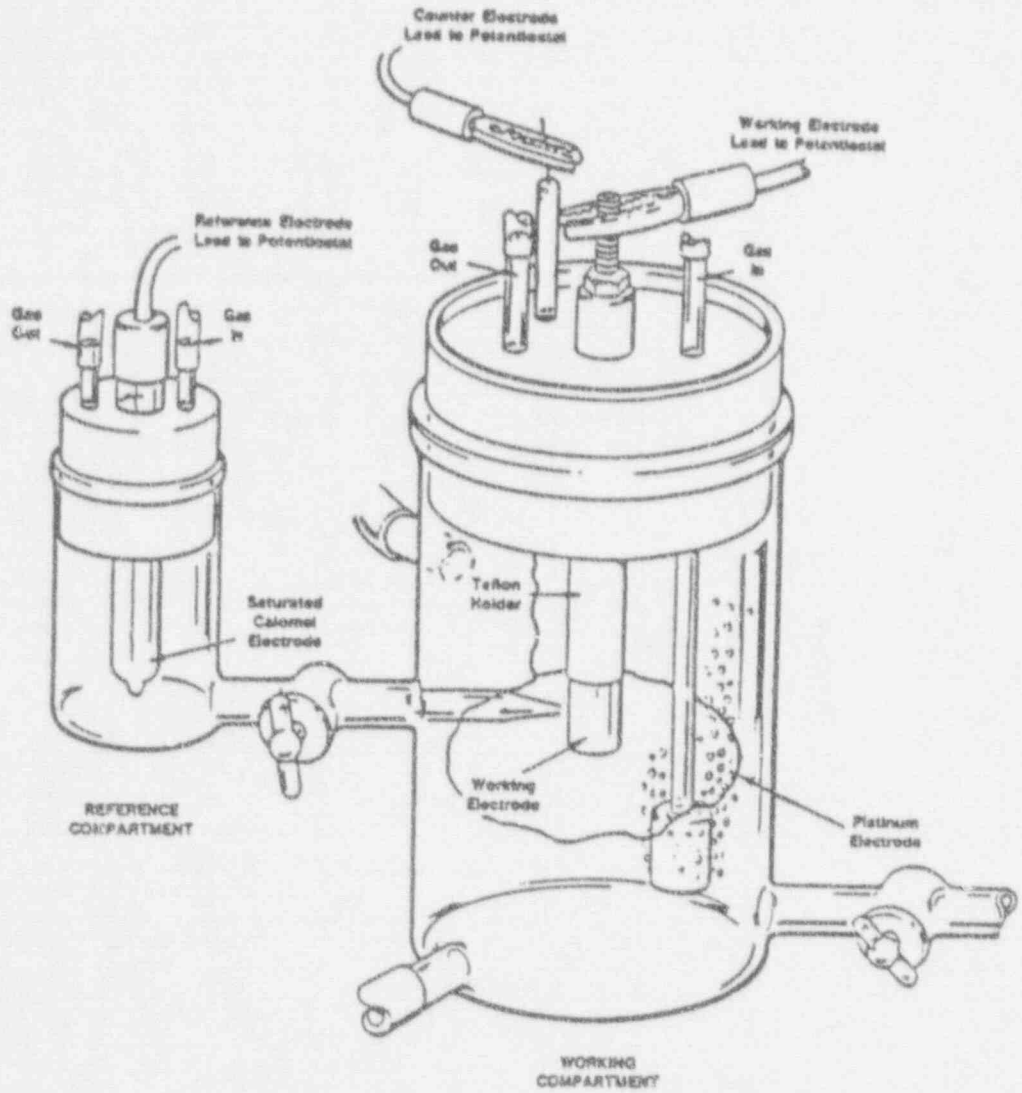

Figure A.2 Electrochemical Cell Used For Ambient Pressure Potentiodynamic Polarization Experiments.

probe or salt bridge. The tip of the probe is placed near the test specimen to minimize measurement errors due to ohmic potential drops.

Partial cathodic and full anodic polarization curves were obtained by scanning at a rate of 0.6 V/h and beginning the scan approximately 100 mV more negative than the free-corrosion potential. The current for the anodic curve was scanned until a current density of approximately 2×10^{-3} A/cm^2 was attained; the potential scan was then reversed until repassivation occurred and the current changes polarity, becoming cathodic.

After completion of the polarization scans, the following polarization parameters were obtained from the polarization curves of potential (E) versus logarithm of current density (log i) when applicable: i_{cor}, E_{cor}, i_{pas}, E_{pit} or E_b, E_{prot} or E_{rp}, i_{max} and E_{max}. Tafel slopes could be obtained from the polarization curves if desired.

APPENDIX B

CPP CURVES OF Fe-Cr-Ni ALLOYS

IN SIMULATED J-13 WATER AND CHLORIDE SOLUTIONS

Table B.1 Comparison Of Polarization Parameters For Alloy 304L In 90°C Simulated J-13 Well Water Containing Various Types And Concentrations Of Salt.

Chloride Concentration ppm	Chloride Type	E_{ocr} V, SCE	I_{ocr} μA/cm²	E_{pit} V, SCE	E_{prot} V, SCE	Comments
1 000	NaCl	-.231	0.11	+0.300	-0.059	Pitting, iridescent film, and crevice attack.
10 000	NaCl	-.241	0.13	+0.163	-0.122	Pitting, iridescent film, and crevice attack.
100 000	NaCl	-.224	0.20	-0.224	-0.330	Pitting and crevice attack.
10 000	$CaCl_2$	-.163	0.05	+0.026	-0.140	Pitting and crevice attack.

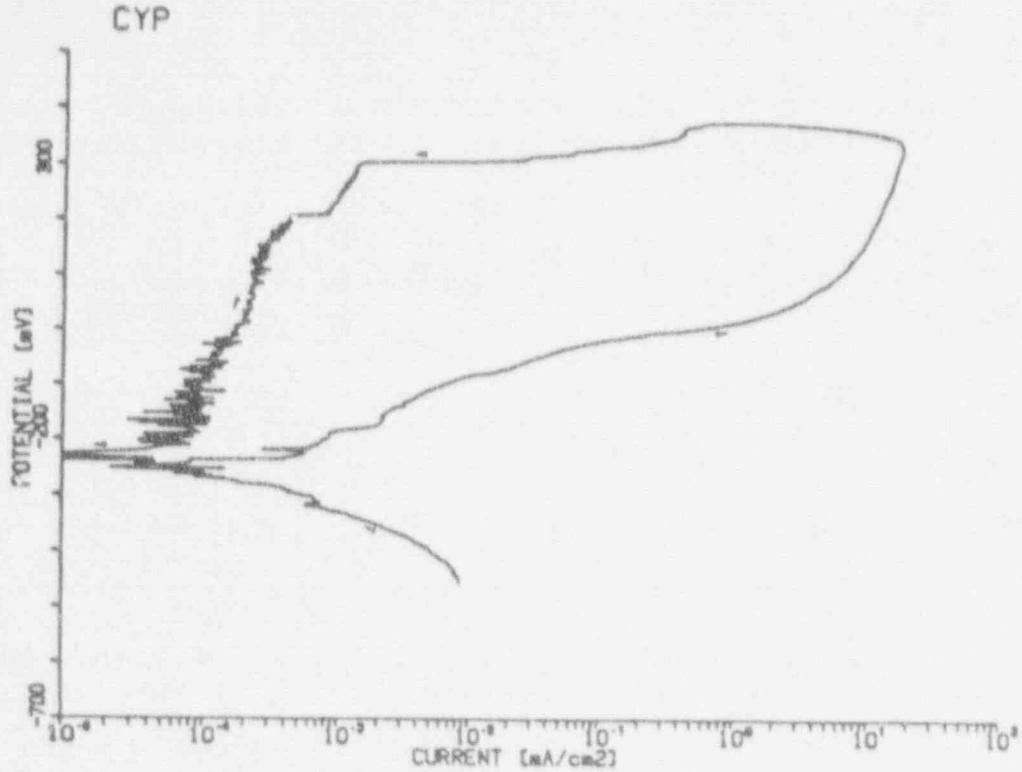

Figure B.1 Polarization Curve For Alloy 304L In 90°C Simulated J-13 Well Water Containing 1000 ppm Chlorides As NaCl.

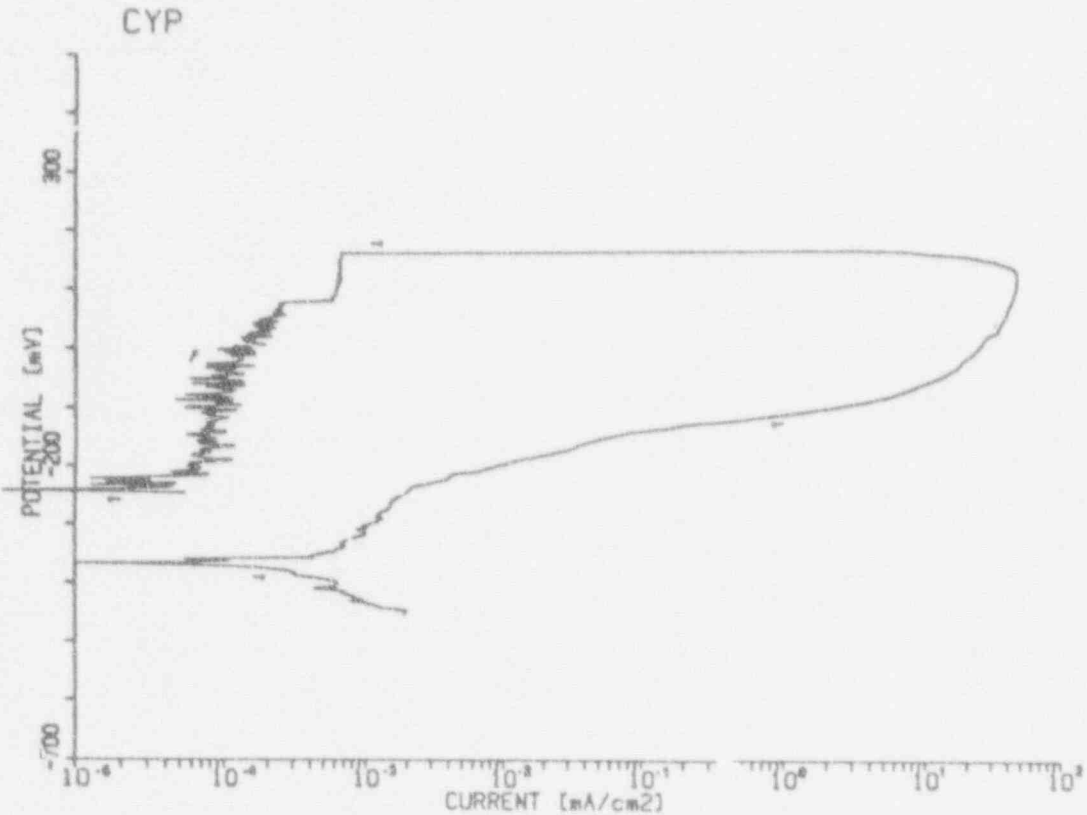

Figure B.2 Polarization Curve For Alloy 304L In 90°C Simulated J-13 Well Water Containing 10 000 ppm Chlorides As NaCl.

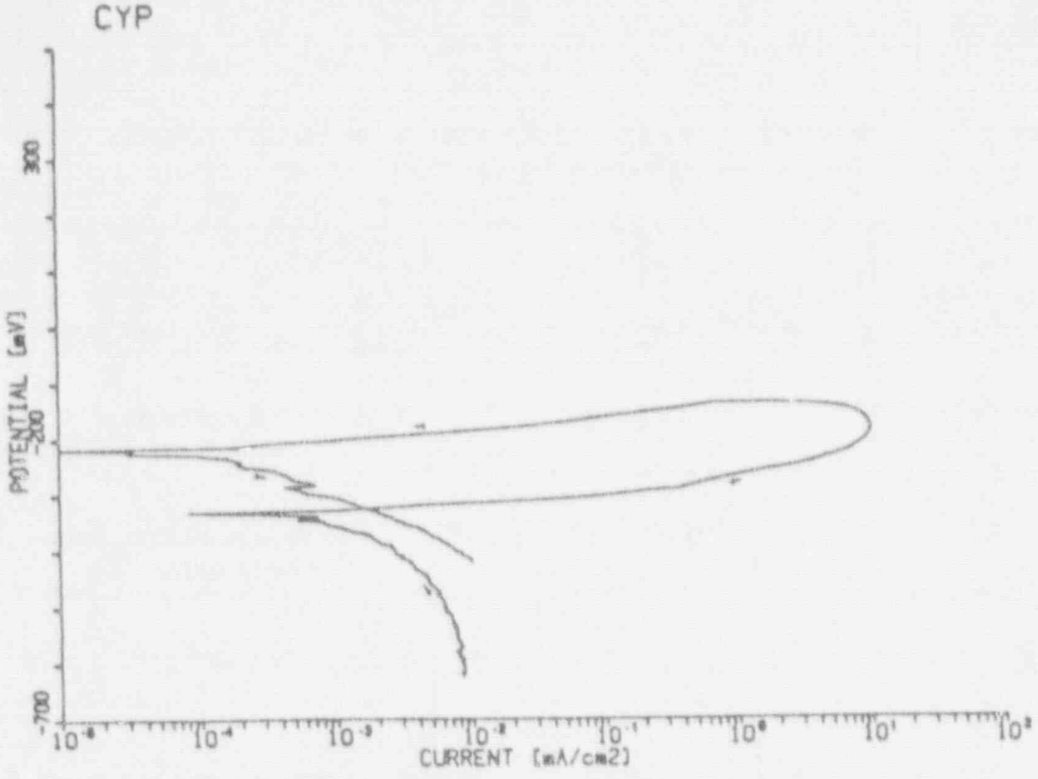

Figure B.3 Polarization Curve For Alloy 304L In 90°C Simulated J-13 Well Water Containing 100 000 ppm Chlorides As NaCl.

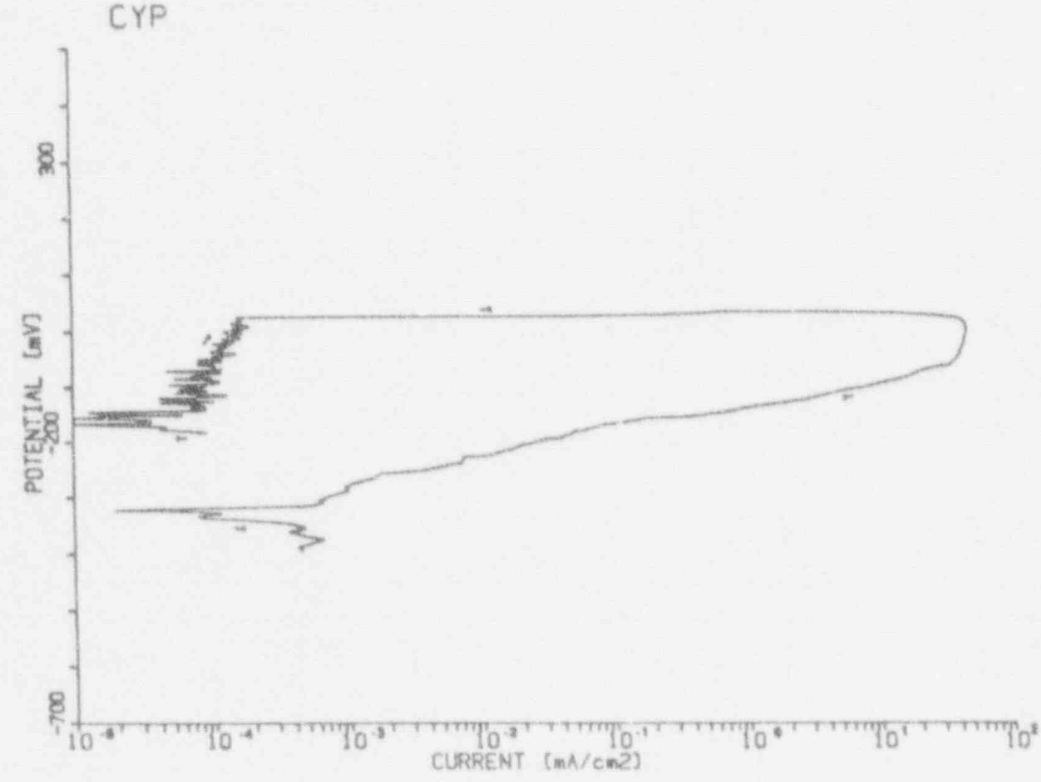

Figure B.4 Polarization Curve For Alloy 304L In 90°C Simulated J-13 Well Water Containing 10 000 ppm Chlorides As $CaCl_2$

Table B.2 Comparison Of Polarization Parameters For Alloy 825 in 90°C Simulated J-13 Well Water Containing Various Concentrations Of Salt.

Chloride Concentration ppm	Chloride Type	E_{cor} V, SCE	I_{cor} μA/cm²	E_{pit} V, SCE	E_{prot} V, SCE	Comments
1 000	NaCl	+0.083	0.30	+0.355	-0.190	Iridescent oxide, pitting and etching, crevice attack.
10 000	NaCl	-0.041	0.60	+0.205	-0.068	Iridescent oxide, pitting and crevice attack.
100 000	NaCl	-0.300	0.10	-0.044	-0.250	Pitting and crevice attack.
10 000	$CaCl_2$	-0.241	0.12	+0.242	-0.150	Pitting and crevice attack.

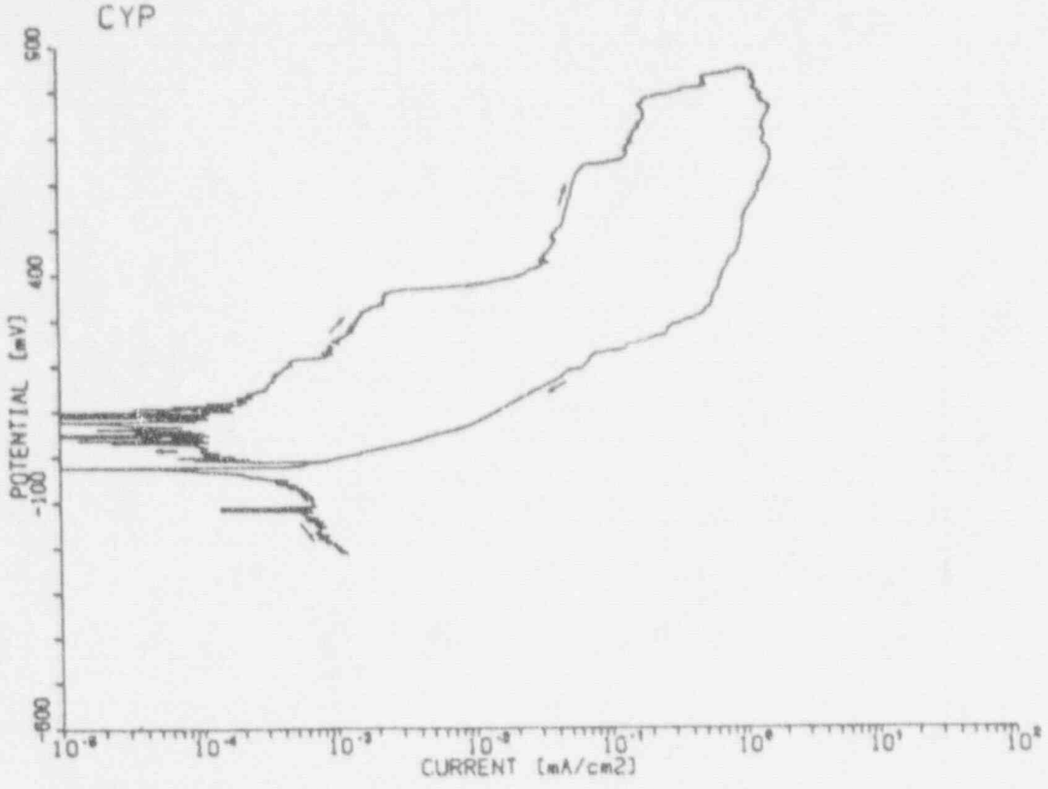

Figure B.5 Polarization Curve For Alloy 825 In 90°C Simulated J-13 Well Water Containing 1000 ppm Chlorides As NaCl.

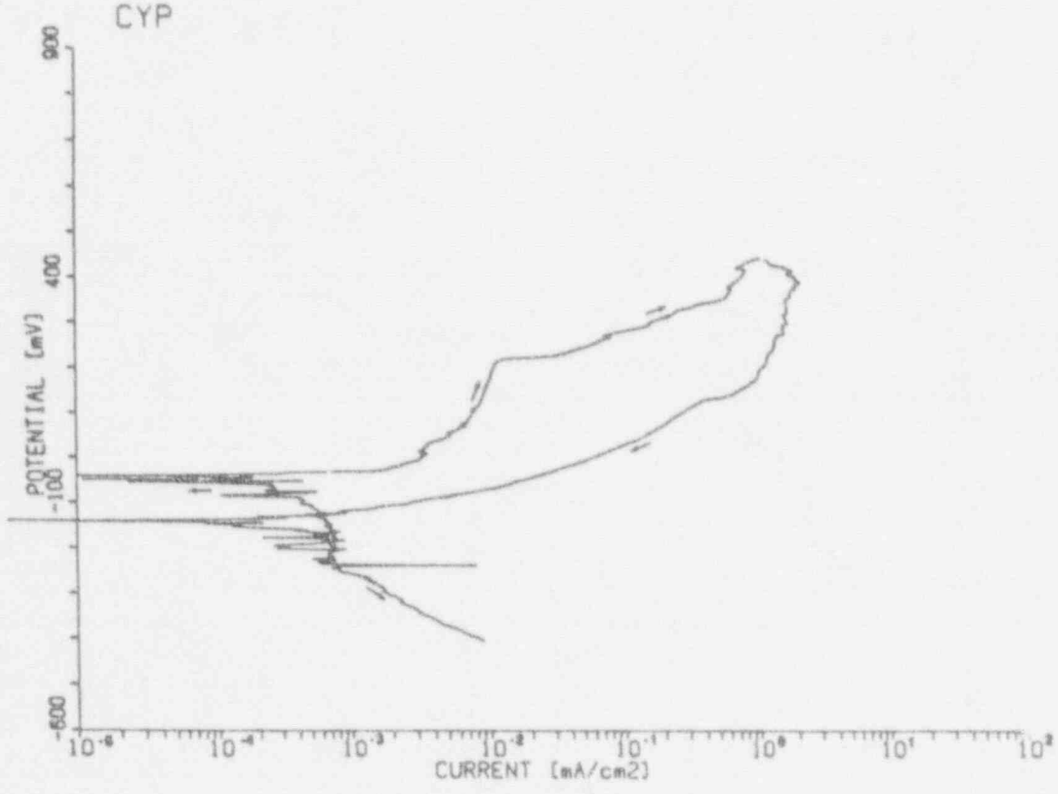

Figure B.6 Polarization Curve For Alloy 825 In 90°C Simulated J-13 Well Water Containing 10 000 ppm Chlorides As NaCl.

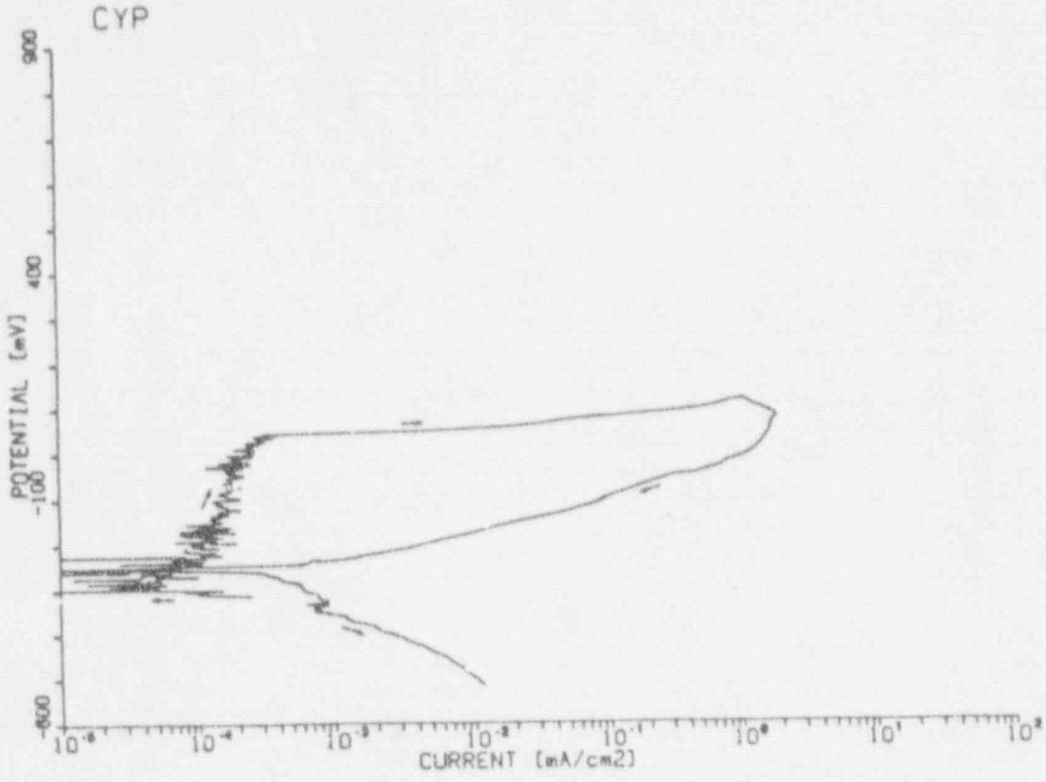

Figure B.7 Polarization Curve For Alloy 825 In 90°C Simulated J-13 Well Water Containing 100 000 ppm Chlorides As NaCl.

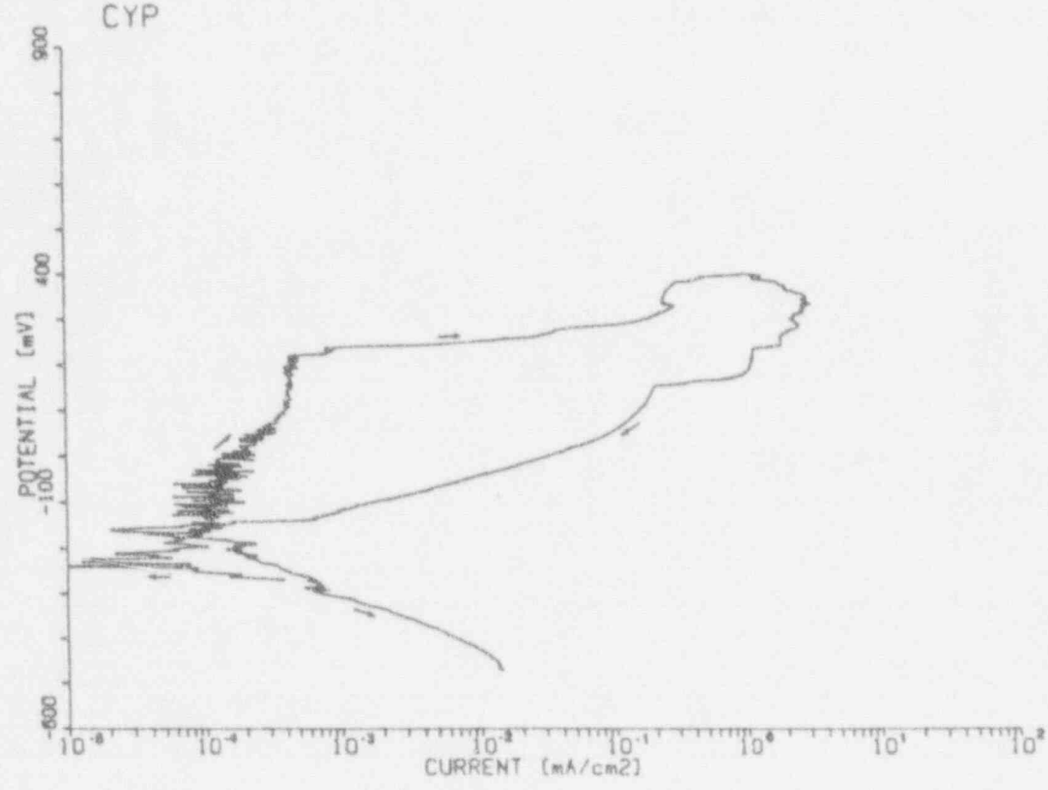

Figure B.8 Polarization Curve For Alloy 825 In 90°C Simulated J-13 Well Water Containing 10 000 ppm Chlorides As $CaCl_2$.

APPENDIX C

CANDIDATE ALLOY COMPOSITIONS

Table C.1 Candidate Alloy Compositions Of U-Bend Specimens Used For The Stress-Corrosion-Cracking Studies In 90°C Simulated J-13 Water In Task 3.

ELEMENT	CDA 102	CDA 715	1825	304L
Cu	99.99%	68.85%	1.71%	0.47%
Ni	---	29.42%	42.20%	9.44%
Fe	---	0.60%	29.06%	Balance
Cr	---	---	22.56%	18.27%
Mo	---	---	2.74%	0.10%
Mn	---	0.60%	0.51%	1.39%
C	---	0.015%	0.02%	0.020%
S	---	0.006%	0.003%	0.015%
Zn	---	0.05%	---	---
P	---	0.004%	---	0.022%
Pb	---	0.01%	---	---
Si	---	---	0.33%	0.54%
Al	---	---	0.06%	---
Ti	---	---	0.81%	---
Co	---	---	---	0.18%
N	---	---	---	0.023%

Table C.2 Candidate Alloy Compositions Of U-Bend Specimens Used For The Stress-Corrosion-Cracking Studies In Solution Numbers 7 And 20 At 90°C, Task 3.

ELEMENT	Solution Number 7		Solution Number 20	
	CDA 102	CDA 715	I825	304L
Cu	99.95%	68.85%	1.76%	0.47%
Ni	—	29.42%	40.22%	9.44%
Fe	—	0.60%	30.41%	Balance
Cr	—	—	23.34%	18.27%
Mo	—	—	2.74%	0.10%
Mn	—	0.60%	0.41%	1.39%
C	—	0.015%	0.02%	0.020%
S	—	0.006%	0.001%	0.015%
Zn	—	0.05%	—	—
P	—	0.004%	—	0.022%
Pb	—	0.01%	—	—
Si	—	—	0.17%	0.54%
Al	—	—	0.04%	—
Ti	—	—	0.89%	—
Co	—	—	—	0.18%
N	—	—	—	0.023%

Table C.3 Candidate Alloy Compositions Of Tensile Specimens Used For The Stress-Corrosion-Cracking Studies In Task 5.

ELEMENT	CDA 102	CDA 715	I825	304L
Cu	99.99%	67.13%	1.71%	0.190%
Ni	—	31.80%	42.03%	8.87%
Fe	—	0.47%	29.84%	Balance
Cr	—	—	21.96%	18.22%
Mo	—	—	3.17%	0.170%
Mn	—	0.56%	0.41%	1.21%
C	—	<0.01%	0.01%	0.021%
S	—	<0.01%	<0.001%	0.023%
Zn	—	0.01%	—	—
P	—	<0.01%	—	0.026%
Pb	—	<0.01%	—	—
Si	—	—	0.17%	0.520%
Al	—	—	0.05%	—
Ti	—	—	0.65%	—
Co	—	—	—	—
N	—	—	—	—

Table C.4 Candidate Alloy Compositions Of U-Bend Specimens Used For The Stress-Corrosion-Cracking Studies In The Long-Term, Boil-Down Tests With 90°C Simulated J-13 Water; Task 7.

ELEMENT	CDA 102	CDA 715	I825	304L
Cu	99.95%	68.85%	1.71%	0.47%
Ni	—	29.42%	42.20%	9.44%
Fe	—	0.60%	29.06%	Balance
Cr	—	—	22.56%	18.27%
Mo	—	—	2.74%	0.10%
Mn	—	0.60%	0.51%	1.39%
C	—	0.015%	0.02%	0.020%
S	—	0.006%	0.003%	0.015%
Zn	—	0.05%	—	—
P	—	0.004%	—	0.022%
Pb	—	0.01%	—	—
Si	—	—	0.33%	0.54%
Al	—	—	0.06%	—
Ti	—	—	0.81%	—
Co	—	—	—	0.18%
N	—	—	—	0.023%

Table C.5 Candidate Alloy Compositions Of U-Bend Specimens Used For The Stress-Corrosion-Cracking Studies In 90°C Simulated J-13 Water Containing Salt; Task 7.

ELEMENT	I825	304L
Cu	1.82%	0.47%
Ni	42.89%	9.44%
Fe	27.72%	Balance
Cr	22.78%	18.27%
Mo	2.74%	0.10%
Mn	0.45%	1.39%
C	0.01%	0.020%
S	0.001%	0.015%
Zn	—	—
P	—	0.022%
Pb	—	—
Si	0.40%	0.54%
Al	0.11%	—
Ti	1.08%	—
Co	—	0.18%
N	—	0.023%

APPENDIX D

PHOTOMICROGRAPHS OF SPECIMENS OF ALLOY 304L

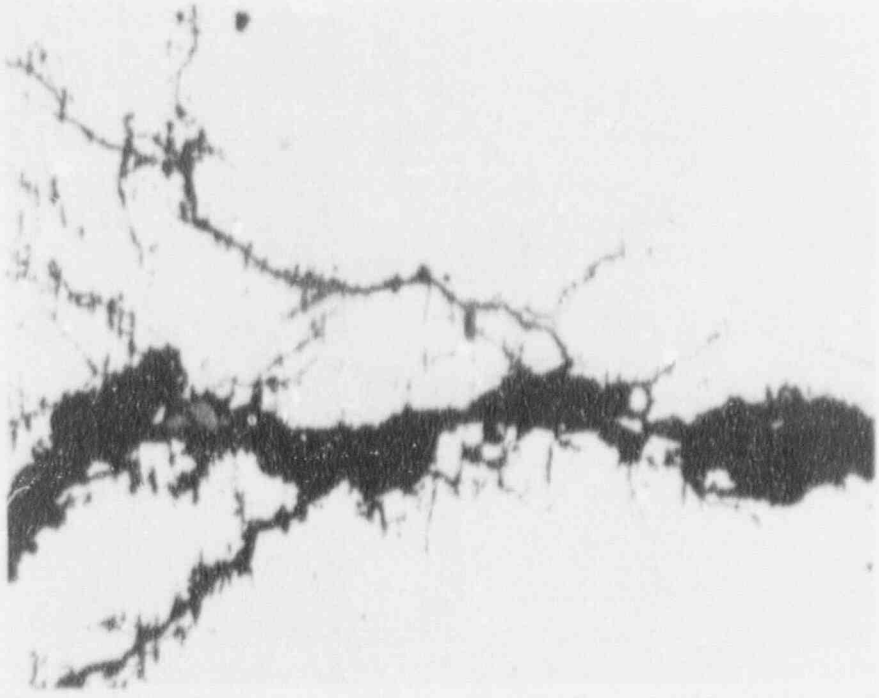

Figure D.1 Photomicrograph Of U-Bend Specimen Of Alloy 304L Following 2855 Hours Of Exposure To Solution No. 20 (With H_2O_2 Additions) At 90°C Showing Transgranular Stress-Corrosion Cracking; 250X Magnification.

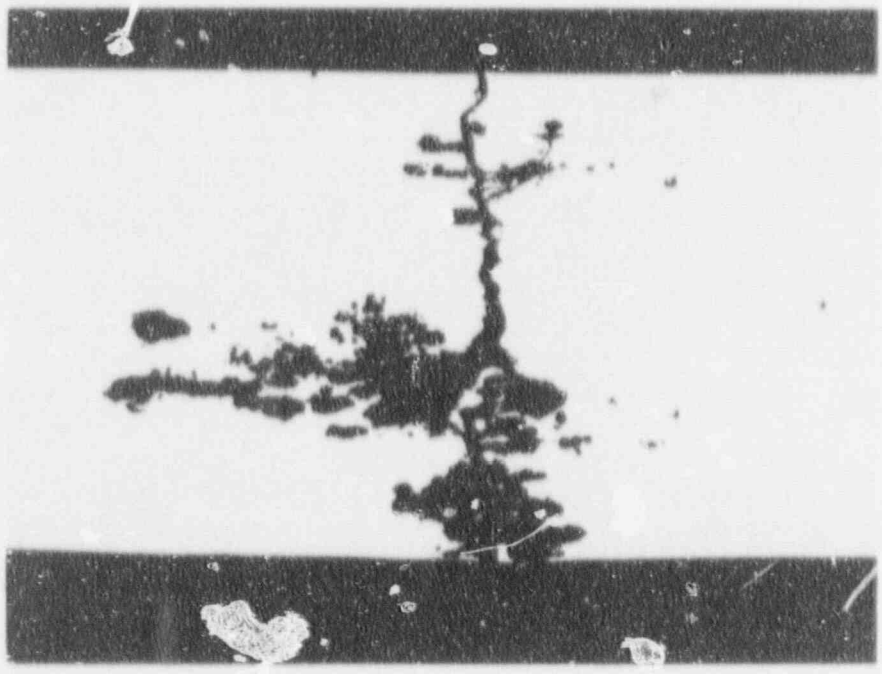

Figure D.2 Photomicrograph Of U-Bend Specimen Of Alloy 304L Exposed To Simulated J-13 Well Water Containing 100 000 ppm Chloride (As NaCl) For 181 Days at 90°C; 50X Magnification.

Figure D.3 Photomicrograph Of U-Bend Specimen Of Alloy 304L Exposed In The Vapor Above Simulated J-13 Well Water Containing 1000 ppm Chloride (As NaCl) For 100 Days at 90°C. H_2O_2 Added Daily; 100X Magnification.

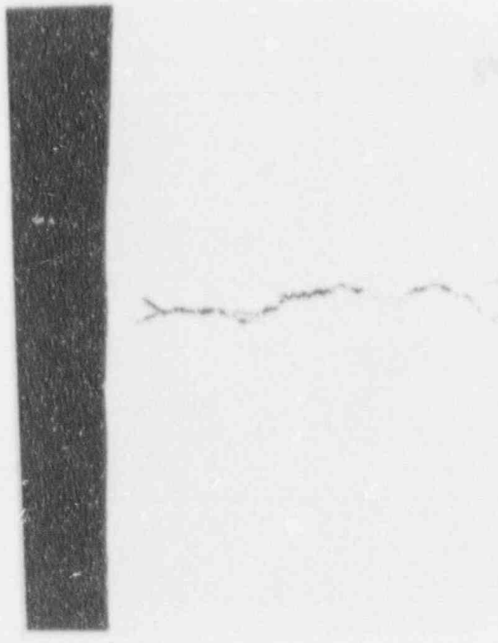

Figure D.4 Photomicrograph Of U-Bend Specimen Of Alloy 304L Exposed In The Vapor Above Simulated J-13 Well Water Containing 10 000 ppm Chloride (As NaCl) For 100 Days at 90°C. H_2O_2 Added Daily; 100X Magnification.

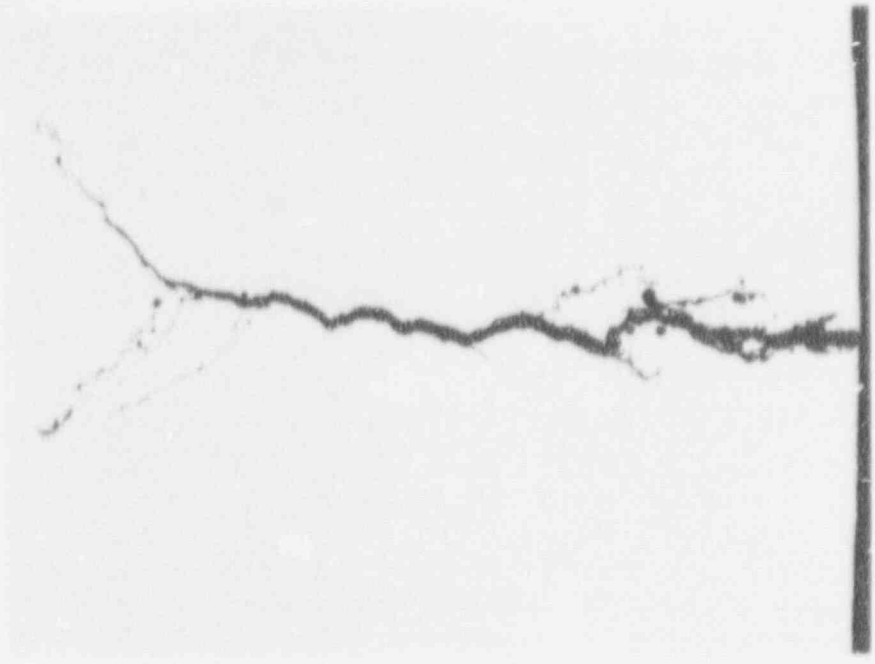

Figure D.5 Photomicrograph Of U-Bend Specimen Of Alloy 304L Exposed In The Vapor Above Simulated J-13 Well Water Containing 10 000 ppm Chloride (As $CaCl_2$) For 100 Days at 90°C. H_2O_2 Added Daily; 100X Magnification.

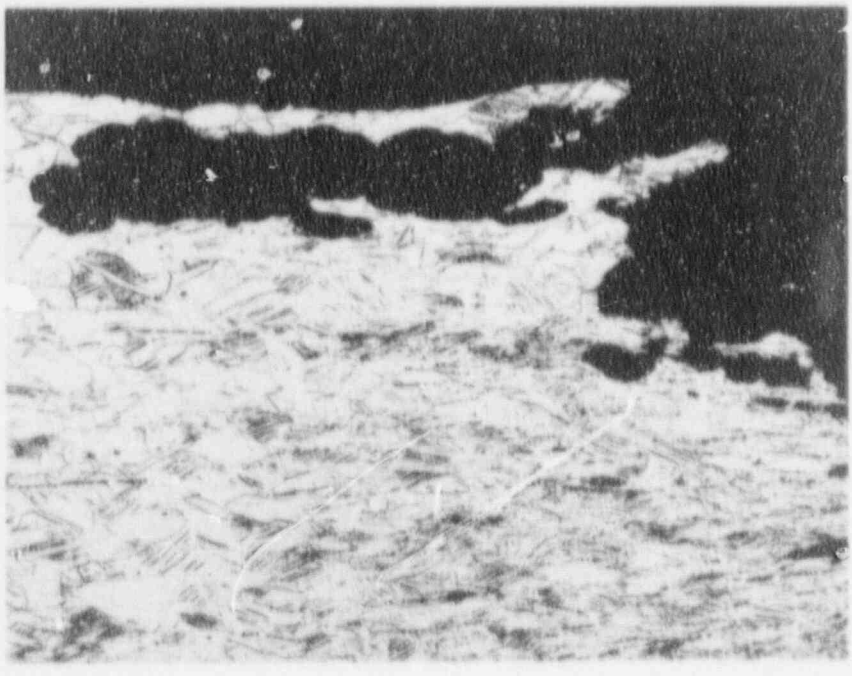

10X a. As Polished

Figure D.6a Photomicrograph Of SSR Specimen Of Alloy 304L Exposed To 90°C Simulated J-13 Water Containing 1000 ppm Cl As NaCl. Specimen Potentiostated To +200 mV (SCE) And Strained To Failure At 1 X 10^{-6} sec^{-1}; (Test No. M20).

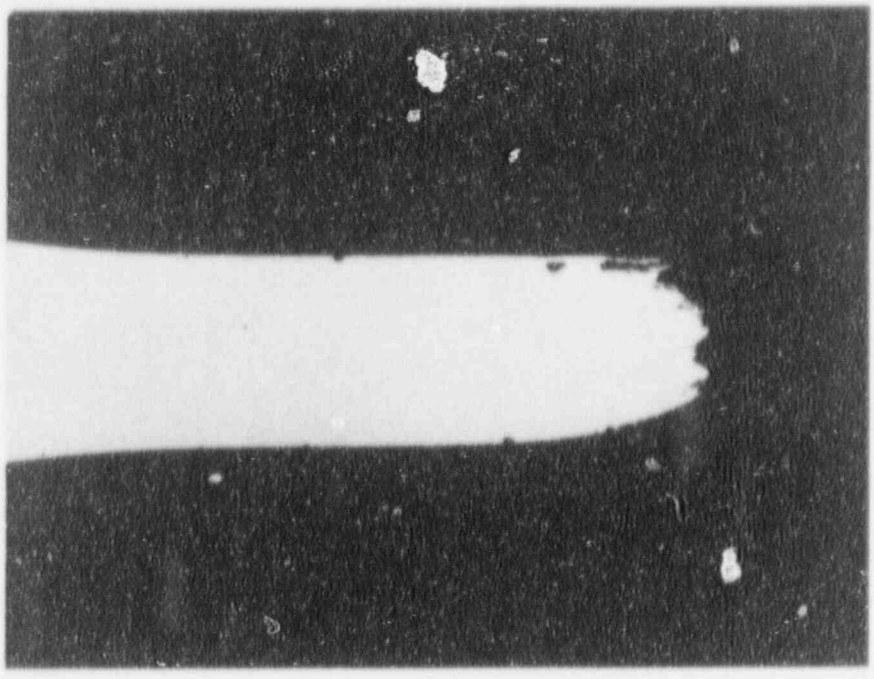

100X b. Etched in 97ml Conc. HCl, 3ml Conc. HNO_3, ½ gm $CuCl_2$

Figure D.6b Photomicrograph Of SSR Specimen Of Alloy 304L Exposed To 90°C Simulated J-13 Water Containing 1000 ppm Cl As NaCl. Specimen Potentiostated To +200 mV (SCE) And Strained To Failure At 1 X 10^{-6} sec^{-1}; (Test No. M20).

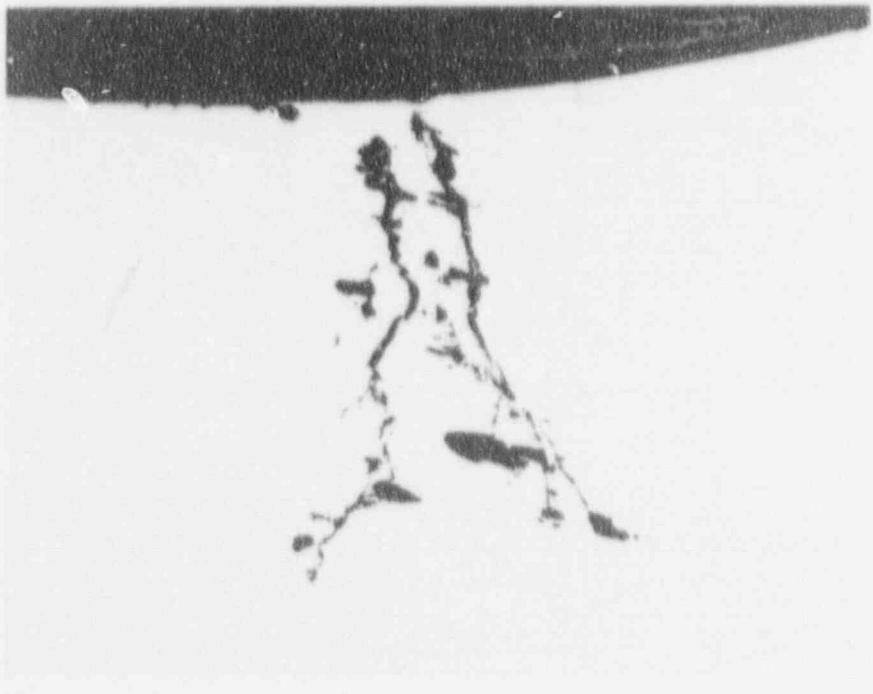

Figure D.7 Photomicrograph Of SSR Specimen Of Alloy 304L Exposed To The Vapor Phase Of Solution Number 20 At 90°C. H_2O_2 Added Daily. Specimen Strained To Failure At 1 X 10^{-7} sec^{-1}; 50X Magnification (Test No. 34).

Figure D.8 Photomicrograph Of SSR Specimen Of Alloy 304L Exposed To The Vapor Phase Of Solution Number 20 At 90°C. Specimen Strained To Failure At 1 X 10^{-7} sec^{-1}; 250X Magnification (Test No. 35).

Figure D.9 Photomicrograph Of SSR Specimen Of Alloy 304L Exposed To 90°C Simulated J-13 Well Water Containing 100 000 ppm Chloride As NaCl. Specimen Polarized To -0.174 V(SCE) (E_{pp} + 50 mV). Specimen Strained To Failure At 1 x 10^{-6} sec^{-1}; 100X Magnification (Test No. 37).

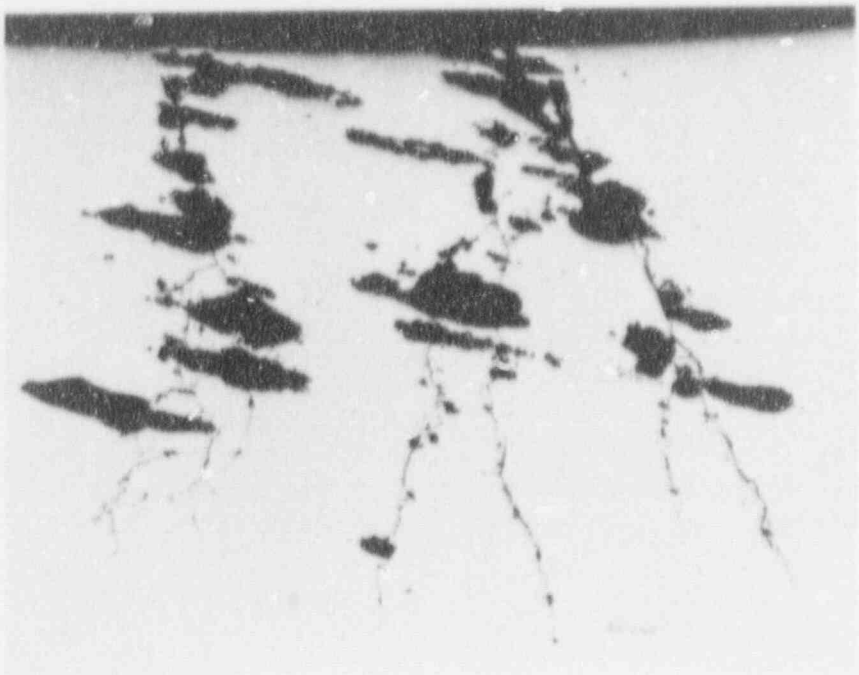

Figure D.10 Photomicrograph Of SSR Specimen Of Alloy 304L Exposed To The Vapor Phase Of 90°C Simulated J-13 Well Water Containing 10 000 ppm Chloride As NaCl. H_2O_2 Added Daily. Specimen Strained To Failure At 1 x 10^{-6} sec^{-1}; 100X Magnification (Test No. 39).

APPENDIX E

PHOTOMICROGRAPHS OF SPECIMENS OF ALLOY 825

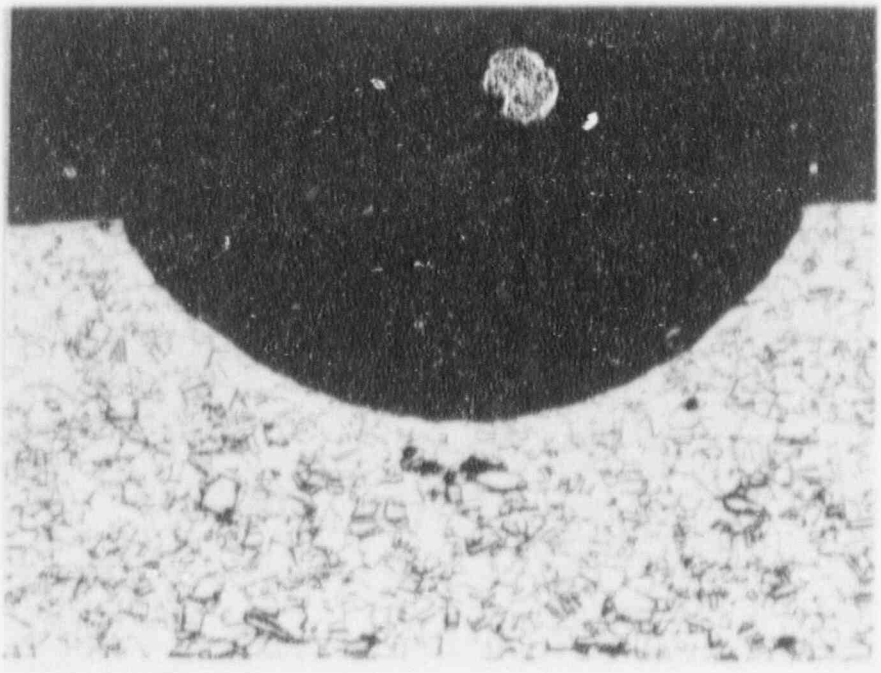

Figure E.1 Photomicrograph Of U-Bend Specimen Of Alloy 825 Exposed In The Vapor Above Simulated J-13 Well Water Containing 10 000 ppm Chloride (As $CaCl_2$) For 103 Days at 90°C. H_2O_2 Added Daily.

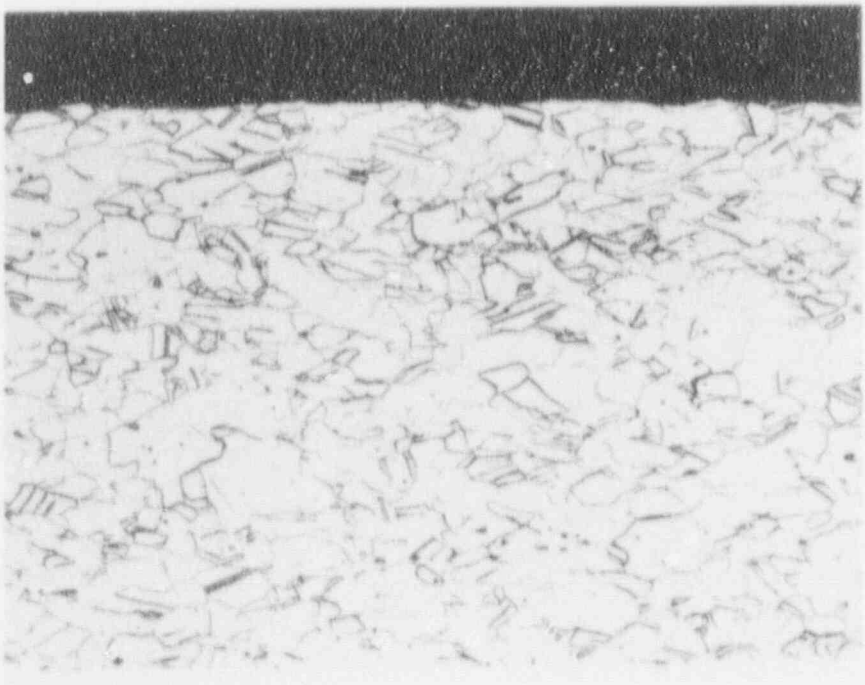

Figure E.2 Photomicrograph Of The Reduced Gage Section Of A Specimen Of Alloy 825 Exposed To The Vapor Phase Of Simulated J-13 Water Containing 100 000 ppm Chloride As Sodium Chloride. Specimen Strained To Failure At 1 x 10^{-6} sec^{-1}; 100X Magnification (Test No. 50).

APPENDIX F

PHOTOMICROGRAPHS OF SPECIMENS OF ALLOY CDA 102

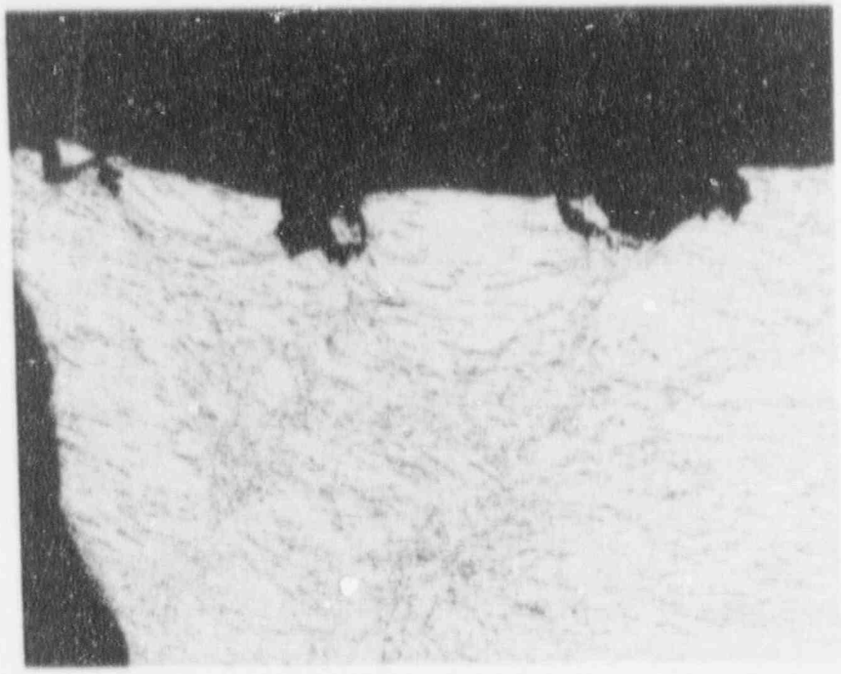

Figure F.1 Photomicrograph Of SSR Specimen Of Alloy CDA 102 Exposed To 0.005M $NaNO_2$ At 23°C And Strained To Failure At 1 X 10^{-6} sec^{-1}; 100X Magnification (Test No. 8).

Figure F.2 Photomicrograph Of SSR Specimen Of Alloy CDA 102 Exposed To 1M $NaNO_2$ At 23°C And Strained To Failure At 1 X 10^{-6} sec^{-1}; 100X Magnification (Test No. 7).

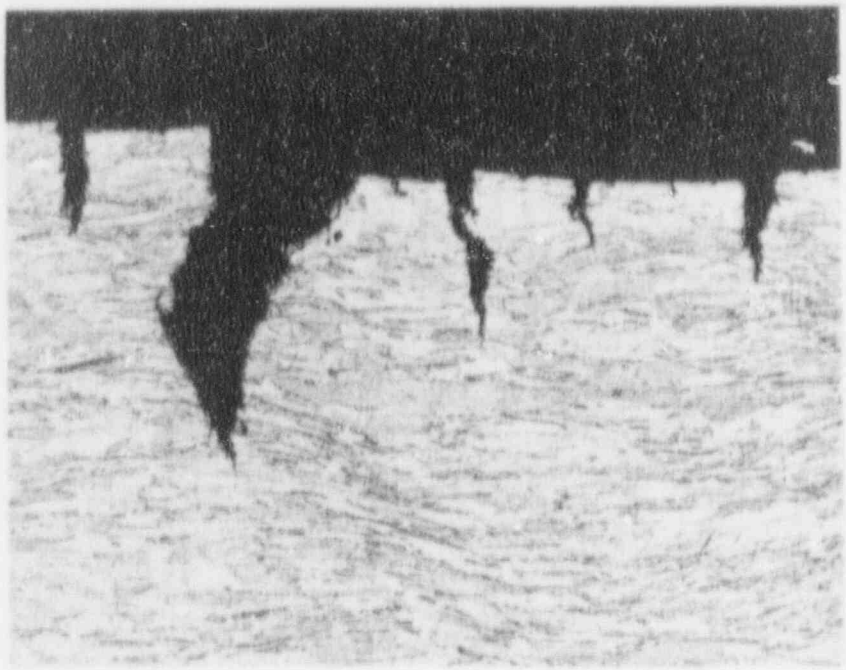

Figure F.3 Photomicrograph Of SSR Specimen Of Alloy CDA 102 Exposed To 0.005M $NaNO_2$ At 23°C And Polarized To +0.200 Volts (SCE). Specimen Strained To Failure At 1 X 10^{-6} sec^{-1}; 100X Magnification (Test No. 19).

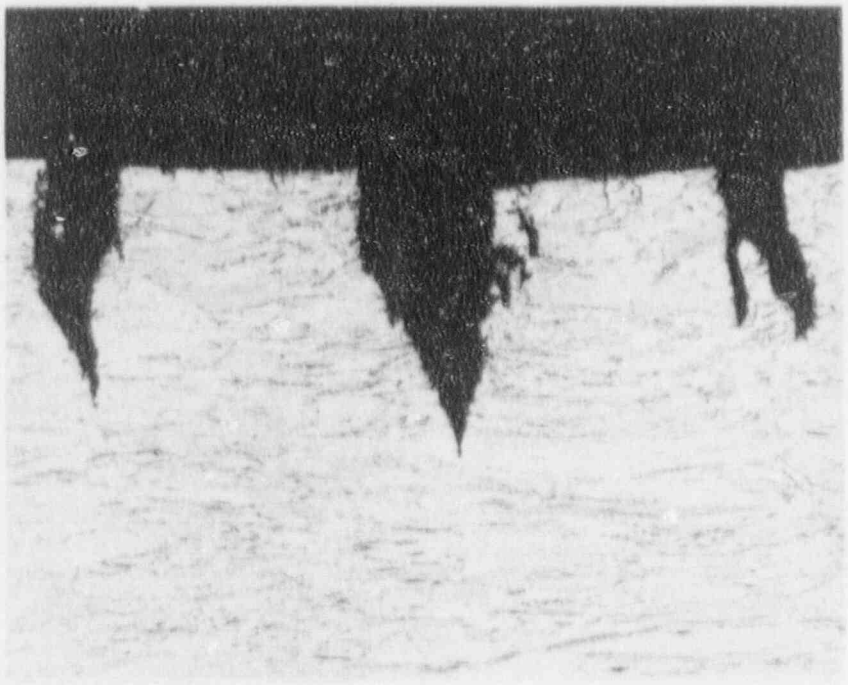

Figure F.4 Photomicrograph Of SSR Specimen Of Alloy CDA 102 Exposed To 0.005M $NaNO_2$ At 23°C And Polarized To 0.174 Volts (SCE). Specimen Strained To Failure At 1 X 10^{-6} sec^{-1}; 100X Magnification (Test No. 20).

Figure F.5 Photomicrograph Of SSR Specimen Of Alloy CDA 102 Exposed To 1M $NaNO_2$ At 23°C And Polarized To +0.061 Volts (SCE). Specimen Strained To Failure At 1 X 10^{-6} sec^{-1}; 100X Magnification (Test No. 17).

Figure F.6 Photomicrograph Of SSR Specimen Of Alloy CDA 102 Exposed To 1M $NaNO_2$ At 23°C And Polarized To +0.068 Volts (SCE). Specimen Strained To Failure At 1 X 10^{-6} sec^{-1}; 100X Magnification (Test No. 18).

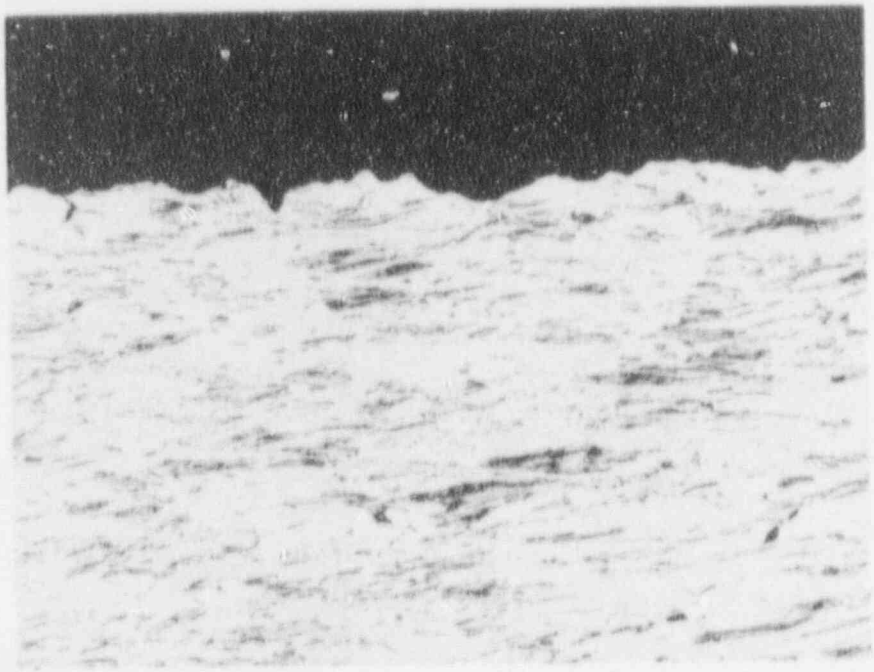

Figure F.7 Photomicrograph Of SSR Specimen Of Alloy CDA 102 Exposed To 0.005M $NaNO_2$ At 90°C And Polarized To +0.234 Volts (SCE). Specimen Strained To Failure At 1 X 10^{-6} sec^{-1}; 100X Magnification (Test No. 29).

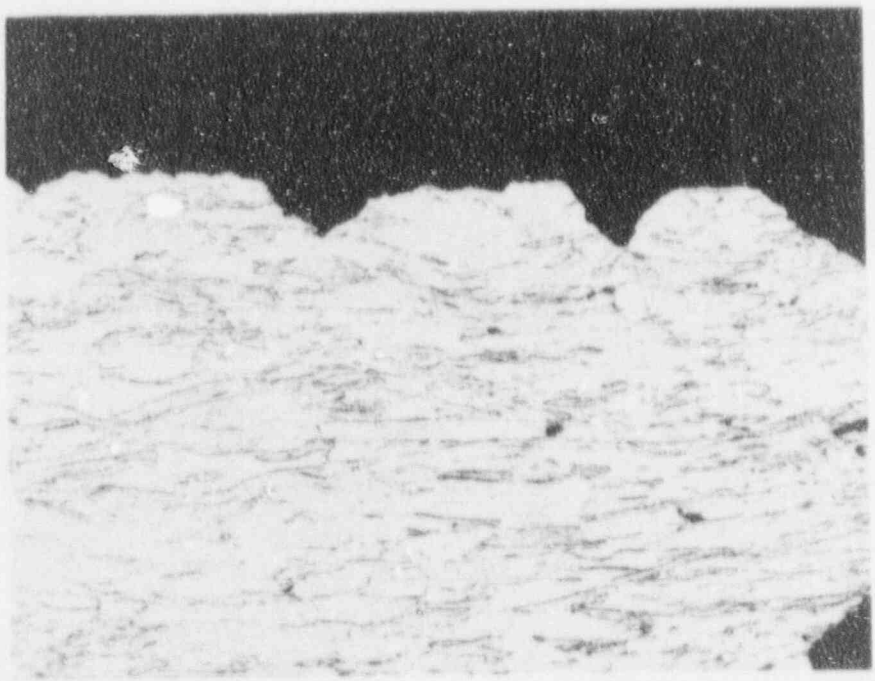

Figure F.8 Photomicrograph Of SSR Specimen Of Alloy CDA 102 Exposed To 0.005M $NaNO_2$ At 90°C And Polarized To +0.246 Volts (SCE). Specimen Strained To Failure At 1 X 10^{-6} sec^{-1}; 100X Magnification (Test No. 31).

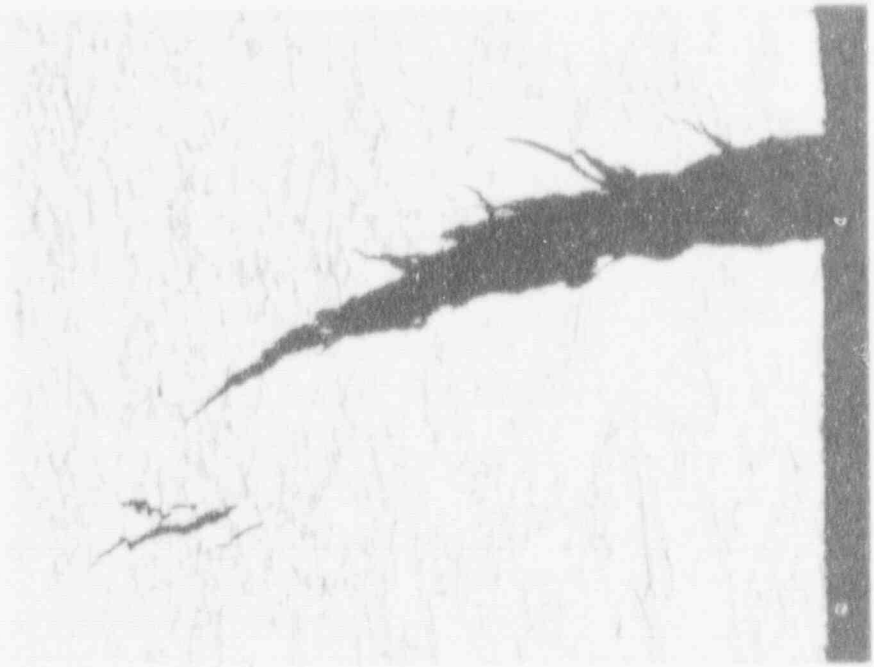

Figure F.9 Photomicrograph Of SSR Specimen Of Alloy CDA 102 Exposed To 1M $NaNO_2$ At 90°C And Polarized To +0.122 Volts (SCE). Specimen Strained To Failure At 1 X 10^{-6} sec^{-1}; 100X Magnification (Test No. 23).

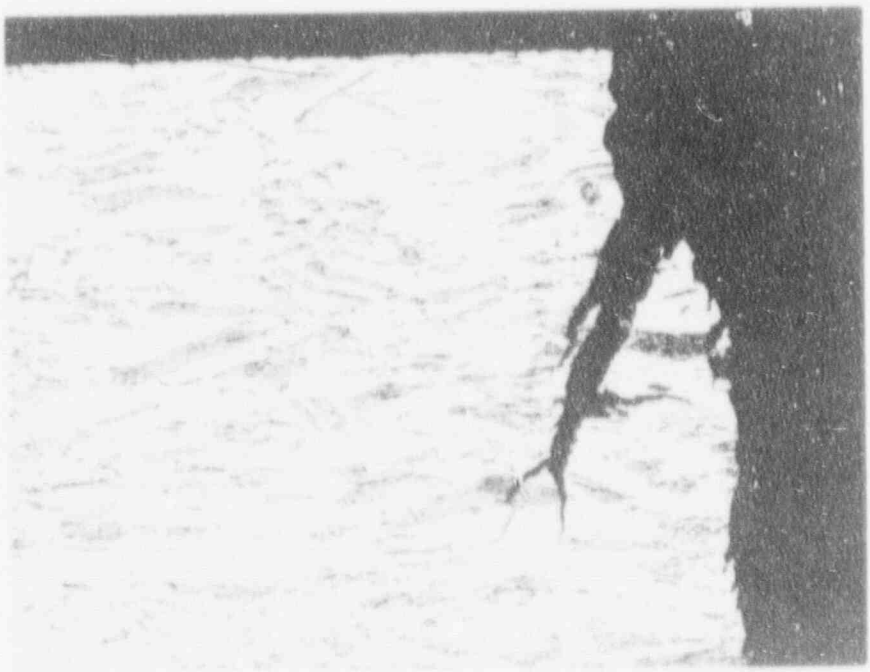

Figure F.10 Photomicrograph Of SSR Specimen Of Alloy CDA 102 Exposed To 1M $NaNO_2$ At 90°C And Polarized To +0.021 Volts (SCE). Specimen Strained To Failure At 1 X 10^{-6} sec^{-1}; 100X Magnification (Test No. 24).

APPENDIX G

PHOTOMICROGRAPHS OF SPECIMENS OF ALLOY CDA 715

Figure G.1 Photomicrograph Of SSR Specimen Of Alloy CDA 715 Exposed To 1M $NaNO_2$ At 23°C And Polarized To +0.033 Volts (SCE). Specimen Strained To Failure At 1 X 10^{-6} sec^{-1}; 250X Magnification (Test No. 28).

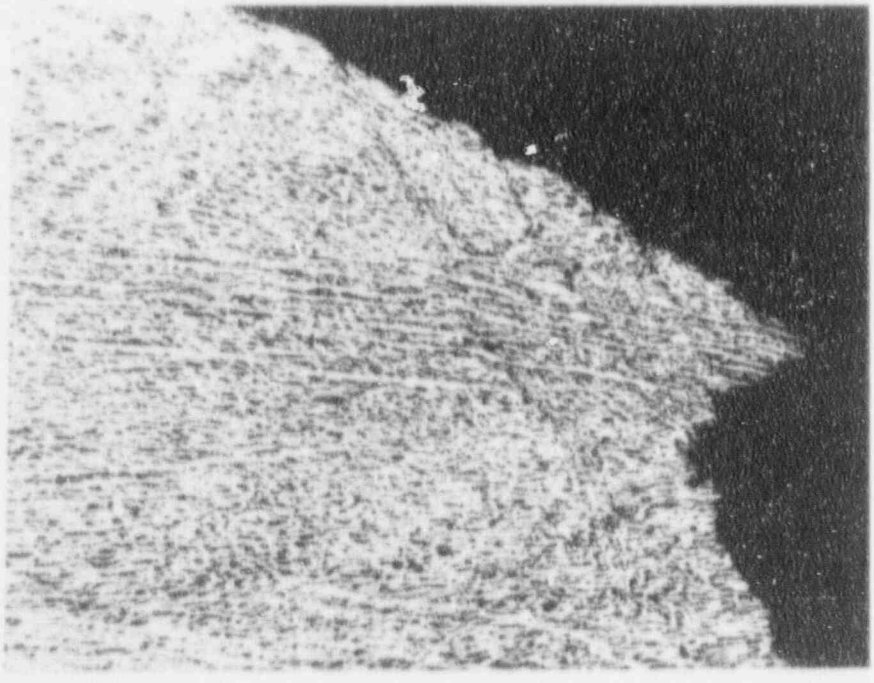

Figure G.2 Photomicrograph Of SSR Specimen Of Alloy CDA 715 Exposed To 1M $NaNO_2$ At 23°C And Polarized To +0.127 Volts (SCE). Specimen Strained To Failure At 1 X 10^{-6} sec^{-1}; 100X Magnification (Test No. 30).

NRC FORM 335 (2-89) NRCM 1102, 3201, 3202

U.S. NUCLEAR REGULATORY COMMISSION

BIBLIOGRAPHIC DATA SHEET

(See instructions on the reverse)

1. REPORT NUMBER (Assigned by NRC, Add Vol., Supp., Rev., and Addendum Numbers, if any.)

NUREG / CR-5710

2. TITLE AND SUBTITLE

Stress-Corrosion-Cracking Studies On Candidate Container Alloys For The Tuff Repository

3. DATE REPORT PUBLISHED

MONTH: May | YEAR: 1992

4. FIN OR GRANT NUMBER

FIN D1092

5. AUTHOR(S)

J. A. Beavers, C. L. Durr

6. TYPE OF REPORT

Technical

7. PERIOD COVERED *(Inclusive Dates)*

12/87 - 12/91

8. PERFORMING ORGANIZATION – NAME AND ADDRESS *(If NRC, provide Division, Office or Region, U.S. Nuclear Regulatory Commission, and mailing address; if contractor, provide name and mailing address.)*

Cortest Columbus Technologies, Inc.
2704 Sawbury Boulevard
Columbus, Ohio 43235

9. SPONSORING ORGANIZATION – NAME AND ADDRESS *(If NRC, type "Same as above"; if contractor, provide NRC Division, Office or Region, U.S. Nuclear Regulatory Commission, and mailing address.)*

Division of Engineering
Office of Nuclear Regulatory Research
U. S. Nuclear Regulatory Commission
Washington, DC 20555

10. SUPPLEMENTARY NOTES

11. ABSTRACT *(200 words or less)*

Cortest Columbus Technologies, Inc. (CC Technologies) investigated the long-term performance of container materials used for high-level waste packages as part of the information needed by the Nuclear Regulatory Commission (NRC) to assess the Department of Energy's application to construct a geologic repository for high-level radioactive waste. At the direction of the NRC, the program focused on the Tuff Repository. This report summarizes the results of Stress-Corrosion-Cracking (SCC) studies performed in Tasks 3, 5 and 7 of the program. Two test techniques were used; U-bend exposures and Slow-Strain-Rate (SSR) tests. The testing was performed on two copper-base alloys (Alloy CDA 102 and Alloy CDA 715) and two Fe-Cr-Ni alloys (Alloy 304L and Alloy 825) in simulated J-13 groundwater and other simulated solutions for the Tuff Repository. These solutions were designed to simulate the effects of concentration and irradiation on the groundwater composition. Possible radiolysis products evaluated included H_2O_2 and $NaNO_2$. All SCC testing on the Fe-Cr-Ni Alloys was performed on solution-annealed specimens and thus issues such as the effect of sensitization on SCC were not addressed.

All four alloys were resistant to SCC in the J-13 well water and in the J-13 well water that was concentrated by a factor of about 80 by evaporation. Alloy 825 also was resistant to SCC in all other environments evaluated including chloride solutions containing up to 100 000 ppm Cl^- and H_2O_2. On the other hand, Alloy 304L underwent SCC in several of the Cl^- containing solutions. Alloy CDA 715 was also resistant to SCC in all other environments evaluated including $NaNO_2$ at concentrations up to 1M. Alloy CDA 102 underwent SCC in $NaNO_2$ environments at concentrations as low as 200 ppm.

12. KEY WORDS/DESCRIPTORS *(List words or phrases that will assist researchers in locating the report.)*

Corrosion
Container Materials
Stress-Corrosion Cracking
U-Bends
Nitrite
Chloride
Copper-Base Alloys
Fe-Cr-Ni Alloys
Simulated J-13 Groundwater
High Level Nuclear Waste Disposal
Tuff Repository

13. AVAILABILITY STATEMENT

Unlimited

14. SECURITY CLASSIFICATION

(This Page)
Unclassified

(This Report)
Unclassified

15. NUMBER OF PAGES

16. PRICE

UNITED STATES
NUCLEAR REGULATORY COMMISSION
WASHINGTON, D.C. 20555

OFFICIAL BUSINESS
PENALTY FOR PRIVATE USE, $300

SPECIAL FOURTH-CLASS RATE
POSTAGE AND FEES PAID
USNRC
PERMIT NO. G-67

UNITED STATES
NUCLEAR REGULATORY COMMISSION
WASHINGTON, D.C. 20555

OFFICIAL BUSINESS
PENALTY FOR PRIVATE USE, $300

SPECIAL FOURTH-CLASS RATE
POSTAGE AND FEES PAID
USNRC
PERMIT NO. G-67